Mariana Rossi

Licenciada em Engenharia Civil

Flat Slabs with Different Longitudinal Reinforcement Ratios Under Horizontal Cyclic Loading

Dissertação para obtenção do Grau de Mestre em
Engenharia Civil – Estruturas e Geotecnia

Orientador: Prof. Doutor António Manuel Pinho Ramos
Co-orientador: Doutor Brisid Isufi

Júri:

Presidente: Prof. Doutor Valter José da Guia Lúcio
Vogais: Prof. Doutor Rui Pedro César Marreiros
Prof. Doutor António Manuel Pinho Ramos

FACULDADE DE
CIÊNCIAS E TECNOLOGIA
UNIVERSIDADE NOVA DE LISBOA

Fevereiro de 2021

Acknowledgements

I would like to thank my supervisor Professor António Pinho Ramos and my co-supervisor Brisid Isufi for all the support, guidance and shared knowledge during the elaboration of this thesis. I am extremely grateful for the trust put in me, patience and guidance to overcome any problems we encountered during this period of time.

Thank you to all the staff from the Civil Engineering department of the Faculdade de Ciência e Tecnologia of Universidade NOVA de Lisboa for all the help, specially to the technicians Jorge Silverio and José Gaspar and the Engineer Vitor Silva for the constant help provided at the laboratory.

I am grateful for all my professors during my Master's studies. In particular, Professor Ildi Cismasiu for the help provided since the beginning of my stay in Portugal and the guidance and support during the entire course. Also, Professor Rui Marreiros for all the help provided during the experimental campaign and all the knowledge shared with me.

I am extremely grateful for all the friends I made while living in Portugal. Thank you for always being by my side and for making me feel at home in Lisbon.

To my friends in Brazil, thank you for always being there for me and giving me strength during the times I needed the most.

Finally, I would like to thank my family for understanding and supporting my decision of studying abroad and for being by my side through every step. Thank you for all your efforts so I could fulfill my dreams, without you I could never have accomplished this.

Abstract

The following dissertation studies the behavior of flat slabs when subjected to constant vertical loads and cyclic horizontal displacements, as a continuation of previous studies developed at FCT/UNL. The main focus of this research is to study the influence of flexural reinforcement on the seismic response of flat slabs. Therefore, three reinforced concrete flat slabs with varying flexural reinforcement ratio were tested, two having the same top reinforcement ratio of ρ=0,64% and one with ρ=1,34%. One of the specimens with lower longitudinal ratio was reinforced with studs as specific punching shear reinforcement. All slabs had overall dimensions of 4,15 × 1,85 × 0,15 m^3 and a gravity shear ratio, ratio between the gravity load and the punching shear resistance, approximately equal to 55%.

For a more complete analysis the results obtained were compared to two other specimens from previous experimental campaigns also conducted at FCT/UNL. These two slabs were designed with top flexural reinforcement ratio (ρ=0,96%) that lies between the two tested in this dissertation, one with no shear-reinforcement and the other with headed studs.

Results showed that the reduction of flexural reinforcement resulted in a more ductile behavior of the specimens and in a higher drift capacity. The high flexural ratio added to one specimen improved the maximum unbalanced moment capacity but also made the slab fail in a more brittle mode. As expected, the specimen with shear headed studs supported the highest drifts and ended up not failing during this experimental campaign, reaching the test setup upper limit.

Keywords

Flat slab, punching shear, reinforced concrete, flexural reinforcement, studs, horizontal cyclic loads

Resumo

A presente dissertação estuda o comportamento de lajes fungiformes submetidas a carga vertical constante e carregamento horizontal cíclico, sendo a continuação de trabalhos realizados anteriormente no Departamento de Engenharia Civil da FCT/UNL. O principal objetivo deste trabalho é estudar a influência da variação da taxa de reforço longitudinal na resposta sísmica de lajes fungiformes. Assim, três modelos de lajes fungiformes com variação da taxa de armadura longitudinal foram fabricados e testados, dois com a mesma taxa de ρ=0,64% e outro com ρ=1,34%. Um dos modelos com baixa taxa de armadura longitudinal foi reforçado com reforço específico ao punçoamento. Todas as lajes possuíam as mesmas dimensões de 4,15 × 1,85 × 0,15 m^3 e razão entre a carga vertical e a resistência ao punçoamento aproximadamente igual a 55%.

Para uma análise mais completa, os resultados obtidos foram comparados com outros dois modelos testados anteriormente na FCT/UNL. Estas duas lajes possuíam uma taxa intermédia de reforço longitudinal (ρ=0,96%), uma sem armadura específica de punçoamento e a outra contendo "*shear studs*".

Os resultados mostraram que a redução da taxa de armadura longitudinal resultou num comportamento mais dúctil das lajes e numa capacidade maior de deslocamentos horizontais. A utilização da taxa mais elevada de armadura longitudinal laje melhorou a capacidade máxima de momentos não balanceados, mas também fez com que a estrutura tivesse uma rotura mais frágil. Como esperado, o modelo com "*studs"* suportou os maiores "*drifts"* e acabou não rompendo durante o ensaio, devido a ter sido atingido o limite do sistema de ensaio.

Palavras-chave

Laje fungiforme, punçoamento, betão armado, armadura longitudinal, studs, cargas horizontais cíclicas

Contents

List of figures

List of tables

Notations

Latin lower case letters

b_0	control perimeter for punching shear
d	effective depth of the slab
d_g	diameter of aggregate
e	load eccentricity
$f_c; f_{cm}$	average concrete compressive cylinder strength
f_{ck}	concrete characteristic compressive strength
$f_{cm,cube}$	average concrete compressive cube strength
f_{ctm}	average tensile strength of concrete
f_{wyd}	yield stress of shear reinforcement
$f_{wyd,ef}$	effective strength of shear reinforcement
f_{yt}	shear reinforcement yield stress
k	factor that takes size effect into account
k_{dg}	parameter regarding the aggregate diameter
k_e	coefficient considering loading eccentricity
k_ψ	parameter depending on the rotation of the slab
m_{Rd}	design resisting bending moment per unit length
m_{sd}	design acting bending moment per unit length
r_s	position of the span length for zero bending moment
s	radial spacing between shear reinforcement perimeters
s_t	tangential spacing between two shear reinforcement perimeters
u_1	control perimeter

v_{min}	minimum punching shear resistance
$v_{Rd,c}$	punching shear resistance for concrete without shear reinforcement
$v_{Rd,cs}$	punching shear resistance for concrete and shear reinforcement
$v_{perp,d,max}$	maximum value of projection of the shear force perpendicular to a basic control perimeter

Latin upper case letters

A_{sw}	punching shear reinforcement area in one perimeter
A_v	effective area in one row of shear reinforcement
E	is the area under force-displacement curve
E_d	dissipated energy
E_s	elastic strain energy
F	force
K_{eff}	effective stiffness
M_{ed}	design unbalanced moment
P_{max}	maximum horizontal force
V_c	concrete nominal shear resistance
V_{Ed}	design acting shear force
V_{Rd}	design shear resistance of both concrete and shear reinforcement
$V_{Rd,c}$	design shear resistance of concrete
$V_{Rd,s}$	design shear resistance for concrete with shear reinforcement
V_s	shear resistance provided by shear reinforcement
W_1	factor related to the shear stress distribution along the basic control perimeter

Greek letters

α	the angle between shear reinforcement and slab
α_s	factor that taking into account the position of the column
β	is the ratio of sides of the column
γ_c	safety factor for concrete
Δ	horizontal displacement
Δ_{Pmax}	maximum horizontal displacement
Δ_r	residual horizontal displacement
Δ_y	yield displacement
ø	diameter of reinforcing bars
λ	parameter regarding concrete properties
λ_s	size effect modification factor
ξ_{eq}	equivalent viscous damping coefficient
$\rho;\rho_L$	flexural reinforcement ratio
σ_{sw}	maximum stress mobilized in the shear reinforcement
ψ	rotation of the slab

Chapter 1

1 Introduction

1.1 Background

Over the years, engineers and researchers worked to develop more efficient technologies and structural systems that also fulfill the constant search for innovation. With civil engineering being everywhere and therefore being a big part of the daily life, many innovative building systems were created making possible diverse styles of edifices.

In the midst of these developed systems, flat slabs (Figure 1) were discovered to be an interesting solution for new buildings. Among the advantages of this system we can emphasize the architectural freedom due to the absence of beams, a much faster construction time than other common structures due to the simple formwork used in flat slabs and it also facilitates the installation of complementary systems (electric, hydraulic, etc.).

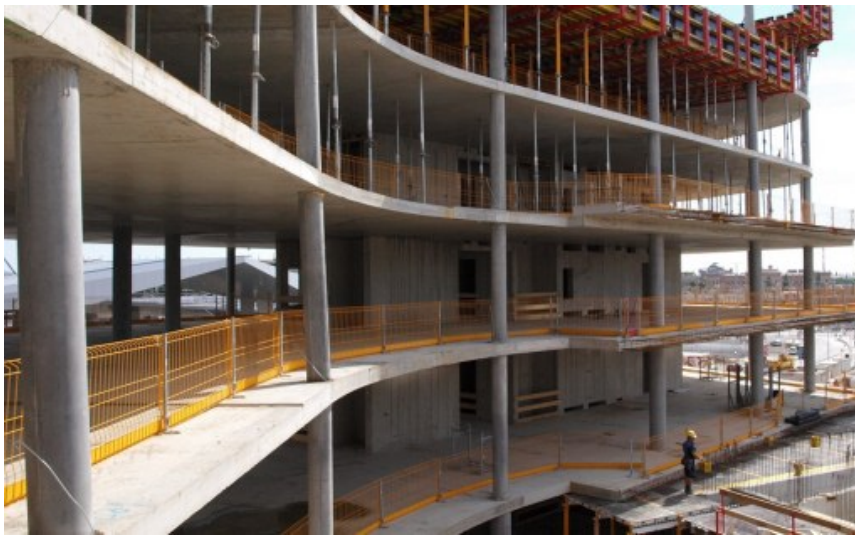

Figure 1 – Flat slab structure (Newswise, 2016)

The rigidity of this system when compared to usual slab-beam-column structures is considerably smaller, specially under combined vertical and horizontal loads. The fact that there

are no beams connecting the column to the slab makes the only possible path for the load to be the direct transfer from the slab to the column. This results in the main disadvantage encountered in this system, the critical connection between the slab and the column. The concentrated load developed in this connection can lead to what is called a punching shear failure, which can cause a progressive collapse of an entire building. This rupture is characterized by the formation of a crack in a conical shape around the column which, when there is shear reinforcement, can be localized between the column and the reinforcement, in the midst of the reinforcement or outside the reinforcement zone.

It is important to emphasize that the removal of beams also makes the structure less rigid and therefore can result in high transversal displacements of the slabs and severe damage when subjected to horizontal forces (earthquakes) unless shear walls or other type of bracing system are used. When this system started to be used not much was known about how it responded to these loads thus, many buildings have collapsed, partially or totally, by punching shear failure. Many even before the construction being totally finished, for example the Harbor Cay Condominium (Figure 2) in Florida, USA, that collapsed during the construction of the fifth floor after not following standards for punching shear reinforcement (Erdogan, 2010). After an earthquake in Christchurch, New Zealand, a three-floor office building partially collapsed, Figure 3 shows the parking lot located in the third floor. It is possible to see in the picture the common punching failure around the columns and how the concrete floor collapsed onto the floor below.

Figure 2 - Collapse of Harbor Cay Condominium in 1981 (Erdogan, 2010)

Figure 3 - Collapse of a building in New Zealand in 2011 (Swanson, 2011)

With the increase of flat slab buildings and also the structural problems that followed it, many studies started being developed for a better understanding of the slab-column connection behavior and in order to develop reinforcement systems that improve the response of these connections to both vertical and horizontal loads. The most common studied shear reinforcements are the increase of the thickness of the slab near the column and the installation of shear headed studs or steel stirrups. The response of these flat slab-column connections to horizontal loads is still not fully understood, reason why there are many studies currently in development for this type of situation. Different test setups combining vertical and horizontal loads have been designed in order to recreate inside a laboratory a situation as similar as possible to a real life structure under seismic action but there are still a lot more improvements to be accomplished.

1.2 Objectives

This dissertation was developed following other studies developed at DEC/FCT/UNL dedicated to punching shear capacity of flat slabs: Almeida et al. (2016), Gouveia et al. (2018), Almeida et al. (2018) and Isufi et al. (2019). Thusly, the specimens developed for this experiment have the same overall dimensions and were tested using the same test setup as the

other studies mentioned. In this case, instead of focusing mainly on the punching shear reinforcement, the main varying factor was the flexural reinforcement ratio. It is an addition to the data already obtained in these previous campaigns and therefore, provides results that enable comparisons in order to improve the knowledge regarding the behavior of flat slab-column connections. The main objectives of this work are:

- Elaboration of three reinforced concrete slabs with varying flexural reinforcement and punching shear reinforcement;
- Better understanding of the seismic behavior of a slab-column connection;
- Analyze the influence of varying flexural reinforcement in flat slabs when subjected to constant gravity load and cyclic horizontal loading.

1.3 Organization of the dissertation

This dissertation is divided in six chapters, with this being the first one with the aim of explaining the fundamental reasons for this experimental campaign regarding punching shear reinforcement in flat slabs and the main objectives to be achieved by the author.

The second chapter is composed by a research of what can be found about punching shear in the literature available. The various sections of this chapter refer first to what is punching shear failure and how it happens followed by the description of a few types of shear reinforcement, some still very common nowadays and others found to be not so effective so their use has decreased over the years. Then some experimental campaigns about flat slabs and punching shear reinforcement are detailed. These published works were found to be relevant to the present dissertation due to the study of different parameters that influence the punching shear capacity of flat slabs and the use of different test setups. The chapter is followed by a description of standard regulations (Eurocode 2, 2010; fib Model Code, 2010; ACI 318, 2019) regarding the design of punching shear reinforcement and at last some important parameters when studying flat slabs under horizontal cyclic loading are described.

In the third chapter the experimental campaign conducted for this dissertation is described. First the specimens design is detailed, as well as the building process of the specimens. Then the properties of the materials used in the specimens are described and also

the tests performed in order to obtain the presented data. The chapter continues to describe the assembly and functioning of the test setup and also all the instrumentation used for this dissertation. At last, it is explained the test protocol followed during this experimental campaign.

Chapter number four begins with the visual observations made for every specimen during the test of each specimen. All the test data obtained with the installed instrumentation regarding forces, displacements and strains are assembled to enable a complete analysis of the results. All aspects were analyzed separately for each tested slab and comparisons were also made among specimens when applicable.

The fifth chapter contains comparisons of the test results here presented with two specimens from previous experimental campaigns also conducted at DEC/FCT/UNL, one with no shear reinforcement and the other with headed studs. The two specimens chosen for comparison had a median longitudinal reinforcement (ρ=0,96%) when compared to the specimens tested in this dissertation and therefore allowed a more complete analysis of the influence of varying flexural reinforcement ratio. The analysis is divided into non-shear reinforced and shear reinforced specimens and parameters such as strength, vertical displacements and lateral stiffness were analyzed.

The sixth and last chapter contains the conclusions obtained from the dissertation presented in this document and some recommendations for future works.

Chapter 2

2 State of the art

2.1 Flat slabs and punching shear failure

Punching shear is a type of failure that can occur to any structural element where there are high forces acting in a concentrated area, for example in flat slabs, bridge decks and foundation systems. In flat slabs, punching shear failure happens due to the non-existence of beams to transfer the loads from the slab to the column. This direct transfer of loads results in a concentrated shear force around the slab-column connection which, if not properly designed and detailed, can suffer punching shear failure (Figure 4). This type of failure is brittle and with the rupture of one slab-column connection the load supported by the surrounding columns increases and it can result in the collapse of the entire structure.

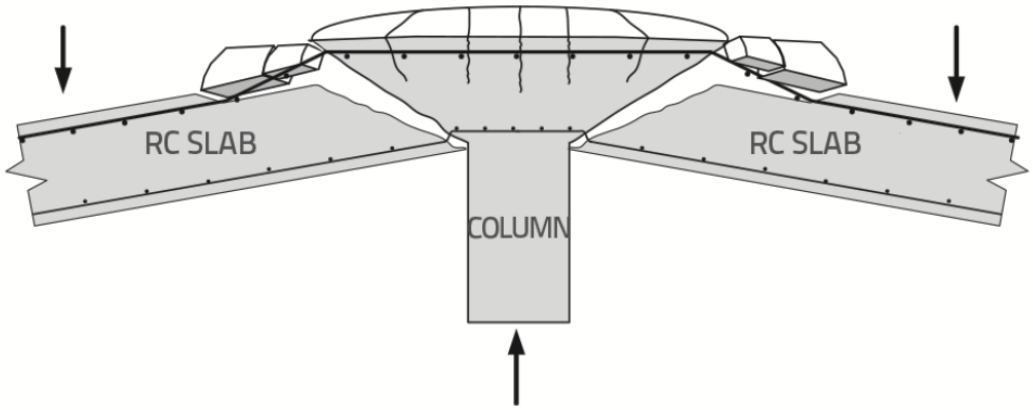

Figure 4 - Punching shear of the slab-column connection (Bartolac et al., 2015)

It is known that many factors influence the punching shear resistance, for example:

- Concrete strength;
- Slab thickness and slenderness;
- Flexural reinforcement ratio;
- Column dimensions;

- Openings in the slab;
- Shear reinforcement.

According to Ruiz and Muttoni (2009) and Ferreira (2010) punching shear failure in flat slabs can occur in three different ways in the presence of shear reinforcement. A brittle failure can occur between the first row of reinforcement and the column, as shown in Figure 5a, by crushing of the concrete on the compressive area. Rupture can also happen through the shear reinforcement, with a diagonal crack beginning at the column and crossing part of the reinforced zone (Figure 5b). At last, failure can propagate to outside the reinforced area, as seen in Figure 5c, resulting in a more brittle and sudden failure when compared to failure through shear reinforcement.

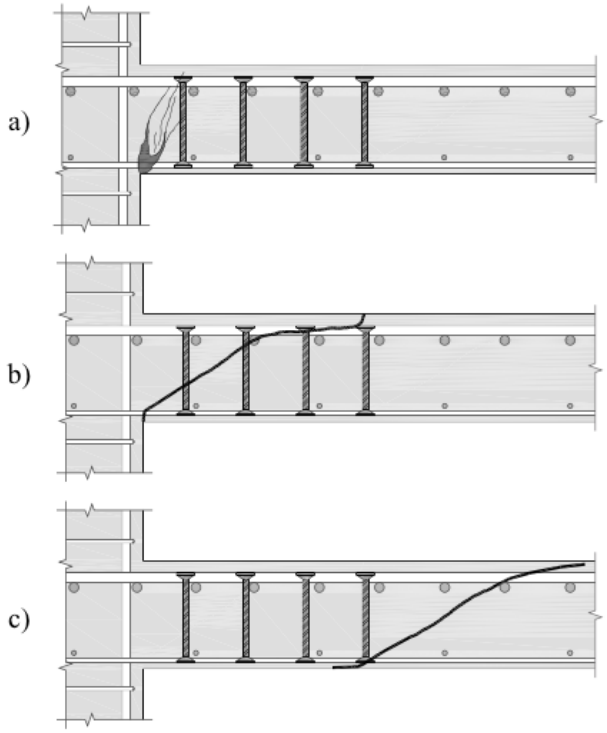

Figure 5 - Punching shear failure modes (Ferreira, 2010)

Codes such as Eurocode 2 (2010), fib Model Code (2010) and ACI 318-19 (2019) have been developed over the years to set a standard and grant safety to the structures when flat slabs are utilized, allowing verifications to analyze if shear reinforcement is necessary and defining design requirements. It is true though that these standards still do not completely specify the

design for flat slabs under seismic actions, at least not when they are part of the lateral load resisting system. This results of the fact that the response of this connection under cyclic loading is yet to be better understood and therefore arises a need for more in-depth studies dedicated to this matter.

2.2 Shear reinforcement systems

Following the growth of flat slabs applications many shear reinforcement systems were developed and improved over the years, therefore this chapter discusses a few important systems that were or still are commonly used in modern constructions. One of the first methods used to improve shear resistance was the increase of the thickness of the slab around the column, being a possible solution also to existing slabs that needed strengthening due to the increase of loads or if it was not initially correctly designed. Other methods to increase the shear resistance of the structure without directly adding shear reinforcement is by increasing the column dimensions or using high strength concrete for the critical zone around the column.

In the past few years several experiments have been developed trying to improve shear reinforcement so there is little or none architectural interference, which is one of the most important reasons why flat slabs are used nowadays.

2.2.1 Bent-up bars

One of the first punching shear reinforcement systems was bent-up bars crossing the column (Figure 6). The main advantage of this system is that the bars work at the same time as flexural reinforcement and as punching shear reinforcement but, since new systems with easier execution and more efficiency were developed, this type of reinforcement is not much used nowadays. Therefore, there are few recent studies focusing on bent-up bars as shear reinforcement, most of them were conducted before 1980.

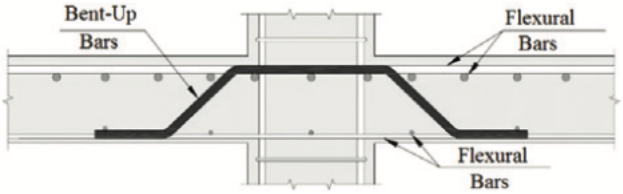

Figure 6 - Bent-up bars (De Oliveira *et al*., 2013)

Unlike other shear reinforcements, the bent-up bar can cross the column (Figure 6) and therefore help prevent progressive collapse of the structure. This was demonstrated in the experimental campaign conducted by Roberson and Johnson (2006), in which bent-up bars passed through the column as top reinforcement but were anchored to the slab as bottom reinforcement.

2.2.2 Stirrups

Stirrups connect the top and bottom longitudinal reinforcement and are one of the most used types of shear reinforcement. As shown below, the disposition of this type of reinforcement can be closed (Figure 7a), open (Figure 7b), continuous (Figure 7c) or inclined (Figure 7d) stirrups. Independently of which stirrups arrangement is applied to the structure it is essential that the corner of each stirrup is connected to a flexural rebar to ensure the full functioning of the reinforcement system.

The use of some types of stirrups is not too common due to some impairments for example, it is difficult to guarantee that open stirrups are properly anchored and the placement of inclined stirrups is not very simple, making it rarely applied. Closed and opened steel stirrups are most common among the applications of this reinforcement system because it is easier to avoid influence on the flexural reinforcement for these two cases.

Several experimental campaigns with the use of steel stirrups on flat slabs have been developed over the years, in most of them specimens were only tested under vertical loading. For example, studies published in Schmidt et al. (2020) and Mabrouk et al. (2017) showed that the application of closed stirrups on flat slabs under increasing gravity load does in fact increase the maximum load capacity of the structure and also improves the ductility of the specimens.

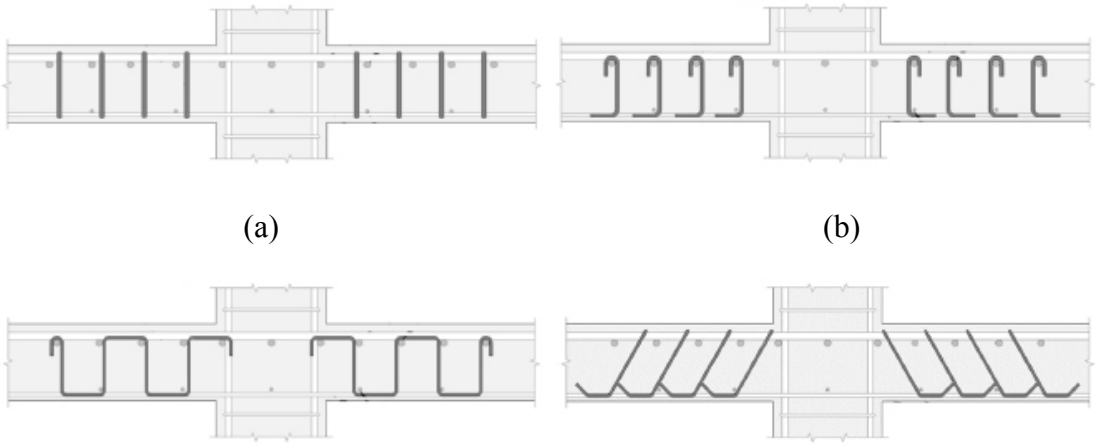

(a) (b)

(c) (d)

Figure 7 - Stirrups (Ferreira, et al., 2016)

Regarding experimental campaigns with flat slabs reinforced with stirrups under both vertical and horizontal cyclic loading, results published in Almeida et al. (2018) showed that the use of this type of shear reinforcement improves not only the drift capacity of the slab but also the ductility and energy dissipation of the structure.

2.2.3 Shearheads

Shearheads are steel profiles embedded in the slab inside or around the connection with the column. The most common types of shearheads are U or C shaped (Figure 8a), which usually go around the column and I shaped (Figure 8b), going through the column. This type of shear reinforcement can improve the slab-column resistance and ductility but can also considerably elevate the costs of the construction.

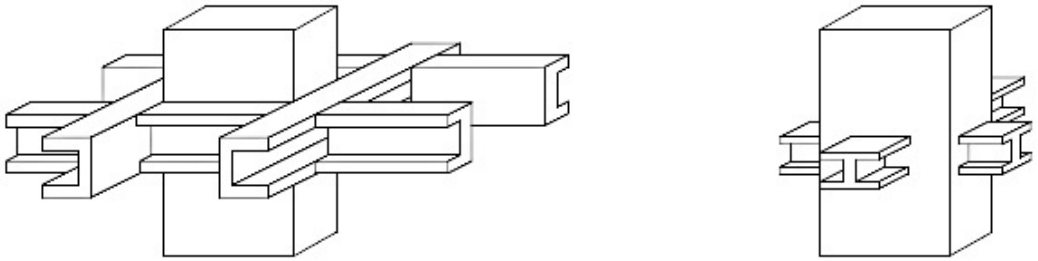

(a) (b)

Figure 8 - Shearheads (Rabello, 2010)

Even though studies focusing on shearheads reinforcement started early with Corley and Hawkins (1968), not many published experimental campaigns with this system can be found in recent literature. Most researches only study the behavior of shearheads as shear reinforcement in flat slabs under vertical load. For example, results published in Badawy et al. (2017) show that by installing I shaped shearheads maximum load capacity is considerably improved but the efficiency of this reinforcement can depend on factors such as shearheads arrangements and cut end angle of the steel profiles.

2.2.4 Headed studs

Headed studs can be used in many structural elements but mostly to improve punching shear resistance in flat slabs. This reinforcement system is known for its easy application and for not interfering with the longitudinal reinforcement bars.

To ensure the correct distance between studs and facilitate the anchorage a thin steel strip is usually used to connect all studs in the same line by welding (Figure 9). The opposite end should also be enlarged, welded or forged separately for each stud, to ensure anchorage on both sides of the steel rebar or rod. Both top and bottom anchorage are essential for the right function of shear headed studs against punching failure.

In recent years there was a growth in the number of experimental campaigns with headed studs in flat slabs, some only for vertical loads (Birkle (2004); Einpaul et al. (2016)) and others combined gravity and horizontal loads (Robertson et al. (2002); Tan and Teng (2005); Isufi et al (2019)). The results obtained in these researches show that the use of headed studs improves the punching shear resistance of flat slabs, resulting in a more ductile structure that can support higher horizontal displacements.

Figure 9 – Headed studs

2.3 Previous studies and experimental campaigns

Over the time many researches have been dedicated to the study of flat slabs and punching shear reinforcement. These studies differ on reinforcement, flexural and shear, and test setups, with naturally more evolved and precise systems in recent years. In this chapter some of these works are briefly explained with an overview of the test setups used and most relevant outcomes.

Experimental campaigns found in literature can be divided into two main categories regarding loading protocols: tests with increasing vertical load or tests with combined vertical and horizontal loads. Due to location, some countries do not have seismic actions as a problem and therefore it is not of interest of some researchers to study the behavior of structures under these actions. Thus, they can develop a simpler test setup that will only apply vertical loads to the specimen.

The different setups found in literature differ on the way vertical and lateral loads are applied to the specimens and also on how they represent boundary conditions at the edge of the slab specimens and columns. There are many ways gravity load could be implemented on test setups, like being applied by hydraulic jacks to load points distributed on the top surface of the slab, when the column is restrained from vertical displacements, or to the top of the column, when the slab is supported on the edges. Lateral displacements are usually applied by a mechanical actuator to the top of the column and, depending on the test protocol, these displacements can be reversed cyclic or monotonic. But there are also test setups that simulate the effects of seismic actions by applying vertical loads acting in opposite directions at opposite borders of the slab. Boundary conditions at the borders of the slab specimens are complicated to be replicated, in many experimental campaigns the borders are free to move or simply supported. Even though these methods are not accurate representations of the real structure, they have been commonly accepted as simplified models and are commonly used (Ramos et al., 2017). The following sub-sections provide more details regarding test setups used in some experimental campaigns.

Most experimental campaigns test only isolated slab-column connections and in a reduced scale because of laboratory space restriction. Recently, with the need of more accurate results, a team of researchers started a project called “SlabSTRESS” (Slab STructural RESponse for Seismic European Design) dedicated to the testing of a real scale flat slab

building under cyclic loading. The building tested in this project had two floors, the first one with no shear reinforcement and on the second floor studs were installed as shear reinforcement. The research is still in development but it is expected to help improve European codes regarding the design of flat slab concrete structures subjected to seismic actions (SlabSTRESS, 2020).

- Hawkins et al. (1974)

Hawkins et al. conducted one of the first experimental campaigns with slab-column connections under cyclic horizontal loads. The authors tested six slab-column connections, four with no shear reinforcement and two with shear reinforcement. Top flexural reinforcement ratio (ρ) varied among the specimens from 0,57% to 1,29%, details are summarized in Table 1. The specimens were subjected to constant vertical load and increasing reversed cyclic displacements. Slabs were rectangular with area of 2,13×3,96m^2, thickness of 152mm and concrete compressive strength was around 30MPa for all specimens. The square cross section of the centered column was 305×305mm^2, with a length of 1,07m above and below the slab.

Table 1 - Specimens tested by Hawkins et al. (1974)

Specimens	ρ (%)	Shear Reinforcement	Failure Mode
S1	1,29	-	Punching
S2	0,90	-	Punching
S3	0,57	-	Punching
S4	1,29	-	Punching
SS1	1,29	ø9,5mm	Crushing of concrete
SS2	0,90	ø6,4mm	Premature punching

The column was pinned on both top and bottom ends, therefore restrained from vertical and horizontal movements but still able to rotate, whereas the slab was free to move. Gravity and lateral loads were applied through two independent jacking systems. Gravity load was applied to the slab through two jacks, each loading a steel beam that was connected to the slab by two steel rods, resulting in four load points symmetrically distributed through the surface of the specimen. Four pairs of push-pull jacks were used for lateral loading, jacks from every pair

were positioned at opposite edges of the slab and acted in opposite directions to simulate seismic action.

The test protocol followed by the authors consisted of first applying the gravity load to the specimen until the target value was reached and keep it constant throughout the entire test. Lateral load was then applied in increasing cycles and for every half cycle the direction of the live load applied at each border was reversed.

All specimens except for SS1 failed in punching. Specimen SS2 had a premature punching failure due to a malfunction of the loading system, where a peak load was applied to the specimen early on the test. With the results obtained, the authors concluded that reversed cyclic loading decreases the stiffness of slab-column connections and that the use of stirrups as shear reinforcement improves the moment transfer capacity of these connections, when designed correctly.

- Pan and Moehle (1993)

An experimental campaign consisting of four flat slab-column connections was conducted by Pan and Moehle (1993). The main objectives of this research were to analyze the effects of lateral loading and the influence of gravity load on lateral behavior. Thus, two of the specimens were tested under uniaxial lateral load and two under biaxial lateral load. Gravity load varied among specimens with same type of lateral load, as shown in Table 2.

Table 2 - Specimens tested by Pan and Moehle (1993)

Specimen	Load	f_c (MPa)	Gravity load (MPa)
1	Uniaxial	33,3	$0{,}12\sqrt{f_c}$
2	Biaxial	33,3	$0{,}12\sqrt{f_c}$
3	Uniaxial	31,4	$0{,}07\sqrt{f_c}$
4	Biaxial	31,4	$0{,}07\sqrt{f_c}$

Specimens were designed at a 60% scale of a flat slab prototype building, resulting is specimens with thickness equal to 122mm and an area of 3,97m^2, assuming the edges of the

specimens were located at the inflection points of the original slab. Centered to all specimens there was a square column with transversal section area 274mm^2 and a height of 1,83m.

Two hydraulic actuators were part of the test setup and connected to the top end of the column, one to apply horizontal loads in the N-S direction and the other in the E-W direction and eight struts with rod-end bearings served as support for the slab edges. Gravity load was applied through lead blocks placed on the top surface of the slab and by the jack installed in the base of the column. A scheme of the test setup used in Pan and Moehle (1993) is displayed in Figure 10.

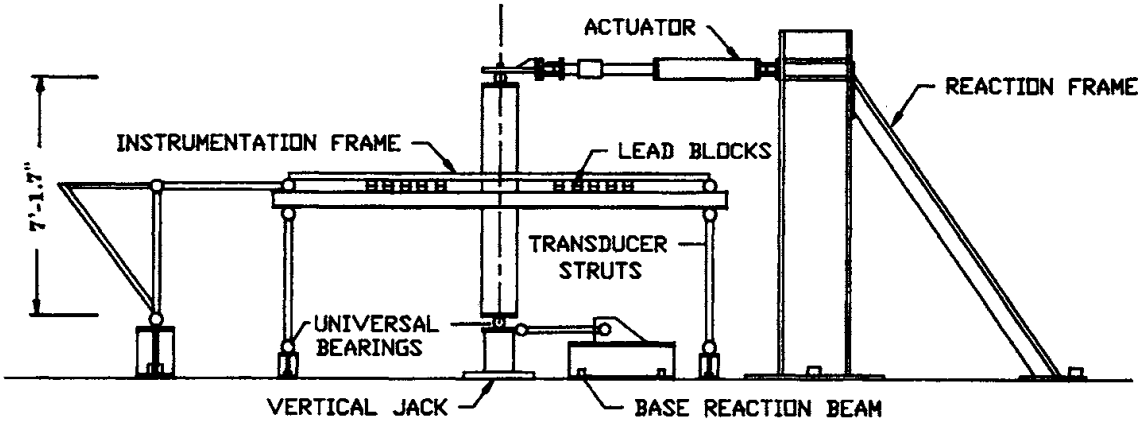

Figure 10 - Test setup used by Pan and Moehle (Pan and Moehle, 1993)

At the beginning of each test, gravity load was applied and kept constant throughout the entire experiment. Lateral loading protocol consisted mainly of applying two complete cycles for a target drift level followed by a complete cycle for half that drift level and then repeating this pattern with higher drifts. For biaxial loading, the displacements were applied first in one direction and held at the target drift while applying the displacement in the orthogonal direction.

All specimens tested by Pan and Moehle (1993) failed in punching shear. The authors concluded that biaxial loading decreased strength, drift capacity, ductility and stiffness of the specimens when compared to the slabs tested under uniaxial load. Pan and Moehle (1993) also noticed that the same parameters were affected by increased gravity loading, showing that it is a critical factor for lateral resistance.

- Emam et al. (1997)

Emam et al. (1997) conducted an experimental campaign with the testing of four interior slab-column connections and tested under vertical and horizontal loads. Two slabs were built with high-strength concrete and two with normal-strength concrete, using two different longitudinal reinforcement ratios. The specimens had overall dimensions of $1900\times1900\times150mm^3$ and centered to the slab's surface there was a square column of area $250\times250mm^2$ and 850mm of length below and above the specimens. Table 3 shows some details regarding the tested slabs in Emam et al. (1997).

Table 3 - Specimens tested in Eman et al. (1997)

Specimen	ρ (%)	f_c (MPa)	Maximum Drift (%)	Maximum Moment (kNm)	Type of failure
HHHC0.5	0,50	75,76	5,2	134,47	Ductile-Flexure
HHHC1.0	1,00	72,32	5,2	162,97	Ductile-Shear
NHHC0.5	0,50	36,76	3,8	100,48	Ductile-Shear
NHHC1.0	1,00	35,37	3,8	127,24	Brittle-Shear

Slabs were simply supported along all four borders and the column was free to move perpendicularly to the slab and were tested under both vertical and horizontal loads. Therefore, three servo-hydraulic actuators were part of the test setup. One was located on top of the column in order to apply the gravity load and two were placed on the side of the column, near the top and bottom tips, to apply the horizontal loads. Figure 11 displays a scheme of the test setup used by Emam et al. (1997). To obtain data from the tests the authors installed load cells, displacement transducers and strain gauges to the test setup and specimens.

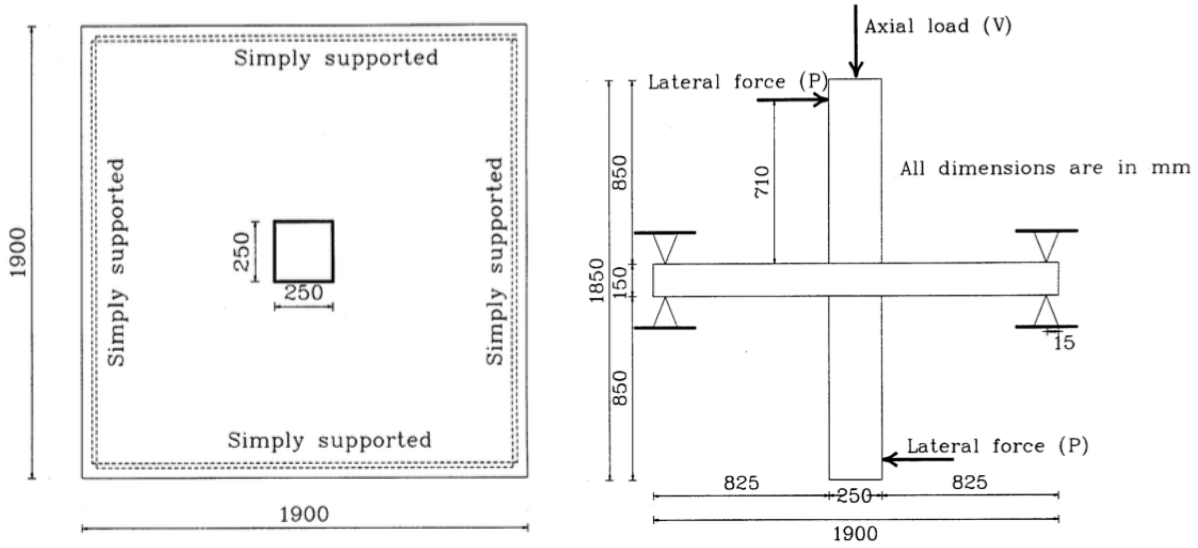

Figure 11 - Test setup used by Emam et al. (Marzouk et al., 2001)

The test protocol followed by Emam et al. (1997) consisted in first applying a portion of the gravity load equal to 125kN, which was kept constant throughout the entire test, and later applying reversed cycles of horizontal loads which were gradually increased until failure of the specimen.

Only specimen HHHC0.5 did not fail in shear, having a ductile-flexural failure and only specimen NHHC1.0 had a brittle failure. It was also noticed by the authors that the drift percentage was not affected by the flexural ratio for specimens with same concrete, but the maximum unbalanced moment was higher for slabs with higher value of ρ.

Finally, Emam et al. (1997) concluded that the use of high-strength concrete can improve the lateral displacement capacity of slab-column connections under seismic loads and the ductility of the structure. The authors also concluded that shear strength and moment capacity of these interior connections were improved in specimens with high-strength concrete.

- Marzouk et al. (2001)

Six flat slabs of 1900×1900mm^2 area and 150mm thickness with a centered column of transversal section 250×250mm^2 were tested during the experimental campaign conducted by Marzouk et al. (2001). The study focused on the seismic response of high-strength lightweight

(HSLW) concrete, therefore two of the six specimens were made of HSLW concrete, two of normal-strength lightweight (NSLW) concrete and two of normal-strength normal aggregate (NSNW) concrete. Between two specimens with same concrete type the longitudinal reinforcement ratio varied form ρ=0,5% to ρ=1,0% and to none of the specimens was added specific punching shear reinforcement. Table 4 displays details about the tested slabs.

Table 4 - Specimens tested by Marzouk et al. (2001)

Specimen	f_c (MPa)	ρ (%)	Maximum unbalanced moment (kNm)	Failure Drift (%)	Failure Mode
HSLW0.5C	70	0,50	135,80	6,2	Flexure
HSLW1.0C	70	1,00	174,00	6,0	Punching Shear
NSLW0.5C	35	0,50	116,20	4,4	Flexure
NSLW1.0C	35	1,00	151,70	5,2	Punching Shear
NSNW0.5C	35	0,50	132,37	-3,8	Flexure
NSNW1.0C	35	1,00	176,40	4,2	Punching Shear

Specimens were subjected to a constant gravity load of 125kN applied at the top of the column and increasing reversed horizontal displacements applied to both top and bottom of the column. Drifts applied to the specimens started at 0,25% until a maximum drift of 7,0% when failure did not occur during lower drifts.

Test setup was the same used in Emam et al. (1997) and represented in Figure 11, with three actuators, one for each load, and the slabs were simply supported at all four borders. During the experimental campaign, first the authors applied gravity load until reaching the target value and then horizontal displacements were applied with gradual increases, as displayed in the graph shown in Figure 12.

From the test results it was noticeable that all specimens with a ρ=0,50% failed in flexure followed by punching of the column whereas specimens with ρ=1,0% experienced a punching shear failure. The authors pointed out the increase of unbalanced moment capacity for specimens with higher reinforcement ratio and how slabs with NSLW concrete presented the lowest values for moment capacity whilst specimens with HSLW and NSNW concrete had similar results regarding unbalanced moment capacity.

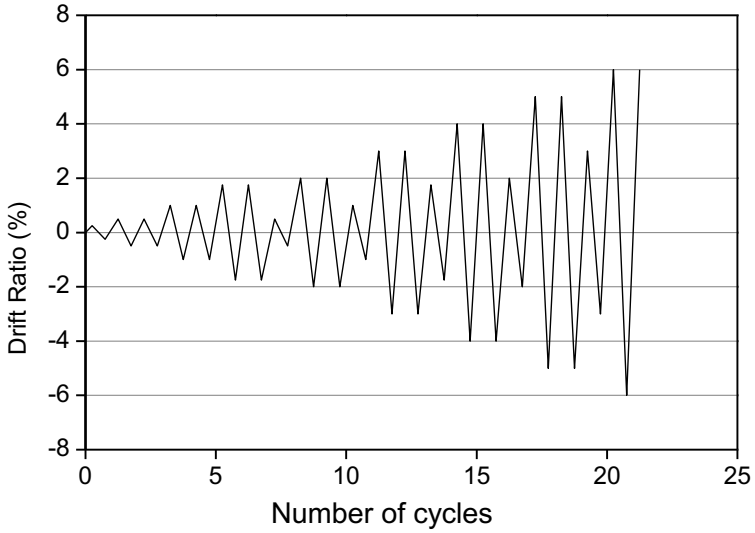

Figure 12 - Drift routine used by Marzouk et al.

The authors concluded that all specimens with a lower flexural reinforcement ratio had a more ductile behavior when compared to those with ρ=1,0%. When comparing specimens with different concrete, HSLW concrete slabs showed a more ductile behavior than the specimens with NSLW and NSNW concrete as it also achieved higher drift ratios and presented a better energy dissipation capacity.

- Robertson et al. (2002)

The study conducted by Robertson et al. (2002) consisted in an experimental campaign with four flat slab-column connections. The focus of the study was to evaluate the behavior of these connections when reinforced by different systems and subjected to seismic load. Three of the specimens were reinforced with specific shear reinforcement, one with closed-hoop stirrups, one with single-leg stirrups and the other with welded-head studs. The fourth specimen was used as reference and therefore no shear reinforcement was added. Details of all four specimens tested in Robertson et al. (2002) can be seen in Table 5.

Table 5 - Specimens tested by Robertson et al. (2002)

Specimen	f_c (MPa)	Shear Reinforcement	Maximum Unbalanced Moment (kN)	Maximum Drift (%)
1C	35,4	-	58,3	3,5
2CS	31,4	Closed stirrups	-68,5	8,0
3SL	43,4	Single-leg stirrups	71,0	8,0
4HS	38,2	Welded-head studs	67,9	8,0

The specimens were designed to represent an interior flat slab-column connection of a prototype building and had overall dimensions of 3000×3000×115mm^3. A centered column of 250mm side and 705mm height above and below the slab surface was connected to the specimens. Bottom of the column was pinned to the laboratory floor and the top was pinned to a servo-hydraulic actuator. In the load direction both edges of the specimens were supported by three pinned-rods, allowing rotation and horizontal moving but restraining movement in the vertical direction. In the borders parallel to the loading direction the edges of the slabs were not restrained.

Concrete weights were suspended from the slab in order to apply the target vertical load and it was kept constant during the entire test. The horizontal load was applied by the hydraulic actuator attached to the top of the column, imposing cyclic reversed displacements until failure of the specimen. Until a 4,5% drift the cyclic displacements were applied in both positive and negative direction, from 5% to 8% drifts displacements were only applied in the positive direction. A full scheme of the test setup used by Robertson et al. (2002) is detailed in Figure 13.

Robertson et al. (2002) concluded that all three shear reinforcement methods improved shear capacity since the only specimen that failed in punching shear was the reference slab, 1C, at a 3,5% drift ratio. The shear reinforced specimens were tested until the test setup limit of an 8% drift ratio and even though they did not fail in punching, it was noticed by the authors that yielding occurred in flexural reinforcement for all slabs but not in the shear reinforcement. It was also concluded by the authors that the use of shear reinforcement improved the ductility of the slab-column connection and the shear strength when subjected to lateral loads.

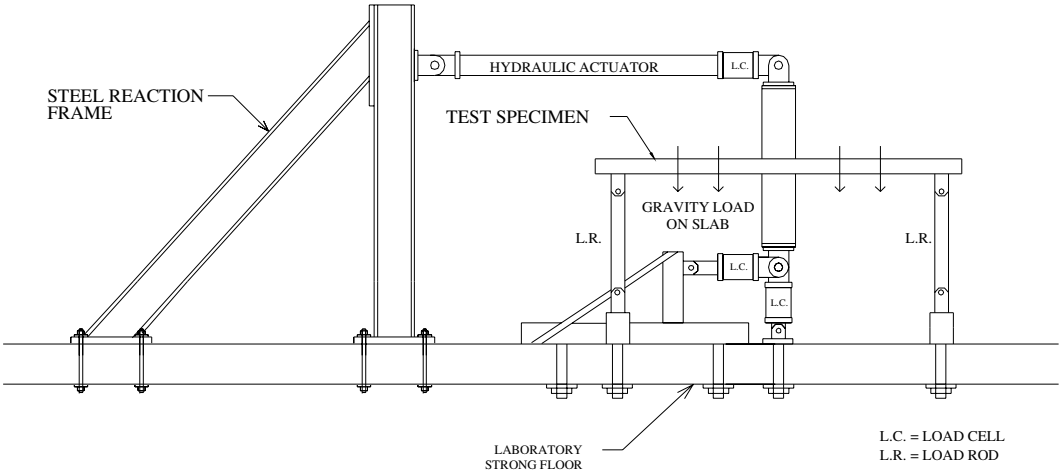

Figure 13 - Test setup used in Robertson and Johnson (Robertson and Johnson, 2006)

- Tan and Teng (2005)

Five interior slab-column connections were tested by Tan and Teng (2005) to study the effect of gravity loading, biaxial loading and the use of studs as shear reinforcement. Specimens were tested under combined vertical and lateral loads, two of the slab-column connections were subjected to uniaxial lateral load and three to biaxial lateral loads. The specimens were designed to represent an interior connection of a flat plate building in a ¾ scale. Thus, specimens' overall dimensions were $4{,}50\times3{,}50\times0{,}15m^3$, with a centered rectangular column of section $0{,}90\times0{,}18m^2$ and total height of 2,25m, and roller supports were placed on the edges of the slabs to simulate the conditions of mid-span of the original structure. Figure 14 shows a scheme of the test setup used in Tan and Teng (2005).

Gravity load was kept constant during the entire experiment and was applied to the slab by placing steel blocks on the top surface of the specimens and also by a hydraulic jack at the bottom of the column. Hydraulic jacks were connected to the top of the column in order to apply lateral displacements. The loading protocol consisted of applying two complete cycles for every drift level until 1,0%. For following drifts, after completing two cycles, one cycle for the previous drift ratio was applied before increasing it again.

Tan and Teng (2005) applied two different levels of gravity shear ratio (GSR) to the specimens, 17% and 28%, as shown in Table 6. To study the effects of studs as specific shear reinforcement, one specimen tested under uniaxial load and one under biaxial load were

reinforced with studs of 150mm height and ø10mm diameter. Studs were placed in a cross distribution around the column, with three rows along the largest side of the column and two along the smaller side. Table 6 presents a summary of all the tested specimens.

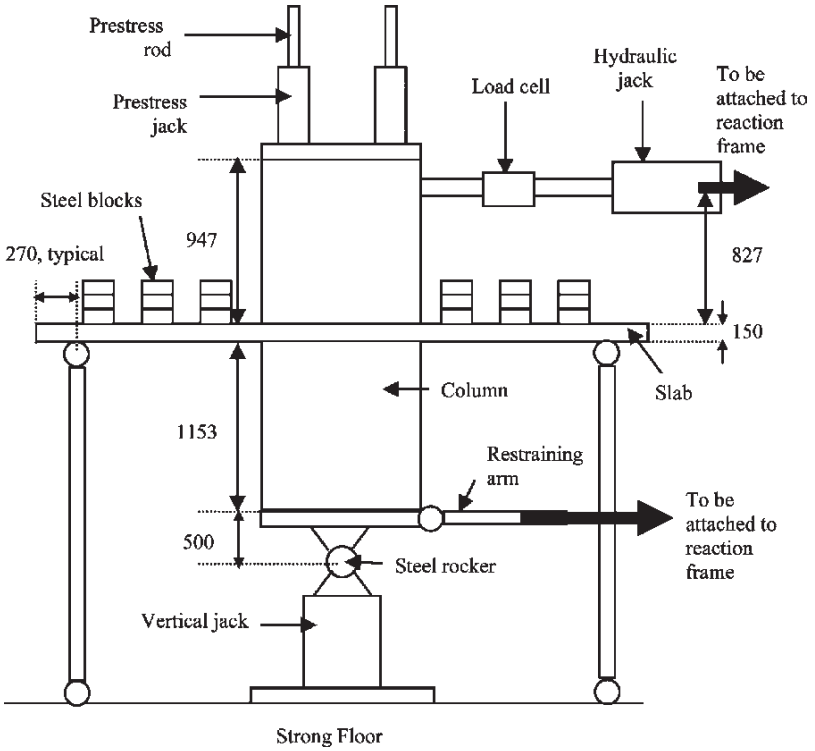

Figure 14 - Test setup used by Tan and Teng (Tan and Teng, 2005)

Table 6 - Specimens tested by Tan and Teng (2005)

Specimen	Lateral Load	GSR (%)	Stud	Ultimate Drift Ratio (%)		Failure Mode
				X	Y	
YL-L1	Uniaxial	17	No	7,32	-	Flexure
YL-H2	Biaxial	28	No	1,96	1,45	Punching Shear
YL-L2	Biaxial	17	No	2,08	2,02	Punching Shear
YL-H2V	Biaxial	28	Yes	4,07	4,29	Flexure-Punching Shear
YL-H1V	Uniaxial	28	Yes	8,14	-	Flexure

All specimens tested under biaxial loading failed in punching shear whereas the two specimens tested under uniaxial load failed in flexure, for higher drifts than the other three slabs. From the results obtained by the authors, it was concluded that biaxial loading decreases

strength, drift capacity, stiffness and ductility of slab-column connections. The increase of GSR was also considered by the authors to have a negative effect on these parameters, but on a smaller scale. However, the installation of studs as shear reinforcement increased the shear resistance of the connection and also drift capacity, ductility and stiffness.

- Robertson and Johnson (2006)

An experimental campaign containing six flat slab-column connections under cyclic horizontal loading was conducted by Robertson and Johnson (2006). The specimens tested by the authors did not have continuity in flexural reinforcement, with the intention of representing designs encountered in older buildings. The design chosen by the authors consisted of top flexural reinforcement not continuous through mid-span and bottom reinforcement not continuous through the column, a common cause of progressive collapse in flat slab structures Thus, the authors decided to add two bottom bars going through the column to prevent the slab from fully collapsing after punching failure. Only one specimen did not have these bars added, ND8BU.

The specimens were tested under constant gravity load and cyclic horizontal displacements and had overall dimensions of 3048×2743mm^2 area and 114mm thickness, with a centered column of section 254×254mm^2. The test setup used in Robertson and Johnson (2006) was the same used in Robertson et al. (2002) and displayed in Figure 13.

Test protocol was divided in two phases, first the horizontal load was applied in both positive and negative drift directions until reaching a 5% drift. After that the displacements were applied only in the positive direction, until a 10% drift ratio. All cycles were repeated three times.

Parameters studied by Robertson and Johnson (2006) were: gravity load, flexural reinforcement ratio (ρ) and bent-up bars in the slab-column connection region. Different parameters explored in each specimen are listed in Table 7 and also gravity shear ratio (GSR) and maximum drift attained before punching shear failure. Concrete compressive strength was around 24MPa for all specimens and ø10mm steel bars were used for flexural reinforcement.

Table 7 - Specimens from Robertson and Johnson (2006)

Specimen	Parameter	GSR (%)	ρ (%)	Maximum Horizontal Load	Maximum drift (%)
ND1C	Control Specimen	25	0,53	-30,9	8
ND4LL	Increased gravity load	37	0,53	-32,4	4
ND5XL	Increased gravity load	48	0,53	-23,7	2
ND6HR	Increased flexural reinforcement	30	0,93	-42,7	5
ND7LR	Decreased flexural reinforcement	36	0,39	-21,8	5
ND8BU	Bent-up bars at slab-column connection	24	0,93	-42,8	5

All specimens failed in punching but slab ND1C failed first in flexure at around 6% drift ratio and punching at 8%. Results obtained during the experimental campaign conducted by Robertson and Johnson (2004) show a decrease of drift capacity when gravity load is increased. Varying the flexural reinforcement did not result in a better drift capacity but the maximum horizontal load capacity followed the flexural variation, increasing when ρ was increased and decreasing with lower ρ. The bent-up bars added to slab ND8BU resulted in a similar reinforcement ratio as ND6HR and therefore similar results but the bent-up bars system served as a mechanism to prevent progressive collapse.

- Drakatos et al. (2016)

An experimental campaign with thirteen flat slab-column connections without specific shear reinforcement was conducted by Drakatos et al. (2016). The focus of the study was to understand the influence of different loads, monotonic and reversed cyclic, in specimens subjected to different gravity load and with variation of flexural reinforcement ratio. Specimens were all the same size, with a 3,0×3,0m^2 area and 0,25m thickness. Slabs overall dimensions were chosen to represent approximately 22% of the span length (L) of the original structure in order to represent the zero moment regions. A centered column with section 390×390mm^2 was connected to all slabs. Top flexural reinforcement ratio varied approximately from ρ=0,75% to ρ=1,50%. Table 8 displays details regarding all thirteen specimens.

Table 8 - Specimens tested by Drakatos et al. (2016)

Specimen	Loading type	ρ (%)	Vertical load (MN)	Maximum Unbalanced Moment (kN)
PD7	Vertical	0,80	0,983	-
PD9	Vertical	1,61	1,040	-
PD1	Vertical + Monotonic	0,79	0,253	525
PD4	Vertical + Monotonic	0,80	0,376	200
PD5	Vertical + Monotonic	0,81	0,517	527
PD3	Vertical + Monotonic	0,81	0,734	462
PD12	Vertical + Monotonic	1,61	0,517	290
PD10	Vertical + Monotonic	1,60	0,734	469
PD8	Vertical + Cyclic	0,81	0,376	196
PD6	Vertical + Cyclic	0,81	0,517	372
PD2	Vertical + Cyclic	0,81	0,734	384
PD13	Vertical + Cyclic	1,61	0,517	286
PD11	Vertical + Cyclic	1,60	0,734	410

The column was secured to the laboratory strong floor and the slab was connected to the column by four threaded bars. Gravity load was applied by four hydraulic jacks, each connected to a steel beam that distributed the load between two load points, therefore eight load points were distributed on the upper surface of the slabs, as shown in Figure 15. Monotonic and cyclic loads to simulate seismic action were imposed by applying two opposite vertical loads at approximately 0,50L of the center of the column in both West and East edges. An actuator was placed on both edges and connected to the slab by steel bridges, as detailed in Figure 15.

Three different types of loading protocols were tested by the authors: symmetrical gravity loads were applied to all specimens but to some specimens the gravity load was combined with monotonic or cyclic loads. In all three protocols the gravity load was applied first, at a speed of 20kN/min, until reaching the target value. For monotonic loaded specimens, one of the actuators located at the East and West borders imposed downward vertical displacements and the other applied a force in the opposite direction until failure. In cyclic loaded specimens the protocol was similar but the two opposite actuators alternated directions of the slab rotation every half drift cycle.

The authors concluded that the increased gravity load decreased the stiffness of the connection and for most cases it also decreased the maximum unbalanced moment. Increasing reinforcement ratio, as expected, increased the stiffness of the specimens but regarding

maximum moments it only significantly influenced specimens with higher ρ value, increasing the obtained moments. It was also concluded by Drakatos et al. (2016) that the application of reversed cyclic loads decreased both moment and deformation capacity of the specimens, in addition to more concrete damage being visibly noticeable.

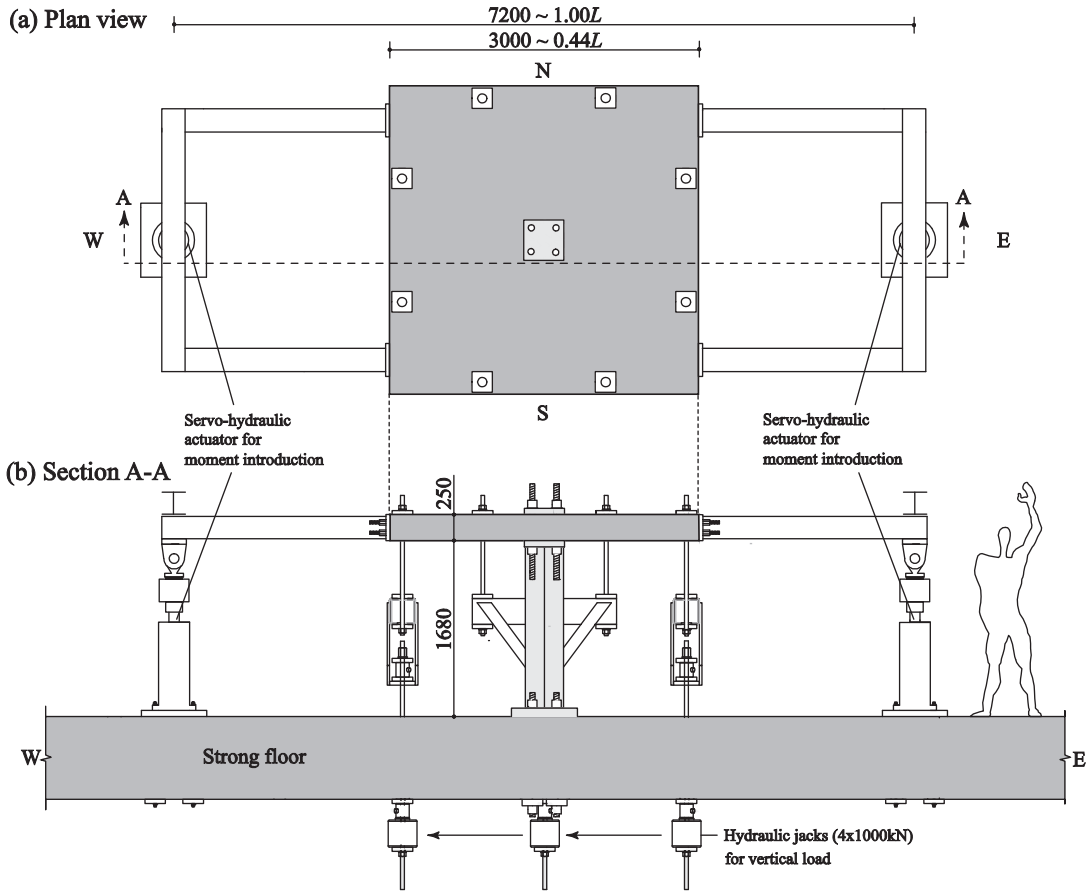

Figure 15 - Test set up used in Drakatos et al. (Drakatos et al., 2016)

- Almeida et al. (2016)

Almeida et al. (2016) developed a research by testing five reinforced concrete slabs one tested under increased vertical load, another under combined gravity and horizontal increased load and the remain three were tested under constant vertical loading and cyclic horizontal displacements. The authors' main objective was to study the influence of shear ratio on flat slabs under vertical load and cyclic horizontal displacements.

The specimens had overall dimensions of 4,15×1,85m^2 in area with a 0,15m thickness and were tested at the Laboratory of Civil Engineering at FCT. The test setup developed and used by Almeida *et al.* (2016) was the same used in this dissertation, therefore it is later explained how the setup works.

The control specimen (MLS) tested by Almeida *et al*. (2016) was tested under centric monotonic loading to help predict the shear capacity of the additional specimens. One specimen, E-50, was subjected to monotonic increased eccentricity and in the last three slabs the authors experimented with varying the gravity load from 30% up to 50% of the shear capacity combined with cyclic horizontal loading. These specimens were named accordingly to the gravity shear ratio applied: C-50, C-40 and C-30. Table 9 displays details from specimens tested by Almeida et al. (2016).

Table 9 - Details of the specimens tested by Almeida et al. (2016)

Specimen	Eccentric Loading	V_g/V_0	V_g (kN)	F_{max} (kN)	Maximum drift (%)	Type of failure
MLS	-	-	323,4*	-	-	Punching
E-50	Monotonic	0,5	212,7	45,8	1,8	Punching
C-50	Cyclic	0,5	203,4	37,4	1,1	Punching
C-40	Cyclic	0,4	167,4	51,4	1,5	Punching
C-30	Cyclic	0,3	131,3	60,8	2	Punching

*Failure load

All five specimens tested by Almeida et al. (2016) suffered a punching shear failure. Results obtained by the authors showed a loss of energy dissipation capacity caused by the cycle repetitions but it was not much affected by the different gravity shear ratio applied to the specimens. Cyclic eccentric loading (C-50) resulted in a more representative loss of stiffness when compared to the specimen under monotonic eccentricity (E-50) and reduced the maximum drift capacity of the slabs. The results obtained also showed that higher horizontal displacements were achieved by specimens submitted to smaller GSR and also bigger horizontal forces were supported by these specimens.

- Isufi et al. (2019)

The research conducted by Isufi et al. (2019) focused on the influence of shear headed studs used as shear reinforcement in flat slabs subjected to seismic actions. The experimental campaign consisted in five concrete reinforced slabs, four reinforced with headed studs in a cruciform layout around the column and one reference specimen (C-Ref) with no shear reinforcement. The slabs dimensions were $4{,}15 \times 1{,}85 m^2$ with 150mm of thickness and connected to centered square steel column. Flexural reinforcement was the same for all five specimens, ρ =0,96%. The four specimens with shear reinforcement differed in number of perimeters of studs around the column, one with three perimeters and the other three with five perimeters but with different gravity shear ratios. The tests were executed in the Laboratory of the Civil Engineering Department at FCT using the same test setup and protocol as the one used in this dissertation, thus it is detailed later on this dissertation.

The specimens were subjected to a constant vertical load throughout the entire test and cyclic horizontal displacements with gradually increased drifts. The imposed gravity loads were chosen in order to achieve a Gravity Shear Ratio (GSR) of around 55% for all specimens except for C-SSR5c, which was nearly 65% GSR. Table 10 displays some details and results of all five specimens tested by the authors.

Table 10 - Detail of specimens tested in Isufi et al. (2019)

Specimen	Perimeters of studs	GSR (%)	Max horizontal force (kN)	Maximum drift (%)	Failure mode
C-Ref	-	54,5	36,0	1,0	Punching
C-SSR3	3	54,7	60,4	4,0	Punching
C-SSR5a	5	54,5	55,2	6,0	Flexure
C-SSR5b	5	53,8	58,9	5,5	Punching
C-SSR5c	5	64,1	47,9	4,0	Punching

The only specimen tested by the author which did not fail in punching was C-SSR5a. All four other specimens suffered a punching shear failure, outside the reinforced area for the shear-reinforced specimens, as a sudden drop of the horizontal load was noticed. The different

vertical load applied to each specimen proved to influence the deflections, even for slabs with similar GSR it was noted that the higher the gravity load the higher were the vertical deflections.

The results obtained by the authors show that the use of studs as specific shear reinforcement improved the drift capacity and also allowed the specimens to support higher horizontal loads. The repeated cyclic horizontal loading caused significant damage at first but a decrease in the rate of stiffness deterioration seemed to happen throughout the tests.

2.4 Standard regulations for punching shear resistance

This chapter briefly summarizes the punching shear resistance standards defined by three design code regulations: Eurocode 2 (NP EN1992-1-1, 2010), ACI 318-19 and Model Code (2010).

2.4.1 Eurocode 2 (2010)

The verification for punching shear resistance by Eurocode 2 (2010) relies on a control perimeter (u_1) distanced 2d from the column (Figure 16). The first step indicated is to calculate the punching shear resistance ($v_{Rd,c}$) for the structure without specific shear reinforcement, using equation (1).

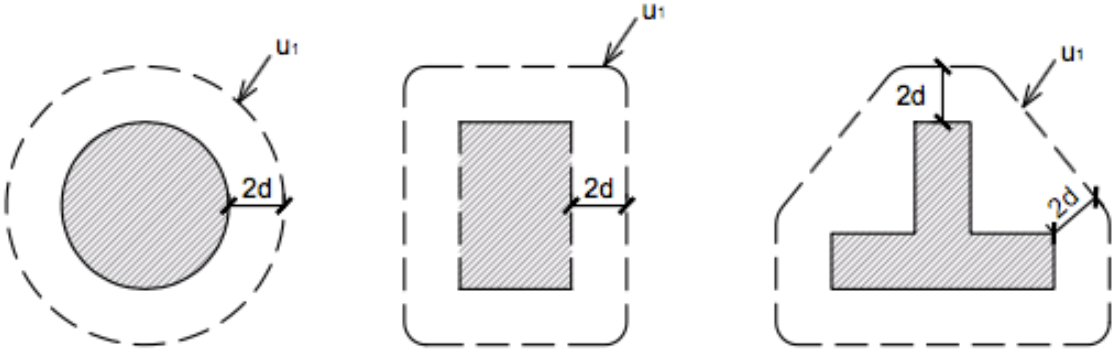

Figure 16 - Control perimeters defined by Eurocode 2 (2010)

$$v_{Rd,c} = C_{Rd,c} k (100 \rho_{\mathrm{L}} f_{ck})^{1/3} \geq v_{min} \quad (1)$$

Where

$C_{Rd,c}$ is given by equation (2) with γ_c being the safety factor for concrete;

k is a factor defined by equation (3);

ρ_L is the flexural reinforcement ratio, obtained by equation (4), where ρ_y and ρ_z are the flexural reinforcement ratio for the directions y and z, respectively;

f_{ck} is the concrete's characteristic compressive strength in MPa;

v_{min} is the minimum shear resistance given by equation (5).

$$C_{Rd,c} = \frac{0{,}18}{\gamma_c} \quad (2)$$

$$k = 1 + \sqrt{200/d} \leq 2 \quad (3)$$

$$\rho_{\mathrm{L}} = \sqrt{\rho_y \rho_z} \leq 0{,}02 \quad (4)$$

$$v_{min} = 0{,}035 k^{3/2} f_{ck}^{1/2} \quad (5)$$

The design shear stress is given by equation (6), with V_{ed} being the acting shear force and β defined by equation (7).

$$v_{Ed} = \frac{\beta V_{ed}}{u_1 d} \quad (6)$$

$$\beta = 1 + k \frac{M_{Ed}}{V_{Ed}} \frac{u_1}{W_1} \quad (7)$$

Where,

k depends on the column geometry, c_1 e c_2, given by table 6-1 from Eurocode 2-1;

M_{ed} is the unbalanced moment in the column;

W_1 is related to the shear stress distribution along the control perimeter u_1 and is defined by equation (8), with dl the control length and e the distance from dl to the moment M_{Ed} action axis.

$$W_1 = \int_0^{u_1} |e| dl \tag{8}$$

If $v_{Ed} > v_{Rd}$, it is necessary to add shear reinforcement. As Eurocode 2 indicates, the concrete resistance ($v_{Rd,c}$) is reduced by 25% and added to the shear reinforcement strength to obtain the final reinforced punching shear resistance ($v_{Rd,cs}$), as shown in equation (9).

$$v_{Rd,cs} = 0{,}75 v_{Rd,c} + 1{,}5 \frac{d}{s_t} A_{sw} f_{wyd,ef} \frac{\sin \alpha}{u_1 d} \tag{9}$$

$$f_{wyd,ef} = 250 + 0{,}25d \leq f_{wyd} \tag{10}$$

Considering,

s_t the radial spacing between two shear reinforcement perimeters;

A_{sw} the punching shear reinforcement area in one perimeter;

$f_{wyd,ef}$ the shear reinforcement's effective stress (equation (10));

α the angle between the shear reinforcement and the slab.

The control perimeter from which shear reinforcement is not needed anymore is given by equation (11) and represented by the dashed line in Figure 17.

$$u_{out} = \frac{\beta V_{ed}}{v_{Rd,c} d} \tag{11}$$

Some distance requirements for punching shear reinforcement arrangements defined in Eurocode 2 (2010) are displayed in Figure 17.

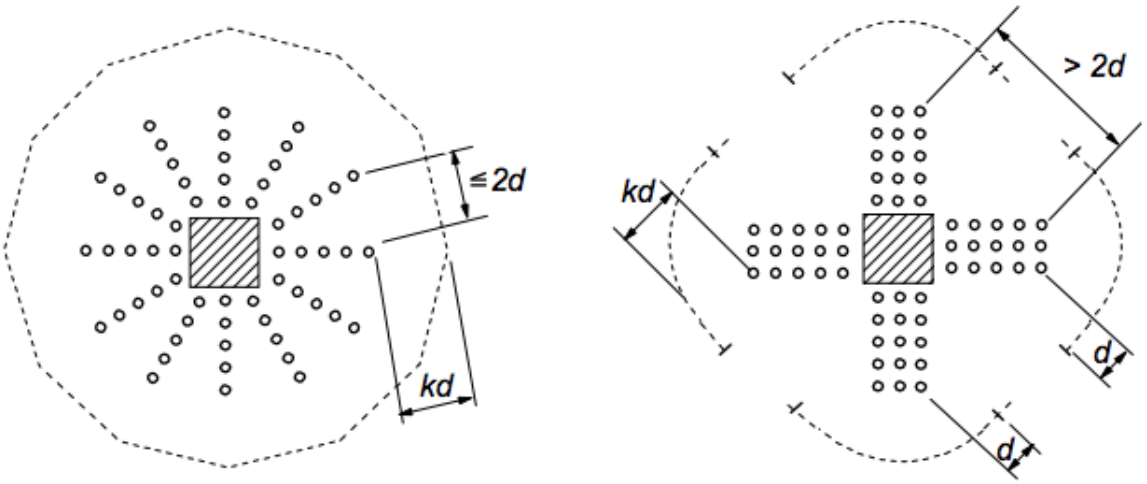

Figure 17 - Control perimeter and shear reinforcement definitions from Eurocode 2 (Eurocode 2, 2010)

2.4.2 fib Model code (2010)

The *fib* Model Code (2010) was developed by the International Federation for Structural Concrete (*fib*) to serve as base for future codes. The approach for punching shear reinforcement is mainly based on the Critical Shear Crack Theory (CSCT), initially studied by Muttoni and Schwartz (1991) and further discussed on Muttoni (2008) and on Ruiz and Muttoni (2009). According to the CSCT, the rotation of the slab (ψ) reduces the shear resistance due to the appearance of a critical shear crack (Figure 18) that spread through the section of the slab into the inclined compression strut carrying the shear force to the column.

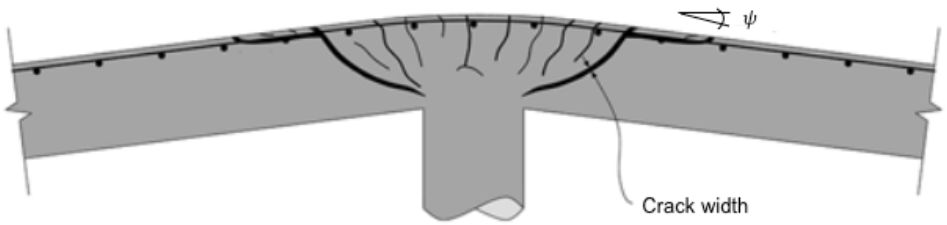

Figure 18 - Critical Shear Crack (Adapted from Muttoni, 2008)

It uses a basic control perimeter (b_0) distanced $0{,}5d_v$ from the column contour, where d_v is the effective depth of the slab. Figure 19 shows b_0 for four types of columns emphasizing that in some cases the perimeter is limited by the edge of the slab.

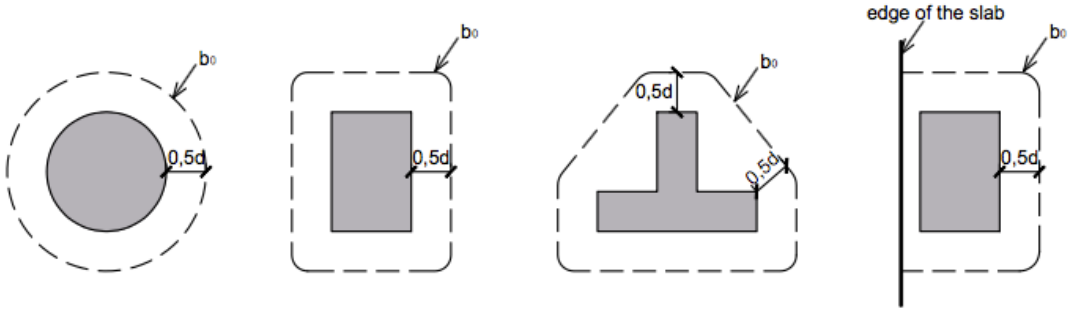

Figure 19 - Basic control perimeter defined by fib Model Code (2010)

The shear resistance (V_{Rd}) suggested by the Model Code (2010) and equation (12) considers both concrete ($V_{Rd,c}$, defined by equation (13) and specific shear reinforcement resistance ($V_{Rd,s}$, obtained by equation (14)). For the concrete resistance calculation, the punching shear-resistance control perimeter b_0 (equation (15)) is used. When $V_{Rd} > V_{Ed}$, punching shear resistance is verified.

$$V_{Rd} = V_{Rd,c} + V_{Rd,s} \tag{12}$$

$$V_{Rd,c} = k_\psi \frac{\sqrt{f_{ck}}}{\gamma_c} b_0 d_v \tag{13}$$

$$V_{Rd,s} = \sum A_{sw} k_e \sigma_{sw} \sin\alpha \tag{14}$$

$$b_0 = \frac{V_{Ed}}{v_{perp,d,max}} \tag{15}$$

Considering

k_ψ a parameter depending on the rotation of the slab and given by equation (16);

k_e coefficient considering the eccentricity of the loading and defined by Table 11 or equation (17) in the case of load eccentricity;

σ_{sw} maximum stress that can be mobilized in the shear reinforcement;

V_{Ed} the acting shear force;

$v_{perp,d,max}$ the maximum value of the projection of the shear force perpendicular to the basic control perimeter.

$$k_\psi = \frac{1}{1{,}5 + 0{,}6\psi d k_{dg}} \leq 0{,}6 \tag{16}$$

Table 11 – Values for coefficient k_e (Model Code, 2010)

Column position	Inner column	Edge column	Corner column
$\boldsymbol{k_e}$	0,9	0,7	0,65

$$k_e = \frac{1}{1 + {}^{e}/_{b}} \tag{17}$$

And also,

k_{dg} is a parameter regarding the aggregate diameter (d_g), defined by equation (18);

e is the load eccentricity (M_{Ed}/V_{Ed});

b is the diameter of a circle with the same surface as the support region;

$$k_{dg} = \frac{48}{16 + d_g} \geq 1{,}15 \tag{18}$$

To calculate the rotation of the slab (ψ), fib Model Code (2010) defines four levels of approximation (LA) numbered from I to IV, with an increase in the accuracy of results for higher levels.

- Level I Approximation: is the simplest of all four levels and does not consider internal forces and bending moment redistributions. An elastic analysis is used to estimate the slab rotation:

$$\psi = 1{,}5\frac{r_s}{d}\frac{f_{yd}}{E_s} \tag{19}$$

  With r_s being the position in the span length where the radial bending moment is equal to zero.

- Level II Approximation considers bending moment redistribution for the calculations, the slab rotation being obtained by equation (20).

$$\psi = 1{,}5\frac{r_s}{d}\frac{f_{yd}}{E_s}\left(\frac{m_{sd}}{m_{Rd}}\right)^{1{,}5} \tag{20}$$

With

m_{sd} the average design acting bending moment per unit length in the support strip;

m_{Rd} the average design resisting moment per unit length in the support strip.

It is essential that the slab rotation is calculated for both directions of the slab, $r_{s,x}$ and $r_{s,y}$, with the highest value being the critical rotation for punching shear resistance.

- Level III Approximation is similar to the equations presented for Level II. The difference relies on the factor 1,5 being reduced to 1,2 due to r_s and m_{sd} being calculated using linear elastic models. Thus, equation (21) is applicable.

$$\psi = 1{,}2\frac{r_s}{d}\frac{f_{yd}}{E_s}\left(\frac{m_{sd}}{m_{Rd}}\right)^{1,5} \quad (21)$$

- Level IV Approximation is the last one therefore provides more precise values of slab rotation based on a nonlinear analysis and taking into account effects such as cracking, tension-stiffening and yielding of the reinforcement.

2.4.3 ACI 318-19 (2019)

The shear strength defined in ACI 318-19 (2019) for a concrete structure with no specific shear reinforcement is given by the smallest concrete resistance contribution (V_c) value obtained in equations (22) to (24). This design code also defines a control perimeter (b_0), distanced at 0,5d from the column contour and it is shown in Figure 20.

$$V_c = 0{,}33\lambda_s\lambda\sqrt{f_c'}b_0 d \tag{22}$$

$$V_c = 0{,}17\left(1+\frac{2}{\beta}\right)\lambda_s\lambda\sqrt{f_c'}b_0 d \tag{23}$$

$$V_c = 0{,}083\left(2+\frac{\alpha_s d}{b_0}\right)\lambda_s\lambda\sqrt{f_c'}b_0 d \tag{24}$$

Where,

λ_s is a size effect modification factor obtained by $\lambda_s = \sqrt{\frac{2}{1+0{,}004d}} \leq 1{,}0$;

λ is a parameter regarding concrete properties, $\lambda = 0{,}75$ for lightweight concrete and $\lambda = 1{,}0$ for normal concrete;

f_c' is the compressive strength of the concrete;

b_0 is the control perimeter, distanced $d/2$ from the contour of the column (Figure 20);

β is the ratio of long to short sides of the column;

α_s is a factor that takes into account the position of the column, values are given in Table 12.

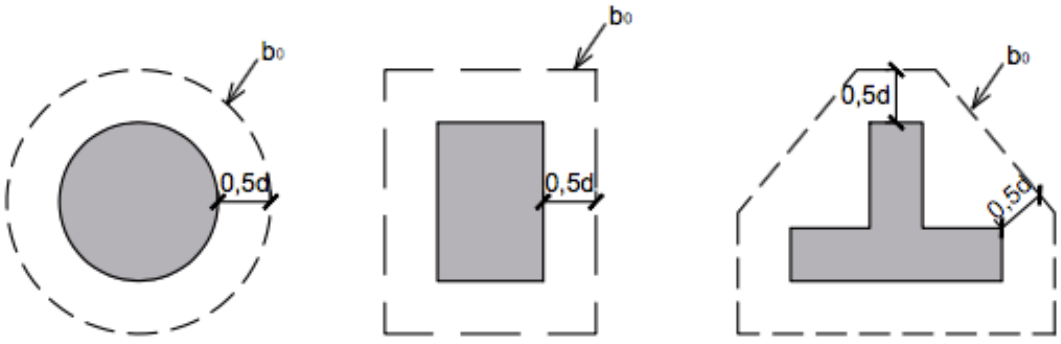

Figure 20 - Control perimeters defined by ACI 318-19

Table 12 - ACI factor values for the column location

Column position	Interior column	Edge column	Corner column
$\boldsymbol{\alpha_s}$	40	30	20

When the shear resistance V_c is not superior to the actions on the structure, it is necessary to add specific punching shear reinforcement. Therefore, the nominal shear resistance is now V_n, obtained by equation (25). The contribution to shear resistance provided by the shear reinforcement (V_s) is given in equation (26).

$$V_n = V_c + V_s \tag{25}$$

$$V_s = \frac{A_v f_{yt} (\sin \alpha + \cos \alpha) d}{s} \tag{26}$$

With,

A_v the effective area of a row of shear reinforcement;

f_{yt} the yield stress of the shear reinforcement;

α the angle between the shear reinforcement and the slab;

s the spacing of the shear reinforcement perimeters, measured parallel to the longitudinal reinforcement.

2.5 Cyclic loading and seismic behavior

Cyclic loads are used in experimental campaigns to understand the behavior of structures under horizontal loads and allow an estimate of the capacity of the structure under a general seismic action. But in reality, seismic actions are not perfect cyclic loads and two earthquakes are never the same because they are composed by dynamic loads with intensity variations during short periods of time.

With the increase of studies and improvement of test setups, some aspects regarding the behavior of flat slab structures under seismic actions have been noticed in most of the studies, for example stiffness deterioration of the structure due to the repetition of horizontal displacements and also the increased damage for higher loads.

In order to estimate the behavior of structures containing flat slabs, three relevant parameters are: Equivalent Viscous Damping, Lateral Stiffness and Residual Deformation Index. These three parameters help to understand the damage that can be caused by such loads and investigate the influence of different variables in the design of structures that might be subjected to seismic actions. Therefore, these three parameters are listed and explained below.

- Equivalent Viscous Damping

The equivalent viscous damping coefficient (ξ_{eq}) is an important parameter to analyze and compare the energy dissipation capacity of the specimens under cyclic loading. The method used for the calculation is presented in Hose and Seible (1999), based on a hysteretic diagram (Figure 21) and relating the energy dissipation capacity and the elastic strain energy of the specimen. The coefficient is calculated separately for the positive and negative parts of the diagram and both are considered to obtain the equivalent viscous damping coefficient, as shown in equation (27).

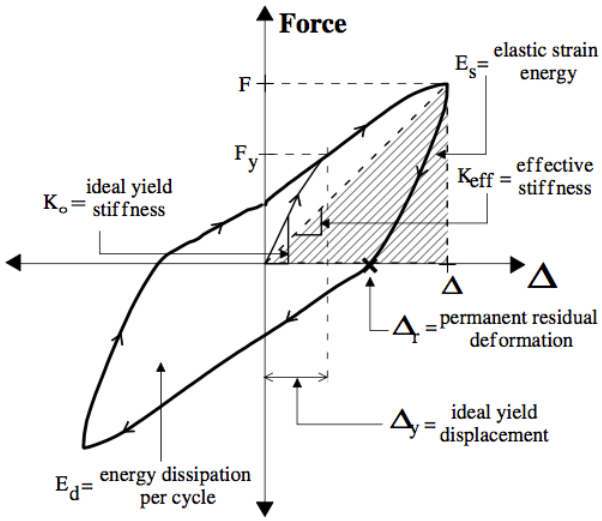

Figure 21 - Equivalent Viscous Damping Ratio and Lateral Stiffness (Hose and Seible, 1999)

$$\xi_{eq} = \frac{1}{4\pi}\left(\frac{E_{d1}}{E_{s1}} + \frac{E_{d2}}{E_{s2}}\right) \quad (27)$$

Where,

E_{d1}: Dissipated energy for positive displacements

E_{s1}: Elastic strain energy for positive displacements

E_{d2}: Dissipated energy for negative displacements

E_{s2}: Elastic strain energy for negative displacements

- Lateral Stiffness

The lateral effective stiffness parameter (K_{eff} in Figure 21) is given by the ratio between the maximum force (F) and the maximum horizontal displacement (Δ), as shown in equation (28).

$$K = \frac{\mathrm{F}}{\Delta} \quad (28)$$

- Residual Deformation Index (RDI)

Another parameter to be considered is the Residual Deformation Index (RDI) commonly studied to quantify the damage on a structure subjected to a seismic action and therefore estimate the reparability of the specimen. Equation (29) shows how the RDI is obtained for structures with symmetric responses during the cyclic displacements, by dividing the permanent residual displacement for each cycle by the ideal yield displacement of the structure (Figure 21). In the case of an asymmetric response negative displacements should also be considered and therefore equation (30) is applied. (Hose and Seible, 1999)

$$RDI = \frac{\Delta_r}{\Delta_y} \tag{29}$$

$$RDI = \frac{1}{2}\left(\frac{\Delta_{r,1}}{\Delta_{y,1}} + \frac{\Delta_{r,2}}{\Delta_{y,2}}\right) \tag{30}$$

Considering,

Δ_r and $\Delta_{r,1}$ the residual displacement for positive cycles;

$\Delta_{r,2}$ the residual displacement for negative cycles;

Δ_y and $\Delta_{y,1}$ the ideal yield displacement for positive displacements;

$\Delta_{y,2}$ the ideal yield displacement for negative displacements;

In order to obtain Δ_y it is necessary to first obtain the envelope curve of the hysteretic diagram and adapt it into a bilinear curve (Figure 22), with same area under both curves. Thus, the ideal yield displacement can be determined by equation (31).

Where Δ_{Pmax} is the maximum horizontal displacement, E is the area under the curve and P_{max} is the maximum horizontal force.

$$\Delta_y = 2\left(\Delta_{Pmax} - \frac{E}{P_{max}}\right) \tag{31}$$

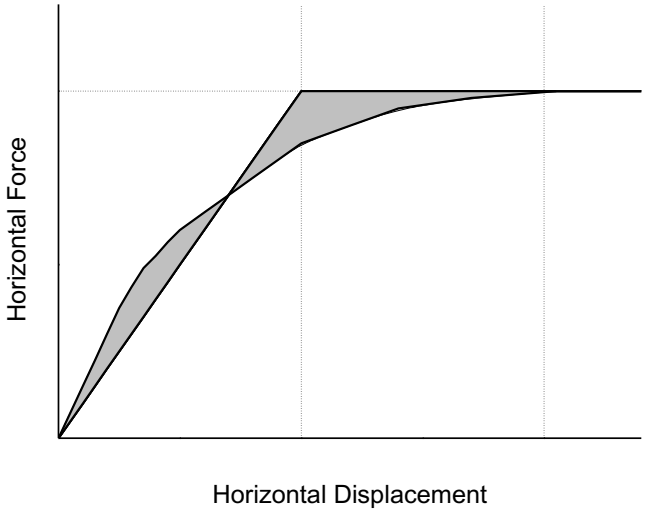

Figure 22 - Elastoplastic curve and bilinear curve

Chapter 3

3 Experimental campaign

The following chapter describes the development of the specimens as well as the characteristics of the materials used. Three reinforced concrete slabs (C-Ref-L, C-SSR5-L and C-Ref-H) with same overall dimensions but longitudinal and shear reinforcement differences among them were tested under cyclic horizontal loading.

The test setup presented below was already installed in the laboratory of the Civil Engineering Department at Universidade NOVA de Lisboa, as it was developed and used in earlier studies. The test setup is detailed below with all the instrumentation that was used in order to obtain the test data analyzed further in this dissertation.

3.1 Description of the specimens

The specimens tested during this experimental campaign were intended to represent an interior flat slab-column connection of an office building and due to restrictions regarding the laboratory area, the specimens size was reduced to 2/3 of the original design. Since the horizontal loads were applied only along North-South axis, the specimens were truncated at approximately mid-span in the longitudinal direction so the positive bending moment at the edge of the specimen corresponds to the maximum value when subjected only to vertical loads. In the East-West direction, envisioning a zero moment region, the slabs were truncated at 22% of the span on each side of the column. Therefore, the three reinforced concrete flat slabs had equal dimensions of an $4{,}15 \times 1{,}85 m^2$ area and 0,15m thickness. All three specimens were connected to a centered steel column of section HEM 120 with a square base plate of $0{,}25 \times 0{,}25 m^2$ and total height of 2,0m. Column is divided in two parts, 1,0m above and 1,0m below the slab, to represent approximately the mid-height of the story.

The first specimen, C-Ref-L, had a top longitudinal reinforcement ratio of ρ=0,64%, with no shear reinforcement. The second slab, C-SSR5-L, presented the same ρ=0,64% but five perimeters of headed studs were installed around the column as specific punching shear

reinforcement. The third and last slab specimen, C-Ref-H, had no shear reinforcement but a higher top longitudinal reinforcement ratio (ρ=1,34%). Punching shear reinforcement could not be added to a specimen with this flexural reinforcement ratio due to the expected high unbalanced moment capacity of such a structure. The test setup used in this experimental campaign was not designed to support forces of this magnitude. These values of flexural reinforcement ratio were chosen to be intentionally lower (C-Ref-L and C-SSR5-L) and higher (C-Ref-H) than the ratios found in specimens tested by Almeida et al. (2016) and Isufi et al. (2019), in order to make comparisons regarding the influence of flexural reinforcement in punching shear resistance.

Flexural reinforcement for specimens C-Ref-L and C-SSR5-L is detailed in Figure 23a. Bottom reinforcement was composed by ø10mm bars spaced at 100mm in both directions and for top reinforcement ø12mm were placed near the column and ø10mm bars outside the column region. Figure 23b displays the longitudinal reinforcement of slab C-Ref-H. For bottom reinforcement bars with ø12mm spaced at 100mm were used in both directions whereas top reinforcement consisted of ø12mm spaced from 60-100mm near the column and ø10mm every 200mm further from the column. Nominal concrete cover was 20mm and longitudinal and transversal cross-sections for all three specimens are displayed in Figures 24-27.

Details of the punching shear reinforcement arrangement added to slab C-SSR5-L are displayed in Figure 28. Dimensions and positioning of shear reinforcement were the same as used in Isufi et al. (2019) to enable valid comparisons. The headed studs were fabricated at the Civil Engineering Laboratory of FCT/UNL and each stud consisted of ø8mm reinforcement steel bars. Five rows of three headed studs were added to each side of the column, thus an area of 6,03 cm^2 of shear reinforcement per perimeter. Every three or five studs were connected to each other by being welded at the top to a rectangular steel bar of 8mm in thickness and 25mm wide to ensure the correct spacing between studs and improve anchorage of the reinforcement. The bottom of each stud was also welded to a 25×25 mm^2 steel bar of thickness 8mm (Figure 29) for better anchorage. A stud rail composed by 3 studs can be seen in Figure 29.

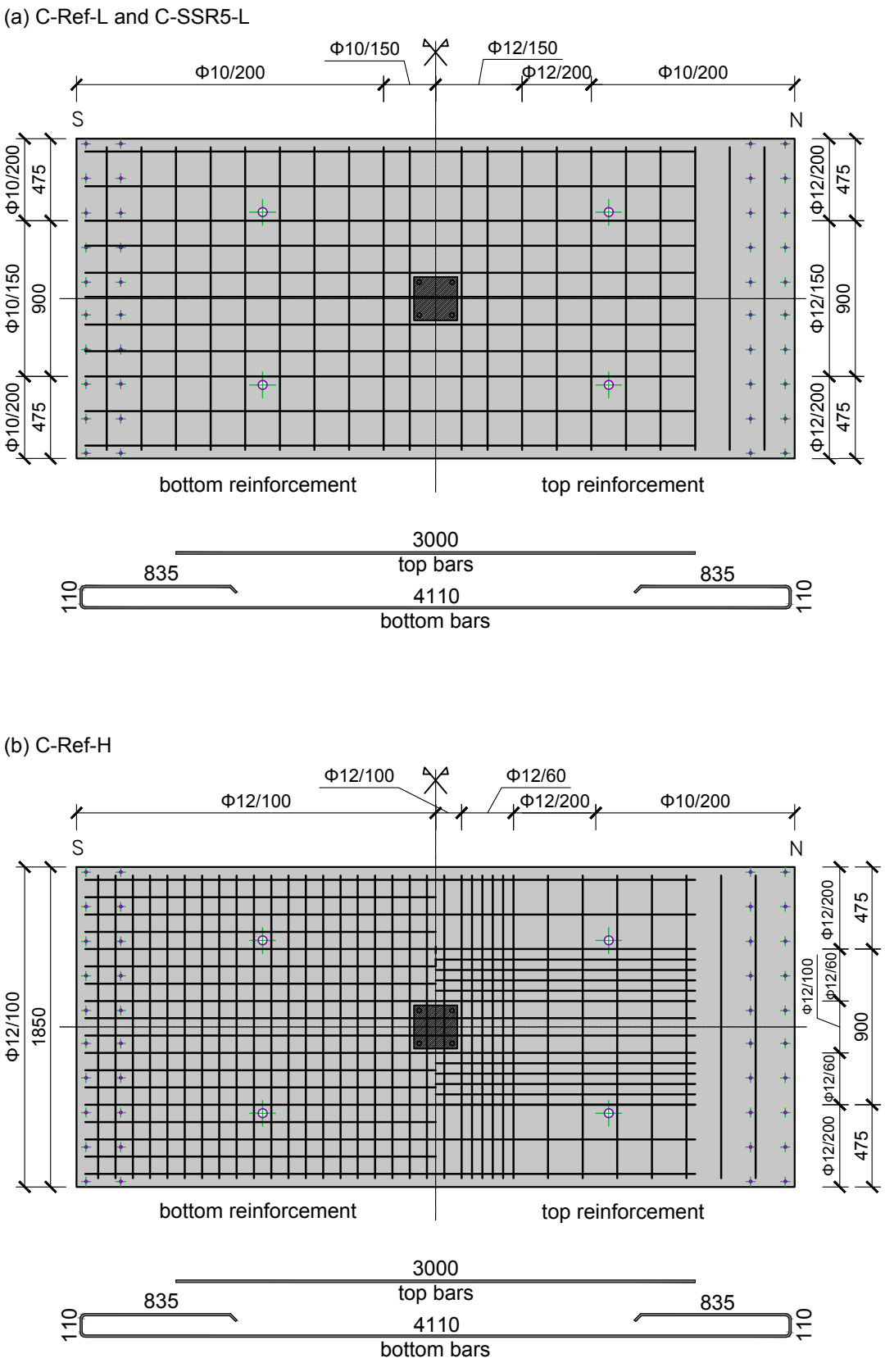

Figure 23 - Detailed longitudinal reinforcement

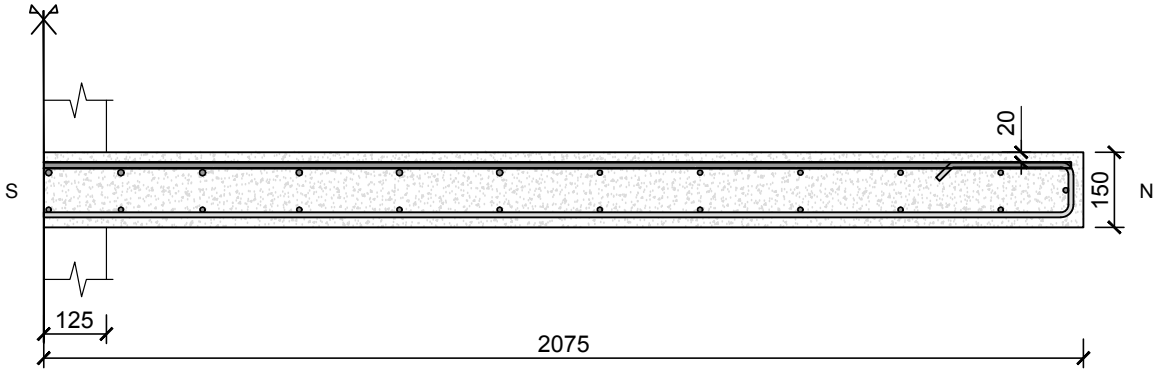

Figure 24 - Longitudinal cross-section of C-Ref-L

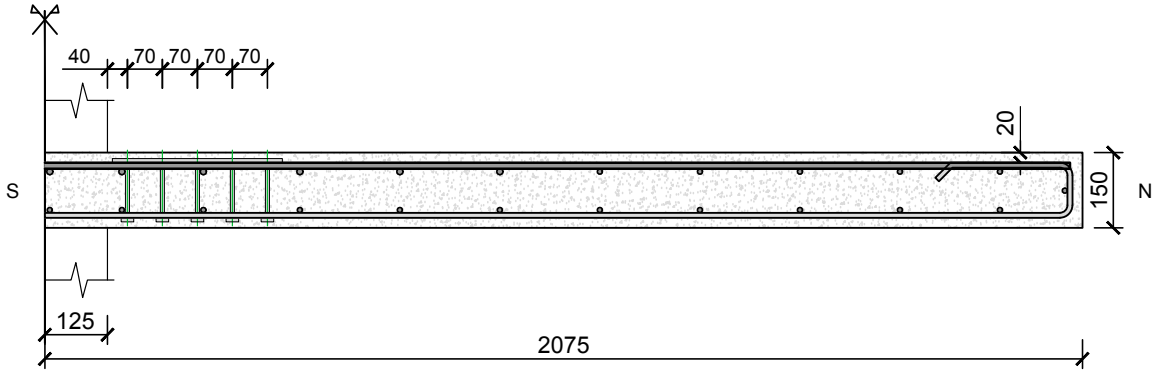

Figure 25 - Longitudinal cross-section of C-SSR5-L

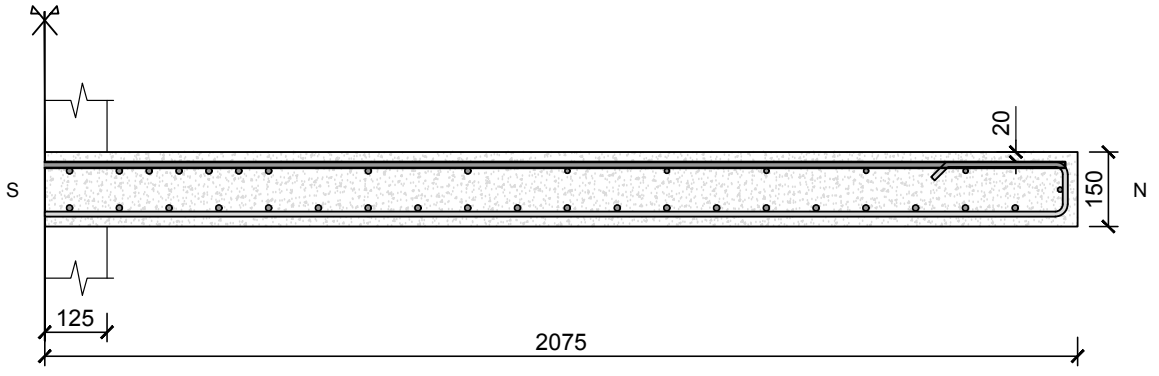

Figure 26 - Longitudinal cross-section of C-Ref-H

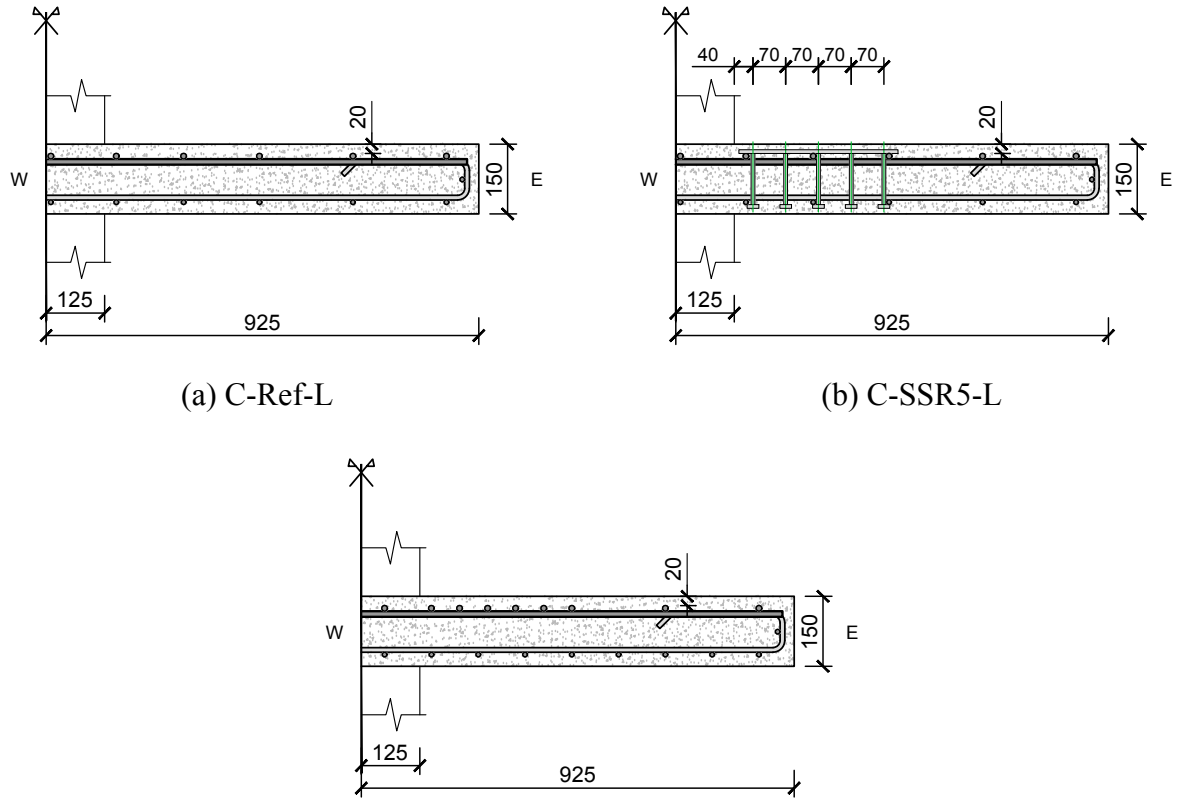

(a) C-Ref-L

(b) C-SSR5-L

(c) C-Ref-H

Figure 27 – Transversal cross section of all three specimens

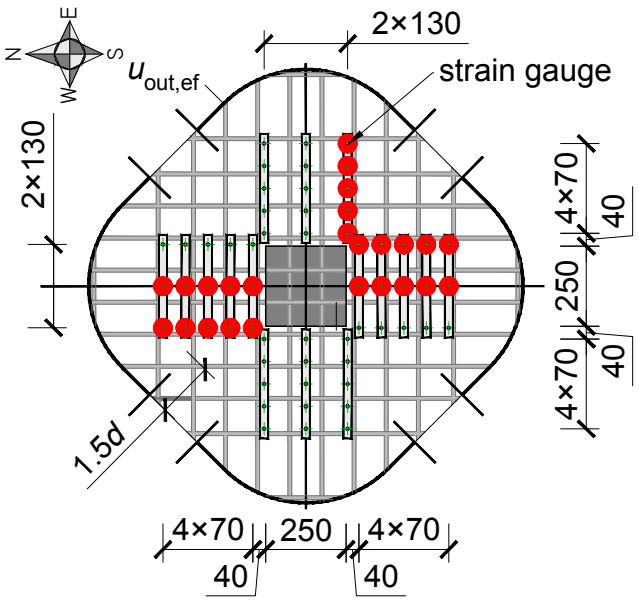

Figure 28 - Punching shear reinforcement – C-SSR5-L

Figure 29 - Studs fabrication

3.2 Development of the specimens

The specimens were built at Concremat and all three were cast in the same mold (Figure 30). Tubes were placed before casting to leave voids for the fastening of the column and the specimen at the test setup, including 20 holes (ø=16mm) on each north and south edges and four in the center of the slab (ø=30mm).

Figure 30 - Molds of the specimens

For specimen C-SSR5-L, after the longitudinal reinforcement was placed, the five perimeters of studs were installed and fixed around the column (Figure 31). Strain gauges were installed and covered with silicon for protection in some reinforcement bars of all three specimens and studs on C-SSR5-L (Figure 28). Some installed strain gauges can be seen in Figure 32.

Figure 31 - Installed studs

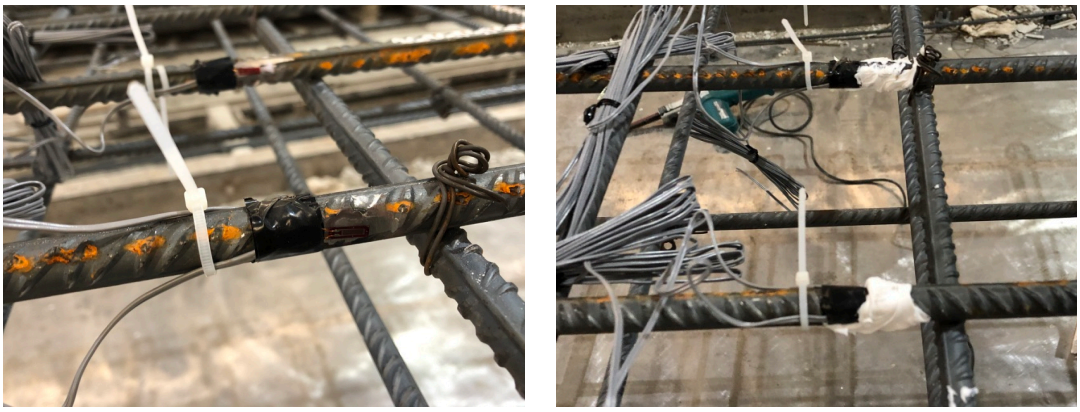

Figure 32 - Strain gauges

In order to test the concrete properties, during the casting of each slab five cubes and ten cylinders were casted (Figure 33).

Figure 33 - Casting of the slabs, cubes and cylinders

3.3 Materials

The concrete used in the specimens was prepared by Concremat and tested partially at the FCT/DEC/UNL Laboratory and at IST, in Lisbon. characteristics of all three slabs are shown in Table 13.

Table 13 - Concrete characteristics

Specimen	f_{cm} (MPa)	$f_{cm,cube}$ (MPa)	f_{ctm} (MPa)	Age (days)
C-Ref-L	31,27	40,12	2,79	49
C-SSR5-L	46,61	53,38	3,37	58
C-Ref-H	41,06	44,41	3,33	75

f_{cm} - average cylinder compressive strength

$f_{cm,cube}$ - average cube compressive strength

f_{ctm} - average tensile strength

The values displayed in Table 13 for both cylinder and cube compressive strength were obtained by the mean value of the results of five samples tested under a compression test (Figures 34 and 35) in accordance with NP EN 12390-3 (2003). The cylinders tested for the compressive strength were mechanically rectified. Five cylinders were subjected to a diametrical compression test to determine the average tensile strength of the material (Figure 36), these tests were carried out in accordance with NP EN 12390-6 (2003).

3.4 Test setup and instrumentation

Over the years many test setups were developed for similar studies proving the complexity of replicating a real structure inside a laboratory, for example due to the reduced space and on how to represent acceptable boundary conditions.

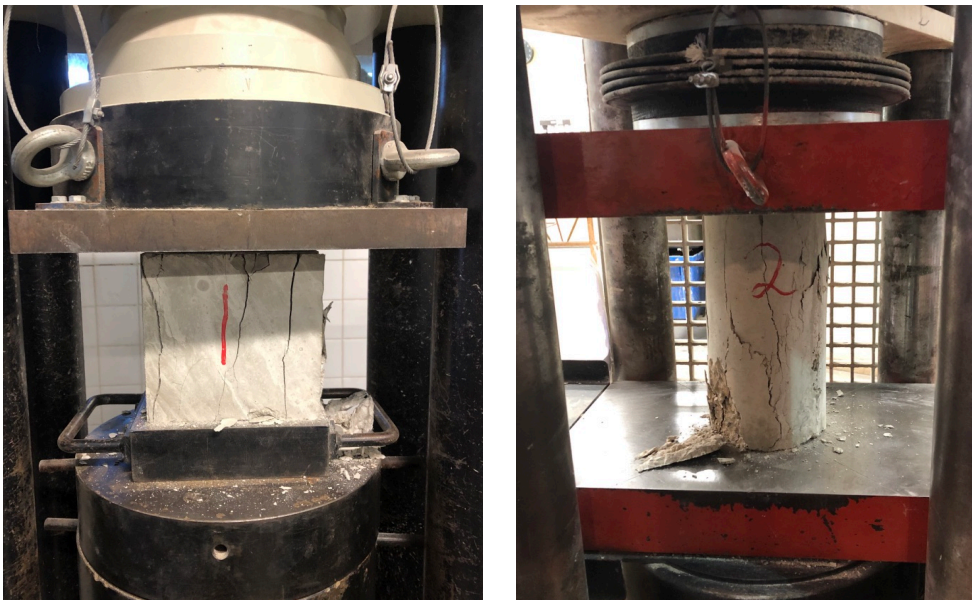

Figure 34 – Cube and Cylinder Compression Test

Figure 35 – Typical Cube and Cylinder after failure

For this experimental campaign the test setup developed at DEC/FCT/UNL was used. The same setup was already used in former experiments regarding flat slabs, such as Almeida et al. (2016) and Isufi et al. (2019). The apparatus is fixed to the laboratory floor and, as explained in Almeida et al. (2016), it was designed to allow equal vertical displacements at the

North and South edges; equal magnitude shear forces, bending moments and rotations at North and South edges; mobility of the inflection point along the N-S direction; high vertical loads. A picture of the test setup used in this project is displayed in Figure 37, different element colors means a different function on the setup.

Figure 36 – Splitting Tensile Test

Figure 37 - Test Setup

The edges' boundary conditions of the test setup were carefully designed to simulate the building continuity. Both North and South borders of the specimen are connected to rigid steel profiles, which are connected to each other by pinned steel struts, allowing equal rotations for the opposite edges. Each strut was equipped with a hydraulic jack and a load cell to adjust the force during the test, monitor the positive bending moments at the edges of the specimen and ensure equal rotations at opposite borders. This system is represented by the green elements in Figure 37 and an elevation of it is shown in Figure 38.

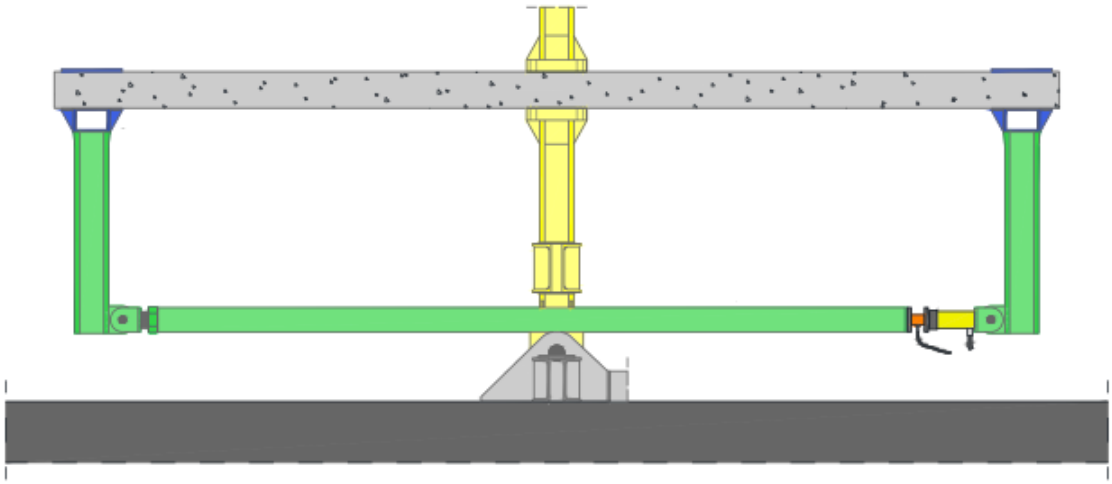

(a) Unloaded specimen

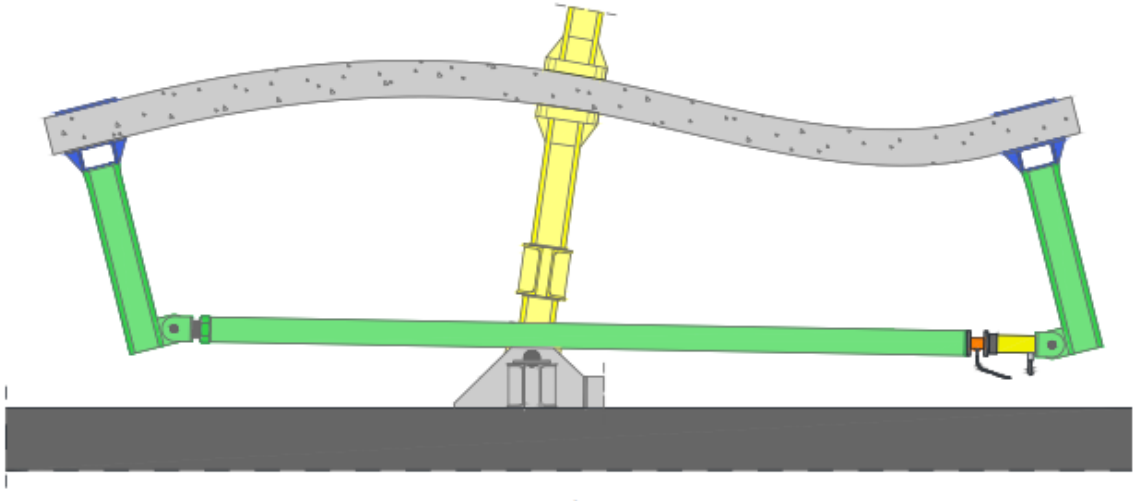

(b) Vertically and horizontally loaded specimen

Figure 38 - Rotation compatibilization system (Almeida et al., 2016)

To ensure equal vertical displacements and shear forces at opposite borders a seesaw system with rigid steel frames connected to the slab by a hinge was installed also in the longitudinal direction. This assembly is composed by the blue elements in Figure 37 and the scheme in Figure 39.

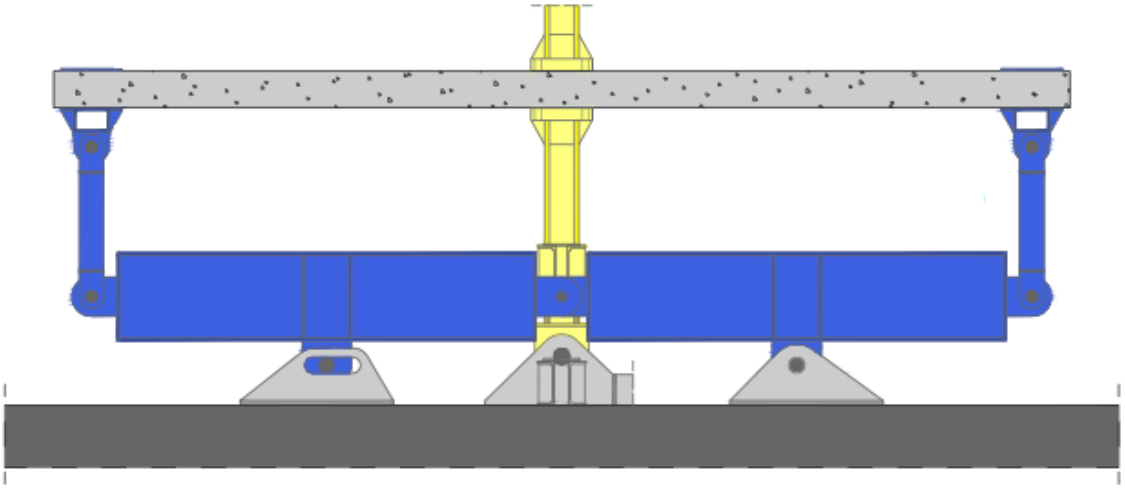

(a) Unloaded specimen

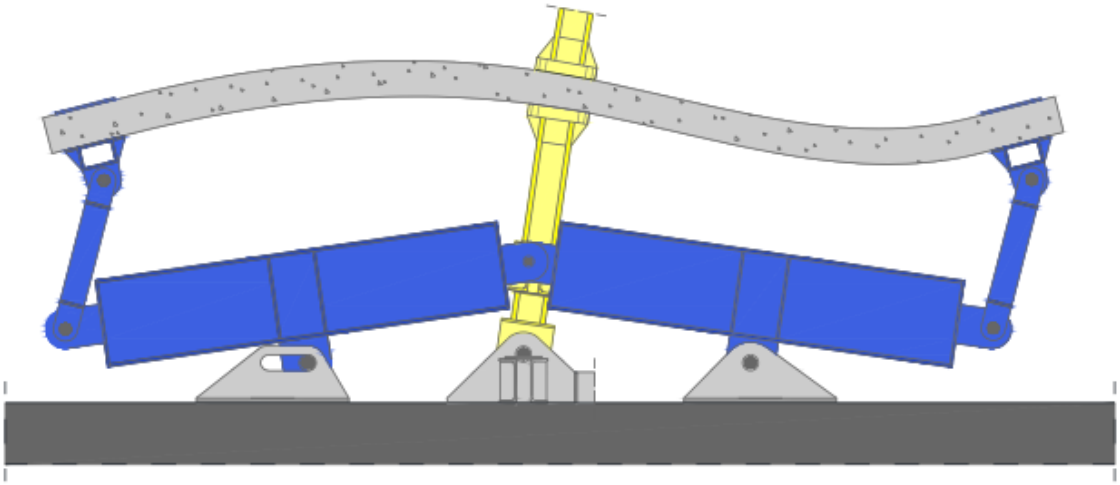

(b) Vertically and horizontally loaded specimen

Figure 39 - Vertical displacement compatibilization system (Almeida et al., 2016)

The steel column has a square rigid base with section 250×250mm^2 and is located at the center of the specimen. It is composed by two parts, one above the slab pinned to the mechanical actuator of the test setup and one below the specimen, which is pinned to the laboratory strong floor. A load cell was connected to the actuator in order to apply the cyclic horizontal

displacements. Both parts of the column are connected by four preloaded threaded rods which also go through the slab to connect it as a system (Figure 40).

Figure 40 - Fixed column below the slab

The vertical load was kept constant during the test and was applied to eight points around the slab upper surface, with location detailed in Figure 41. Four spreader steel beams were placed connecting every two load points equally distribute the gravity load around the top surface of the specimen. To each beam a hydraulic jack and a load cell with maximum capacity of 200kN (CLC-200KNA by TML) were installed (Figure 42) and connected to a pressure controller (Figure 43) in order to apply and control the gravity load during the entire experiment. A steel tendon was connected to each hydraulic jack and load cell, this way the forces were applied through the tendons to a rigid steel profile connected to the bottom part of the column and therefore keeping the vertical loads constant and not affected by the horizontal displacements and deflection of the slab.

An actuator attached to the laboratory reaction wall is connected to the upper end of the column in order to apply the reversed horizontal cyclic displacements (Figure 44). A load cell and a wire displacement transducer are connected to the actuator to measure the horizontal force and displacement applied to the top of the column, respectively. A complete scheme of the described test setup can be seen in Figure 45.

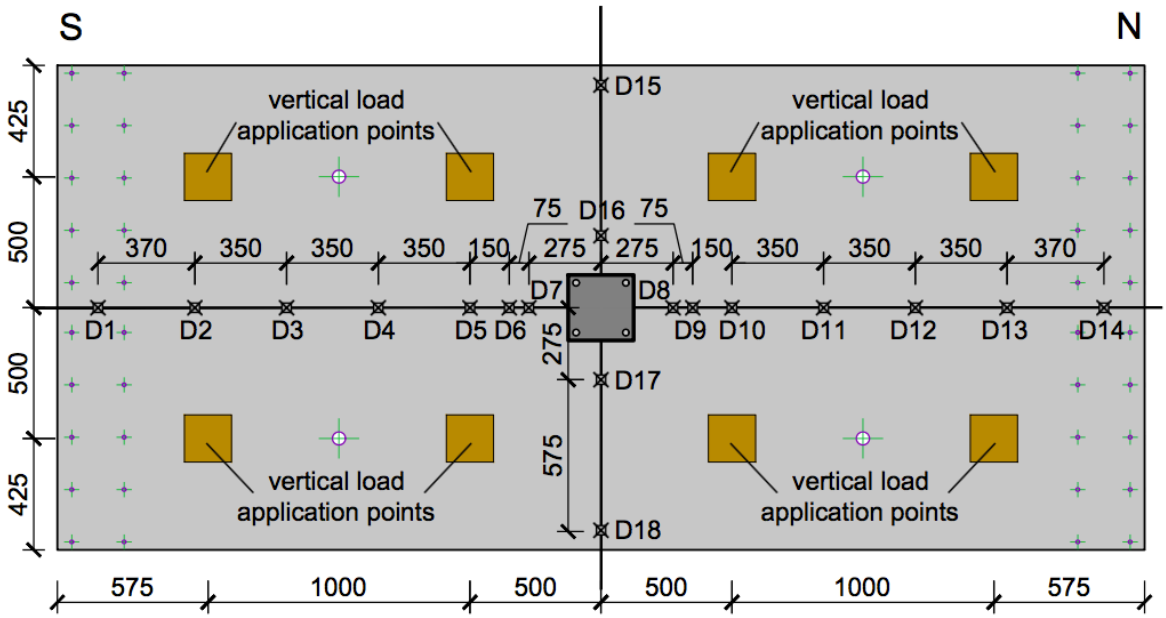

Figure 41 - Loading points and displacement transducers arrangement

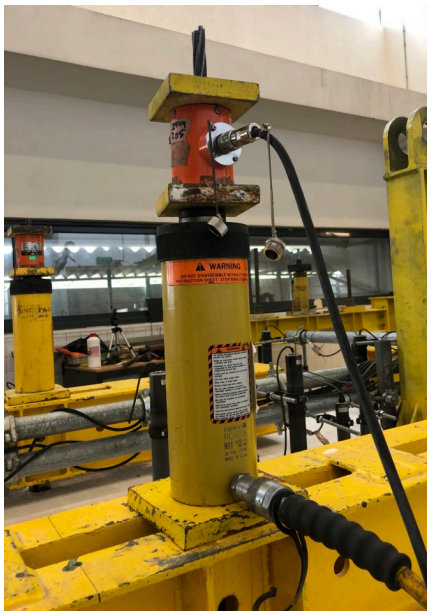

Figure 42 - Hydraulic jack

Eighteen displacement transducers (Figure 46) were positioned on the upper surface of the slab to obtain data regarding vertical displacements (refer to Figure 41 for detailed positioning). Fourteen of the transducers were placed along the N-S center line (D1 – D14) and four in the E-W direction (D15 – D18). The transducers used varied in measuring range when placed in the longitudinal direction. Closer to the border of the slab (D1-D3 and D12-14) wired displacement transducers with a measuring range of 1270mm were used (SP3 by Measurement

Specialties, Figure 46a). Mid-way transducers (D3-D5, D10 and D11) the measuring range was 100mm, CDP-100 by TML (Figure 46b) and next to the column (D6, D7, D8 and D9) an equipment with a smaller range of 50mm, CDP-50 by TML, was used. In the transversal direction all displacement transducers (D15-D18) were CDP-100 by TML. HBM Spider 8 equipment (Figure 47) was used to log the data from the displacement transducers to a computer.

Figure 43 - Pressure controller

Figure 44 – Mechanical actuator before being connected to the specimen

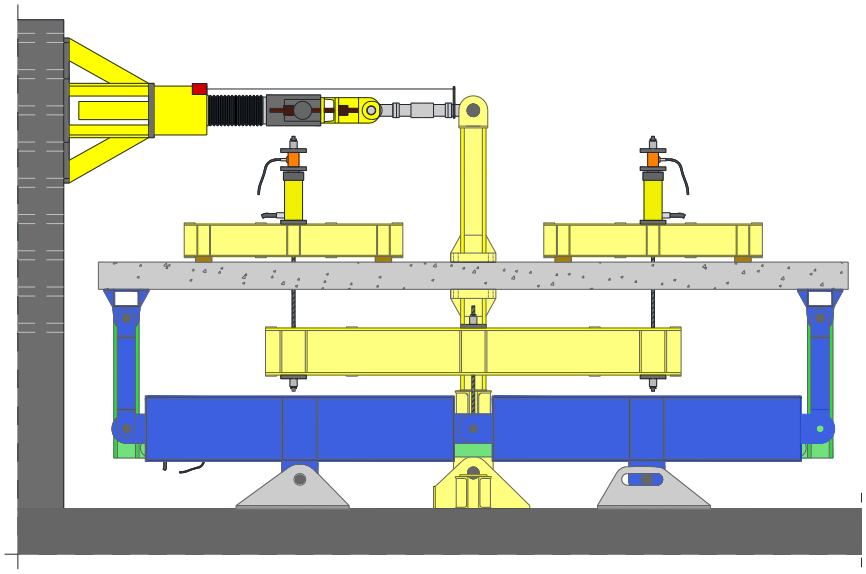

Figure 45 - Scheme of the test setup (Almeida et al., 2016)

(a) 1270mm measuring range

(b)100mm measuring range

Figure 46 - Displacement transducers

To obtain data from the flexural reinforcement bars strain gauges were installed in twelve bars. For each location two strain gauges were positioned on opposite sides of the rebar. Figures 48 and 49 display the positions for the strain gauges in top and bottom reinforcement for all specimens. Strain gauges were also installed in twenty-five studs. Due to the smaller

dimension of the studs' rebar, only one strain gauge was installed in the middle of each stud. The location for this instrumentation is shown in Figure 28.

Figure 47 - HBM Spider 8 data loggers

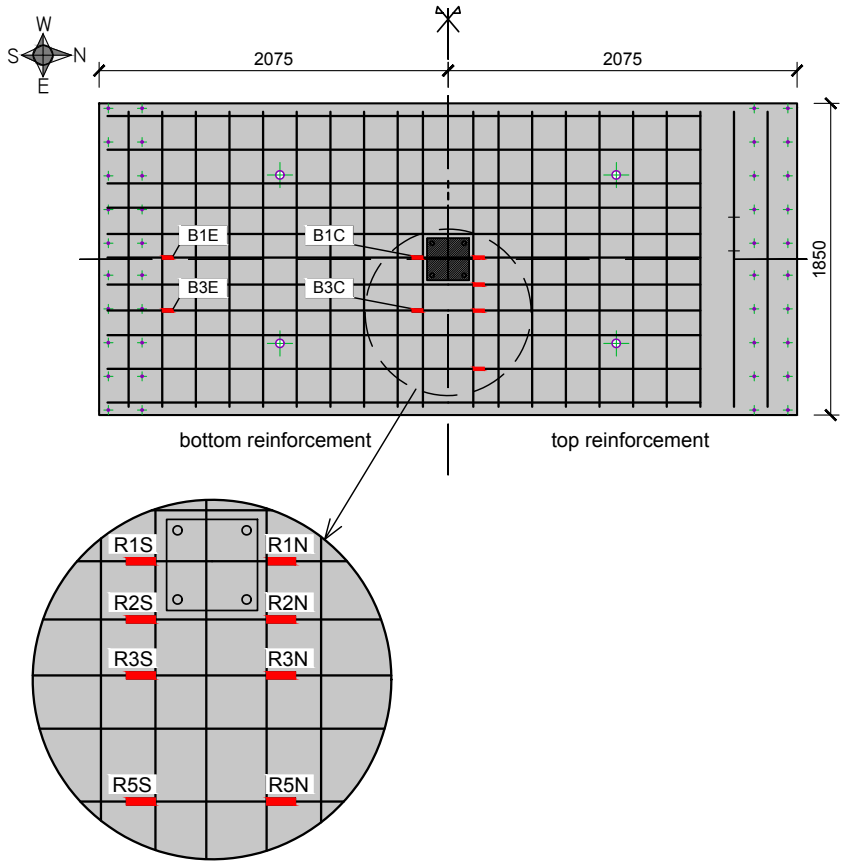

Figure 48 - Longitudinal reinforcement strain gauges - C-Ref-L and C-SSR5-L

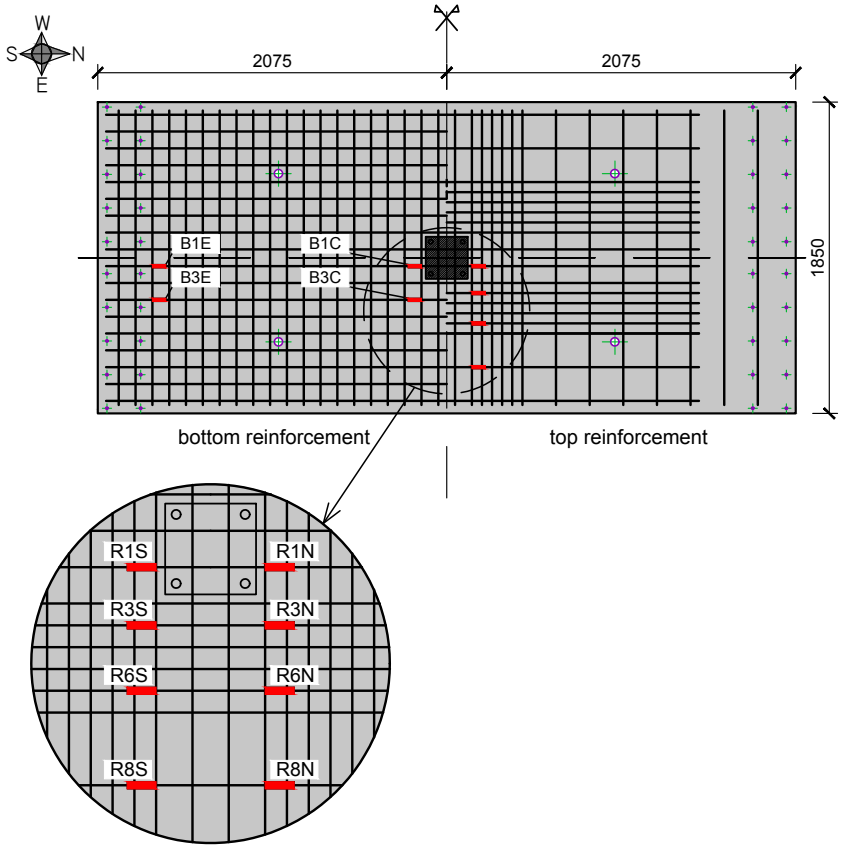

Figure 49 - Longitudinal reinforcement strain gauges - C-Ref-H

To log the data measured by the strain gauges they were all connected to a HBM QuantumX data logger, displayed in Figure 50.

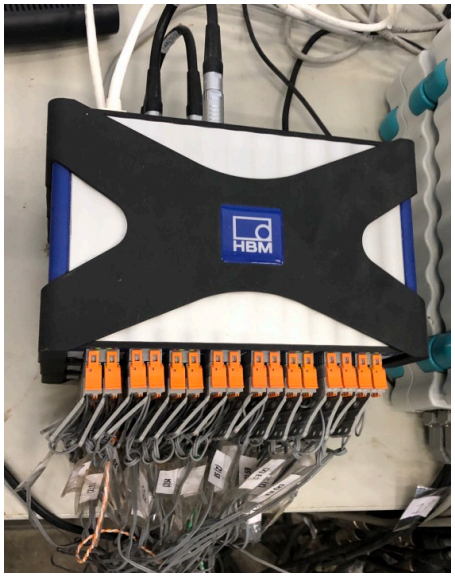

Figure 50 - HBM QuantumX for strain gauges data

On both North and South borders of the test setup an inclinometer (Figure 51) was installed to monitor the rotation of both borders. It was connected to a computer and monitored throughout the test to ensure that rotations on the opposite borders were equal. When needed, rotations were adjusted by altering the force in the struts, which were equipped with a load cell and a hydraulic jack each, as shown in Figure 52.

Figure 51 – Inclinometer SST300

Figure 52 - Load cells and hydraulic jacks installed to the struts

3.5 Preparation of test setup

In order for the experimental campaign to occur successfully and in a secure way, it was necessary to follow a sequence of assemblage of the test setup and correct placement of the

specimens and instrumentation. First the setup was cleaned so the specimens could be placed, Figure 53 shows the test setup prior to the placement of any specimen. Slabs were carried by a crane holding the specimen in four points distributed symmetrically through the top surface (Figure 54a). Specimens were only released from the crane after they were fastened in both north and south edges (Figure 54b) and load was added to the struts (19kN for C-Ref-L, 21kN for C-SSR5-L and 26kN for C-Ref-H) through the hydraulic jacks and load cells shown in figure 52, to ensure zero rotation at the borders of the specimens.

Figure 53 - Test setup before specimen was placed

After both North and South borders were secured, top surface of the slab was grinded in the location where the centered column was being placed with a crane. Epoxy resin was also applied to the surface before placing the column in order to fill and remaining voids, as displayed in Figure 55. Threaded rods (M24) were fastened and pre stressed into the four holes and distributed in the column surface and the empty space around the rods was filled with grout to ensure a split-resistant connection.

The assemble of the test setup continued by connecting the mechanical actuator to the top of the column through a pinned connection, fixing the metal tubes that hold the displacement transducers to the column (Figure 56a) and placing the plates onto the loading points (Figure 56b). Later all eighteen displacement transducers were fixed to the metal tube and the wires from transducers and strain gauges were connected to the data logger.

(a) (b)

Figure 54 - Placing of the specimens

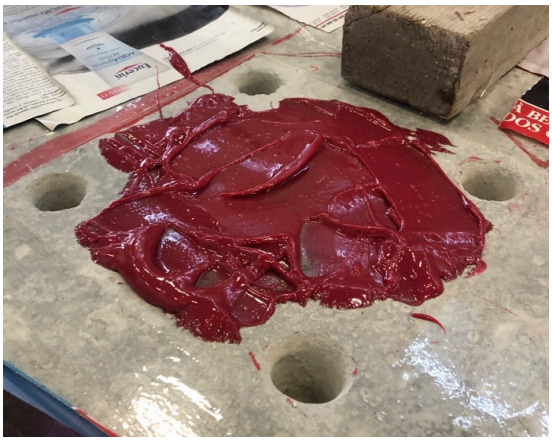

(a) Epoxy resin (b) Placement of the top column

Figure 55 - Installation of the steel column

Again with the help of a crane, all four metal spreader beams were positioned to their respective location around surface followed by the installation of the hydraulic jacks, load cells and tension tendons. A top view of the complete test setup is displayed in Figure 57.

(a) Metal tubes fixed to the column

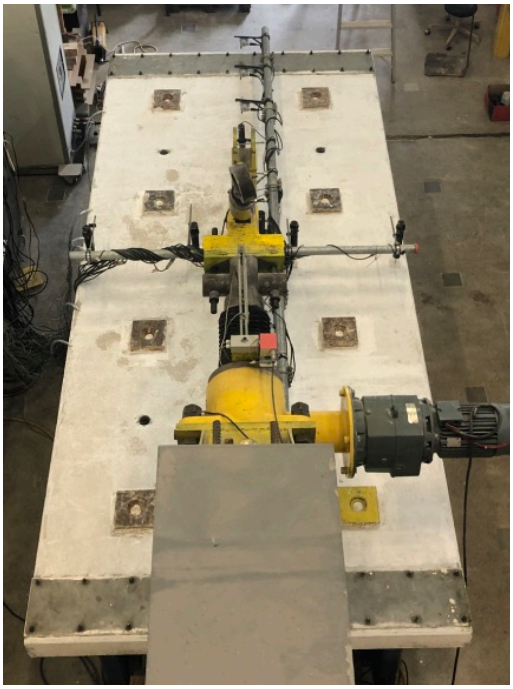

(b) Loading points

Figure 56 - Tubes for displacement transducers and loading points

Figure 57 - Test setup with displacement transducers and steel beams in place

3.6 Test protocol

All three tests followed the same protocol. Gravity load (V_g) was kept constant during the entire experiment and horizontal displacements were gradually increased. The total vertical load applied to each slab is shown in Table 14 and it is the sum of the specimen self-weight and the part of the test setup used to apply the vertical loading. The table also presents the Gravity Shear Ratio (GSR), obtained by the ratio V_g/V_0, where V_0 is the shear resistance, calculated according to EC2 (2010) as shown in equation (32). The value for GSR was intentionally around 55% for all specimens to allow reasonable comparisons with previous experimental campaigns conducted at FCT/UNL that used the same GSR value.

$$V_0 = 0{,}18k(100\rho_1 f_c)^{1/3}ud \tag{32}$$

With f_c values described in Table 13, u is the control perimeter distanced $2d$ from the column, ρ_1 is the longitudinal reinforcement ratio, limited by 0,02, and k is given by:

$$k = 1 + \sqrt{200/d} \leq 2 \tag{33}$$

Tests started with gravity load being applied and gradually increased until reaching the target value for each specimen. After the desired gravity load was reached and kept constant, horizontal displacements started to be applied by the actuator to the top end of the column. The drift ratio is the horizontal displacement divided by the total column height (2m) and during testing it was increased by 0.5% for different cycles, the maximum being 6,0% (limit of the test setup). Until the 3.5% drift ratio the cycles were repeated 3 times, two times for 4,0% and one cycle for the following drifts until failure. Complete protocol for horizontal displacements is shown in Figure 58.

Table 14 - Vertical loads

Specimen	d (mm)	V_o (kN)	V_g (kN)	GSR (%)
C-Ref-L	117,30	284,17	165,23	58,1%
C-SSR5-L	117,16	324,16	181,53	56,0%
C-Ref-H	117,73	399,30	219,10	54,9%

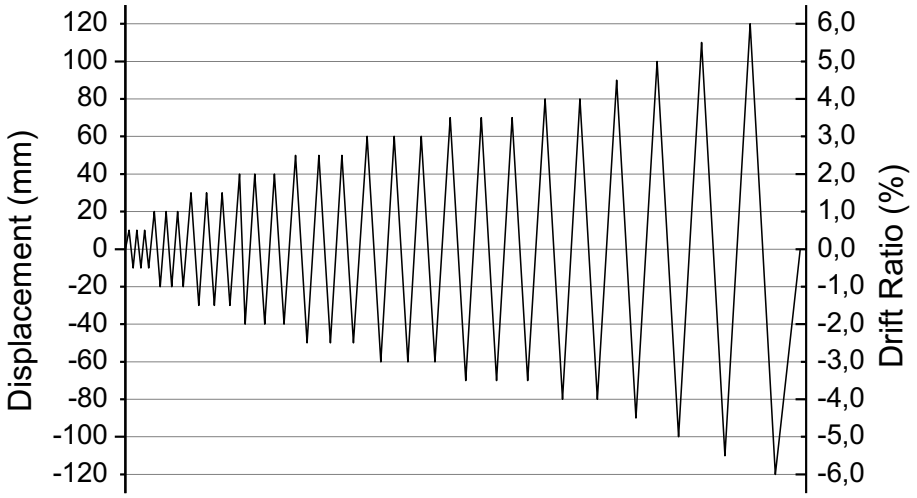

Figure 58 – Test protocol for all specimens

Chapter 4

4 Experimental results and analysis

In this chapter the test results obtained during the experimental campaign are presented and discussed. First the responses noted during the experimental campaign are described and supported by photographic content. Following the responses, data from each specimen is analyzed separately and finally a comparison among the three slabs is conducted to conclude which effects the different flexural reinforcements accomplished.

Some of the results presented in this chapter were obtained directly from the test instrumentation previously described in this paper, for example deflections along both longitudinal and transversal directions and loads. Part of the data here presented was not directly obtained by the results given by the equipment, but was calculated based on the extracted data, for example strain, lateral stiffness, inflection points, equivalent viscous damping and residual deformation index.

4.1 Test responses

Below are described for each specimen the physical aspects noted during the experiments, highlighting cracks caused by the positive and negative bending moments that appeared as higher drifts were imposed to the slab.

4.1.1 C-Ref-L

During the first step, vertical loading, small flexural cracks appeared near the column in the top slab surface. As the horizontal cyclic displacements started cracks emerged near the column (top surface) and for positive moments at the north and south edges of the slab (slab's bottom surface). At a 1,0% drift ratio cracks on the upper side of the slab edges appeared and negative moment cracks developed further from the column as the existing ones grew wider (Figure 59).

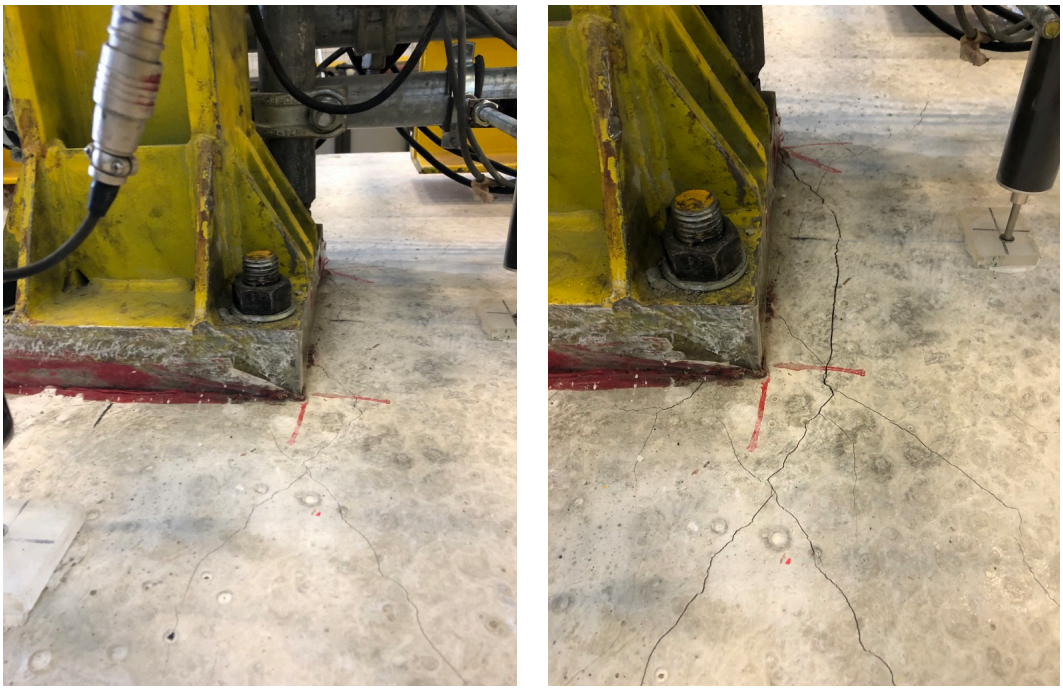

(a) 0,5% drift ratio (b) 1,0% drift ratio

Figure 59 - Cracks near the column in specimen C-Ref-L

The brittle failure occurred near the end of the first 1,5% drift ratio cycle (Figure 60), after the cracks for positive and negative moment kept increasing in the first half of the cycle.

Figure 60 – Punching Shear failure specimen C-Ref-L

4.1.2 C-SSR5-L

Small flexural cracks near the column at the top slab surface appeared during the gravity load phase. Flexural cracks for both positive and negative bending moments started to emerge with the increase of horizontal displacements. At a 2,5% drift ratio some cracks appeared at the bottom face of the specimen, near the column, as some damage was visible. On the upper face some pieces of concrete cover started to break. Figure 61 displays the cracking at different drifts during the test.

The slab damage continued to grow and become more visible as the drifts were increased. The test ended after one cycle for the 6,0% drift ratio with no failure of the specimen in punching shear.

During the testing of this specimen the actuator had some functioning problems, so the test had to be stopped at 1,5% drift ratio and the vertical loading had to be removed until the test setup was correctly working again. Gravity load was applied again and drifts continued to be imposed from where the test was previously stopped. No significant effects were noticed by this unexpected stop in the test.

4.1.3 C-Ref-H

With the application on the gravity load some flexural cracks near the column at the top slab surface and the slab north and south edges at the slab's bottom surface emerged. At the 0,5% drift ratio cycles more cracks appeared in both positive and negative bending moment regions of the specimen. The cracks kept growing during the application of 1,0% cycles and at the third and last cycle failure occurred (Figures 62 and 63).

(a) 1,5% drift ratio

(b) 3,5% drift ratio

(c) 4,5% drift ratio

(d) 5,5% drift ratio

Figure 61 - Cracks in Specimen C-SSR5-L

(a) 0,0% drift ratio (b) 1,0% drift ratio

Figure 62 - Cracks Specimen C-Ref-H

Figure 63 - Punching shear failure C-Ref-H

4.1.1 Saw-cuts

After specimens were tested, longitudinal saw-cuts were made and are shown in Figure 64. In the saw-cut from C-Ref-L the usual crack for punching shear failure is noticeable right outside the column due to the non-existence of specific shear reinforcement. It is visible an almost vertical and small crack near the column edges, meeting the larger crack at the bottom.

In Figure 64 it is visible that the bottom crack in C-SSR5-L is extended further from the column in comparison with the non-shear reinforcement specimens, as a result of the usage of studs. Nearly vertical cracks can be seen between the column borders and the first row of shear reinforcement, taking the entire height of the slab and with more inclined cracks approaching the first stud.

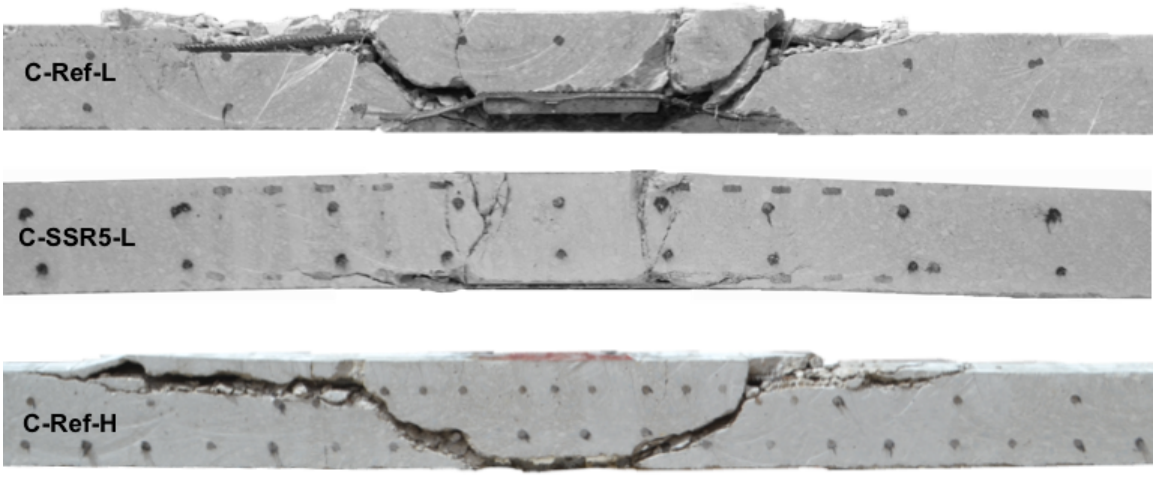

Figure 64 - Saw-cuts of all three specimens

As expected, the rupture seen in C-Ref-H happens near the column, similar to the other non-shear reinforcement specimen (C-Ref-L). In this case the extend of the damage on the upper surface of the specimen was bigger than the one seen in C-Ref-L, although the crack width was smaller.

4.2 Deformation and failure load

The failure of a specimen subjected to a horizontal cyclic test was considered when a 20% decrease of the horizontal load was achieved, thus hysteretic diagrams relating horizontal force and displacement, drift ratio and unbalanced moment were created for a better understanding of the specimens' cyclic behavior (Figures 65-67).

The hysteretic diagram for specimen C-Ref-L is shown in Figure 65. The slab-column connection reached the highest horizontal load (36,40kN) during the first half of the first 1,5%

drift and before ending the full cycle the horizontal load quickly decreased as failure and consequently abrupt damage were noted.

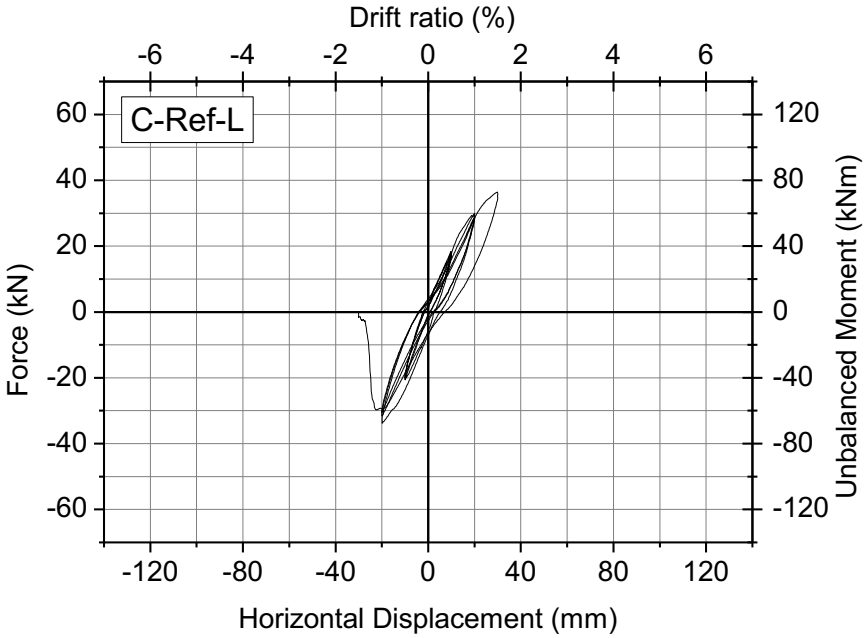

Figure 65 - Hysteretic diagram C-Ref-L

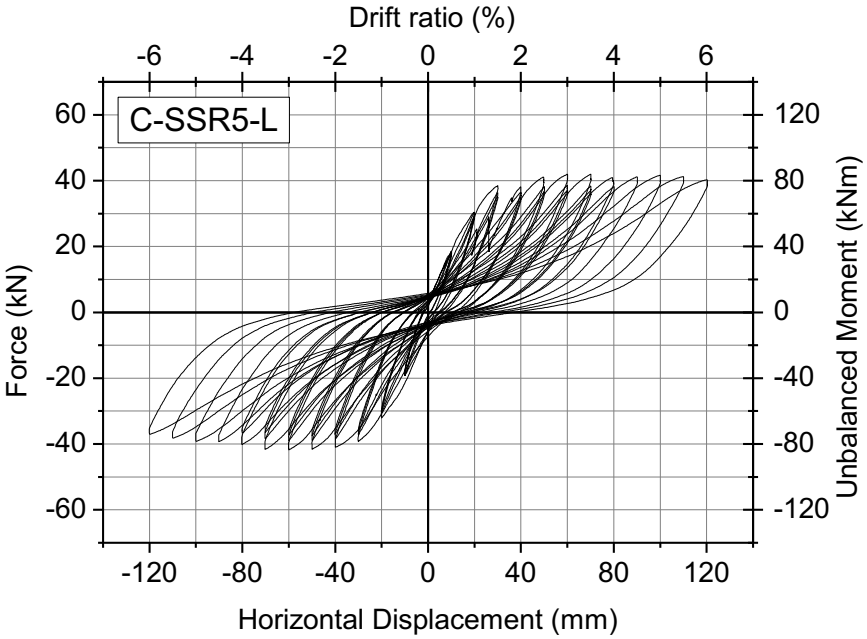

Figure 66 - Hysteretic diagram C-SSR5-L

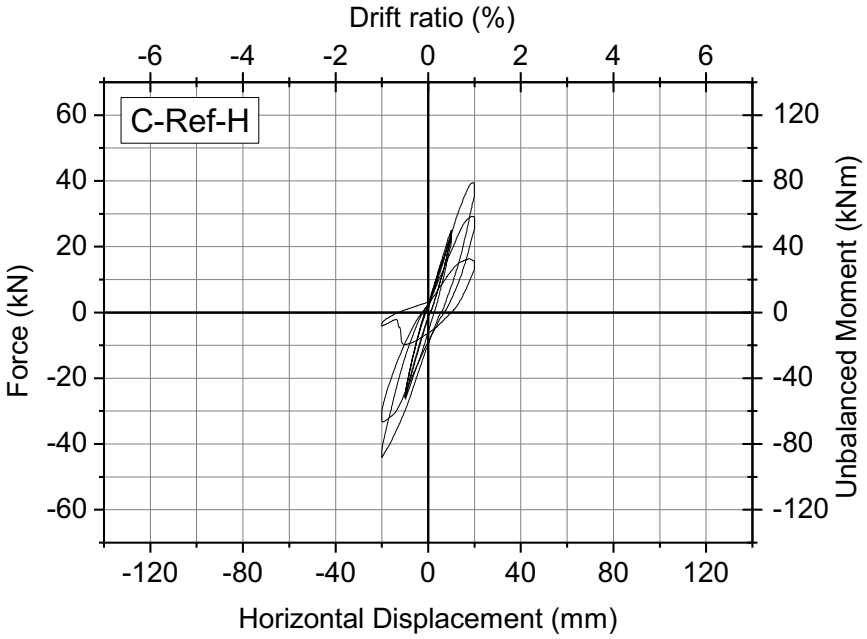

Figure 67 - Hysteretic diagram C-Ref-H

The only specimen that did not reach punching failure was C-SSR5-L, resulting in a very stable hysteretic diagram (Figure 66). The test reached the maximum horizontal force of 41,92 kN during the 3,0% drift ratio cycle and for the following drifts the maximum load showed a small decrease reaching a more significantly decrease of 8% for the last drift ratio.

The maximum horizontal load for C-Ref-H was reached at the first cycle of the -1,0% drift and the specimen failed during the third and last cycle of that same drift. With a higher stiffness, this slab degraded much quicker than the slabs with low flexural reinforcement ratio, given by the fast decrease of the maximum horizontal force shown in Figure 67.

Figure 68 shows the backbone curve for horizontal positive displacements for all three specimens during the first cycle of each drift. Curves for low flexural reinforced slabs were similar until specimen C-Ref-L was near failure, at 1,50%. A horizontal plateau can be noted for C-SSR5-L at approximately 2,50% drift ratio. Neither of the non-shear reinforced specimens reached a horizontal plateau, although it can be noticed by the similar behavior with C-SSR5-L that the curve of C-Ref-L was starting to lose stiffness.

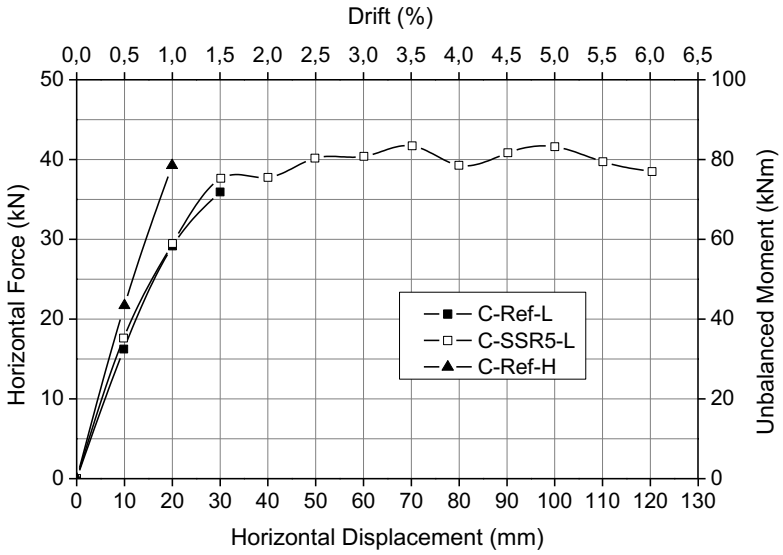

Figure 68 – Backbone curve for horizontal displacements

Table 15 shows a summary of the maximum horizontal load values for each specimen with the respective drift ratio. In the table it can also be seen the failure drift ratio and the unbalanced moments, obtained by multiplying the horizontal force by the column height.

Table 15 - Maximum Horizontal Forces

Specimen	Max Horizontal Force (kN)	Unbalanced Moment (kN.m)	Drift	Failure Drift	Failure Mode
C-Ref-L	36,40	72,80	1,50%	-1,10%	Punching
C-SSR5-L	41,92	83,84	3,00%	>6,00%	Flexural yielding (no failure)
C-Ref-H	44,08	88,16	-1,00%	-0,50%	Punching

4.3 Equivalent viscous damping coefficient

As stated before on section 2.5, the equivalent viscous damping coefficient is an important parameter regarding the energy dissipation capacity of a structure. Therefore, a value of ξ_{eq} was calculated for each drift for all three specimens and it is displayed in Figures 69-71.

For all specimens the first cycle for the same drift ratio showed a higher value of ξ_{eq}, meaning that the energy dissipation decreases as a drift is repeated. Although, for specimen C-Ref-L the values for second and third cycles increased for the higher drift due to an increase of energy dissipation and therefore more damage to the specimen.

The highest ξ_{eq} for Slab C-SSR5-L was during the first cycle of the experiment, another peak value could be noted at the 2,0% drift but only after the 4,5% drift ratio was reached that a continuous growth of ξ_{eq} values and therefore more damage to the structure could be noticed.

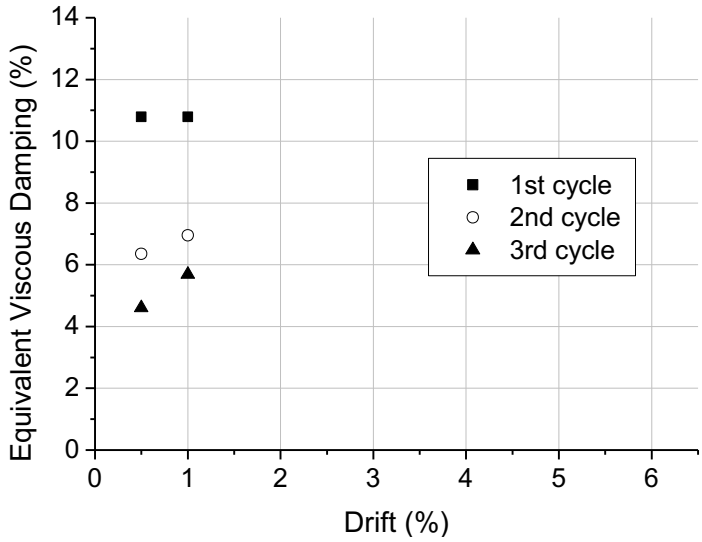

Figure 69 - Equivalent viscous damping coefficient for specimen C-Ref-L

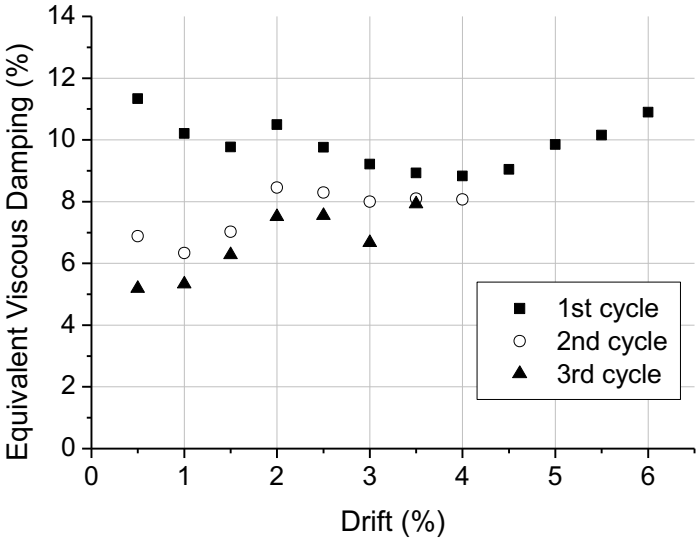

Figure 70 - Equivalent viscous damping coefficient for specimen C-SSR5-L

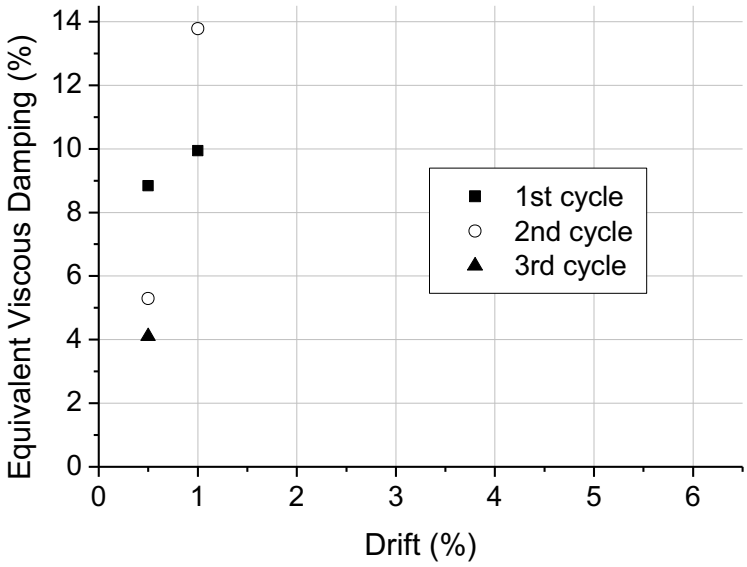

Figure 71 - Equivalent viscous damping coefficient for specimen C-Ref-H

Damping values for specimen C-Ref-H were higher for the 1,0% drift ratio, as the specimen showed more damage and reached failure at the last cycle of that same drift. The second 1,0% drift cycle had the highest value of ξ_{eq} among the three specimens, ξ_{eq}=13,78%, due the low elastic strain energy resulted from the excessive damage on the specimen when approaching failure (equation (27)).

When reaching failure and significant physical damage, the value of ξ_{eq} for specimens C-Ref-L and C-Ref-H raised abruptly but since those cycles were not completed, they are not shown in the diagrams above. Since slab C-SSR5-L did not reach failure, it did not present an enormous value of ξ_{eq}, but a growth of this coefficient value can be seen as the end of the test is reached due to the increased damage.

4.4 Residual Deformation Index

Specimens C-Ref-L and C-Ref-H did not reach global yielding therefore it was not possible to obtain the residual deformation index for these two slabs. Whereas since C-SSR5-L reached higher drifts it was the only specimen that allowed the RDI calculation. The bilinear approximation into the elasto-plastic curve of C-SSR5-L and the backbone curve of the

hysteretic diagram for this specimen are displayed in Figure 72, and RDI values for each drift of positive cycles is shown in Figure 73.

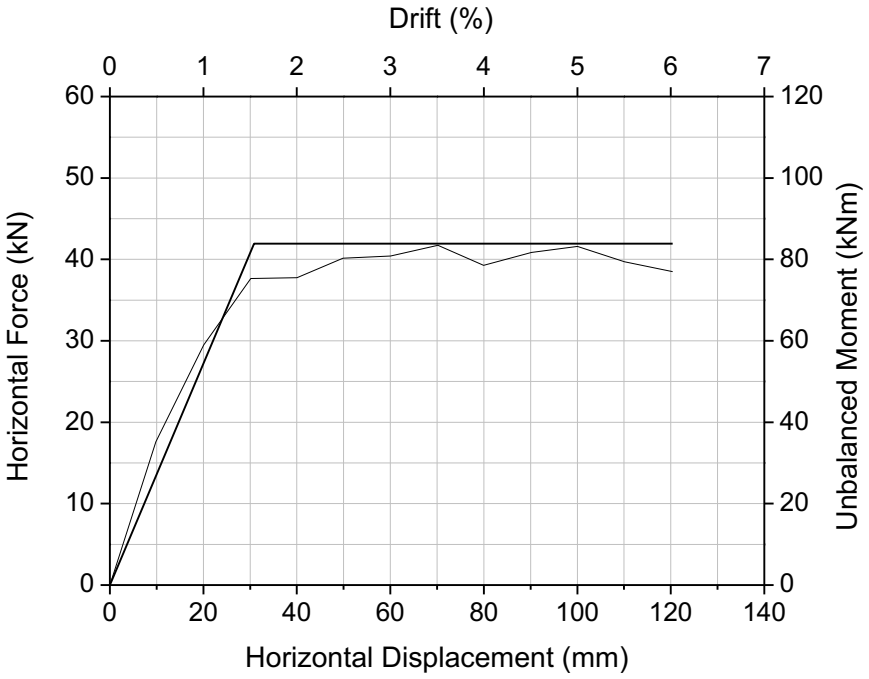

Figure 72 - Elasto-plastic curve for C-SSR5-L

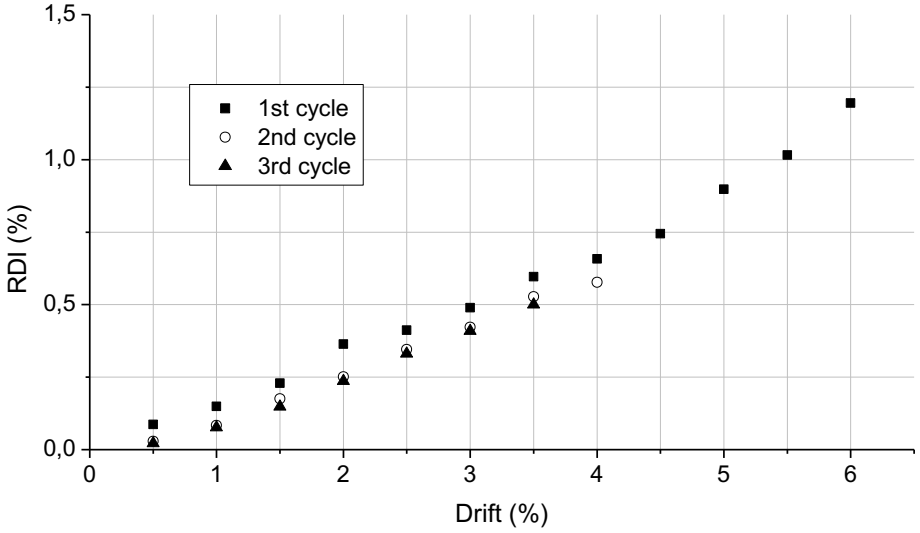

Figure 73 - RDI curve for C-SSR5-L

Since the RDI estimates the damage suffered by a structure that is subjected to cycle loading, it is noticeable from Figure 73 that, as expected, the value of RDI grows as bigger drifts are imposed to the specimen whilst for repetitive cycles it decreases.

4.5 Deflections

As stated before, displacement transducers were used to measure the deflection of the specimens along the N-S and E-W directions, hence the data obtained with these equipment's are presented and analyzed below.

4.5.1 N-S deflection

The deflections measured along the N-S direction for the first cycle of each drift are shown in Figures 74-76. At a 0,0% drift ratio only gravity load was applied and, as expected, vertical deflections could already be seen in all three specimens at this point, with comparable values, even though deflections in specimen C-Ref-H were smaller probably due to the higher reinforcement ratio. The cyclic horizontal loading causes a stiffness decrease, resulting in higher vertical displacements as bigger drifts were applied while maintaining the gravity load constant.

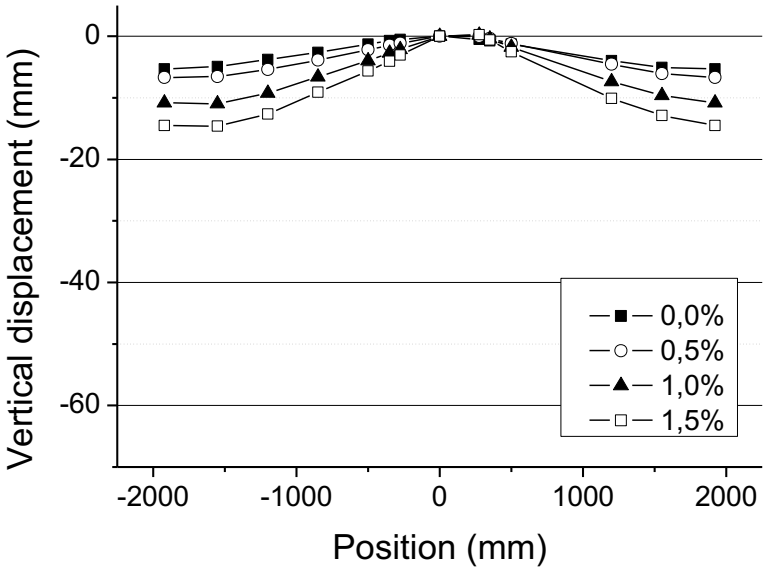

Figure 74 - Longitudinal Deflection C-Ref-L

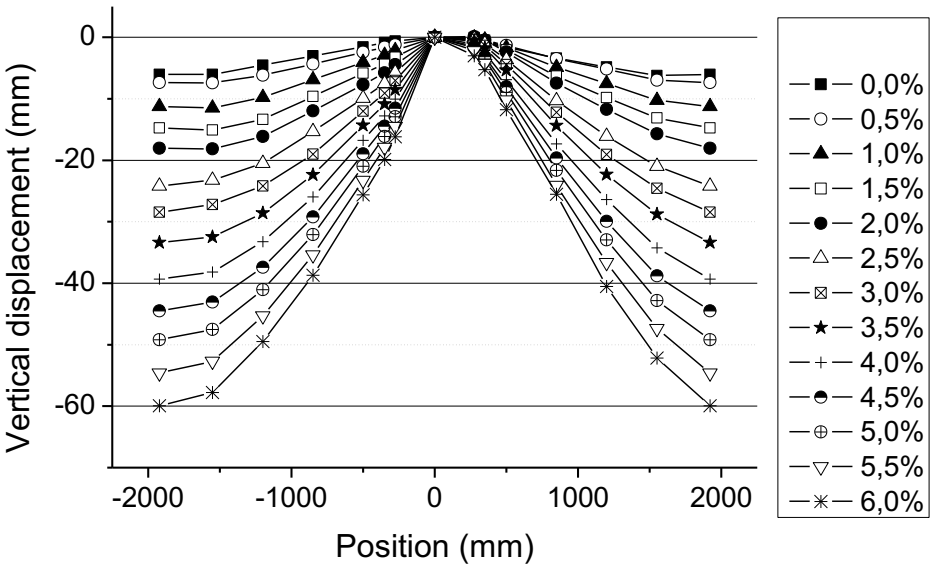

Figure 75 - Longitudinal Deflection C-SSR5-L

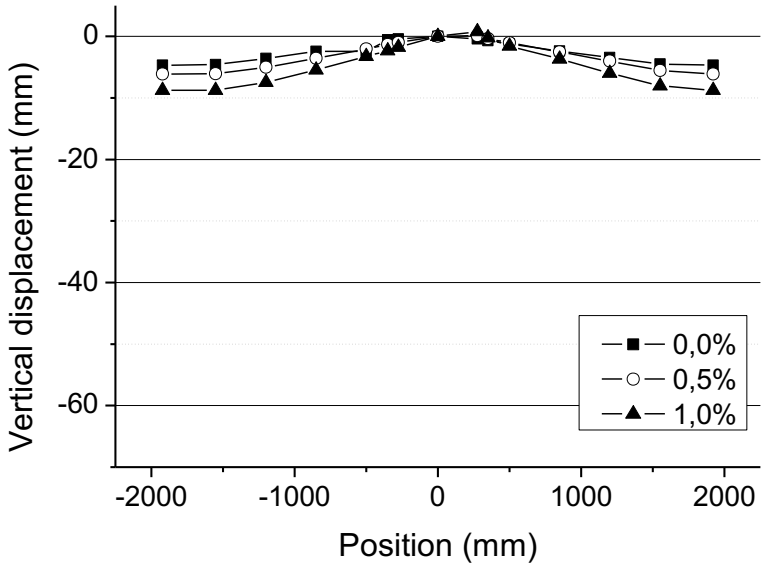

Figure 76 - Longitudinal Deflection C-Ref-H

Specimens C-Ref-L and C-SSR5-L had the same longitudinal reinforcement but the studs applied to C-SSR5-L allowed bigger drifts. It can be seen from Figure 77 that for equal drifts the shear-reinforced specimen showed slightly bigger displacements. This could be explained by the higher vertical load applied to this slab, but the difference between the values becomes lower when larger drifts are imposed and as C-Ref-L approaches failure.

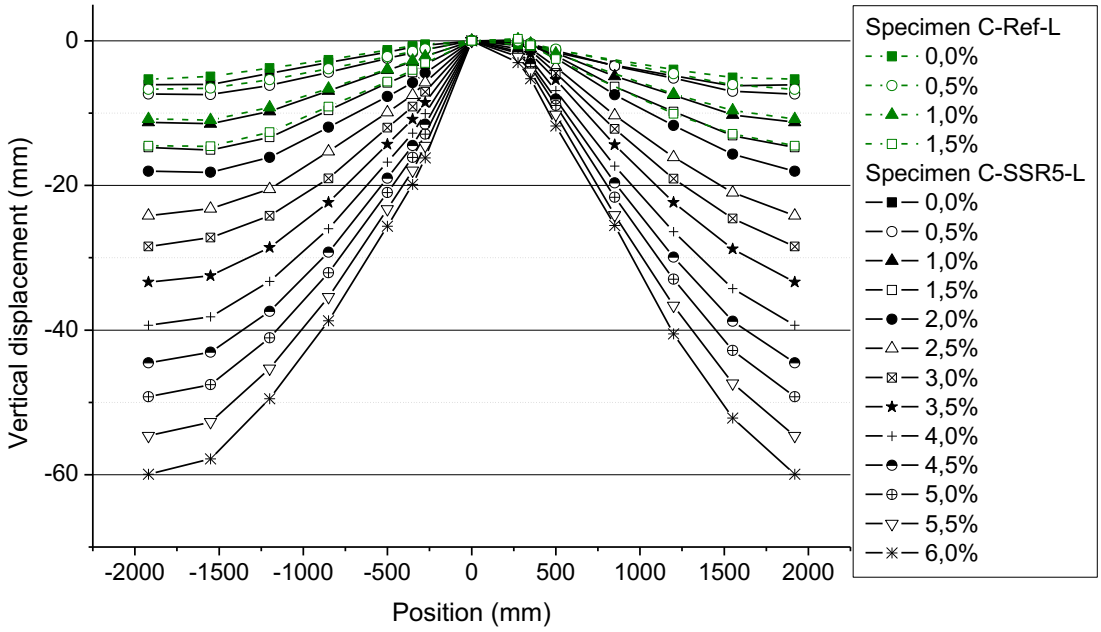

Figure 77 - Longitudinal Deflection C-Ref-L and C-SSR5-L

With a higher longitudinal reinforcement ratio than C-Ref-L, specimen C-Ref-H showed lower deflections for same drift ratios (Figure 78). Throughout the experiment, the more rigid structure of the high flexural reinforcement specimen resulted in smaller deflection increases when compared to the growth of the values in C-Ref-L.

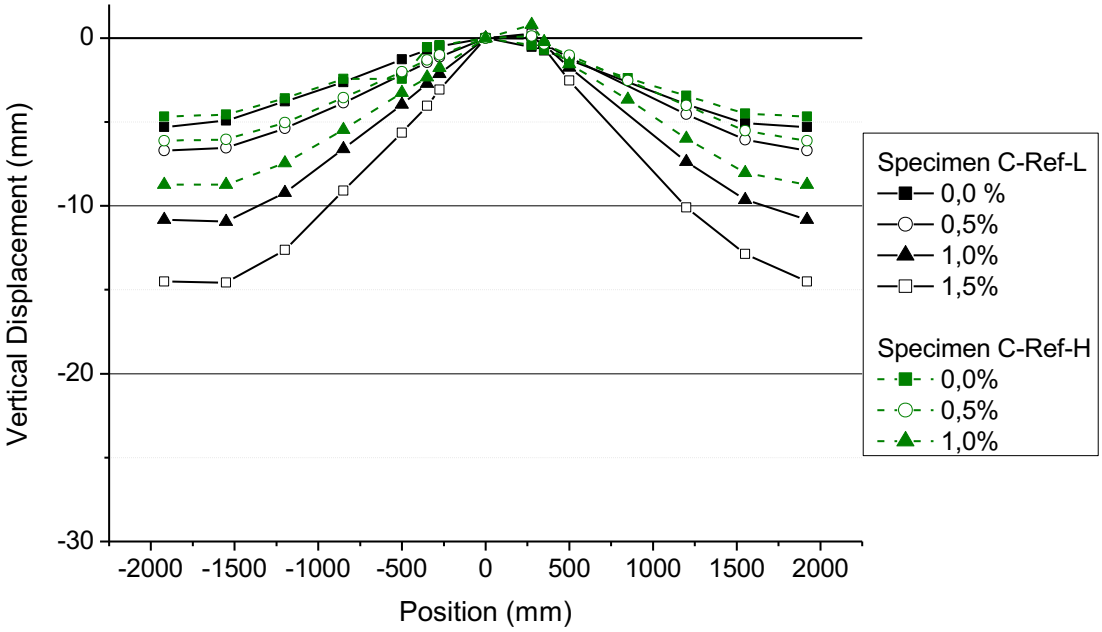

Figure 78 - Longitudinal Deflection C-Ref-L and C-Ref-H

4.5.2 Inflection points

When analyzing the diagrams from Figures 74-76 it is clear the existence of an inflection point on both North and South span of the slabs. Therefore, for each specimen the data from the vertical displacements was used to obtain an approximate fourth degree equation for the deformed slab along the N-S direction, at each step of the experiments. For every step there were two equations, one for each side of the column, and with these data it was possible to obtain the inflection points along the entire test as it varies with time. The values are displayed in Figures 79-81 with the inflection points varying through test time and the position 0,0 being the center of the column, positive side represents the northern part of the slab and consequently the negative side is the southern part. The respective drifts are marked in red on the right side of each inflection point diagram.

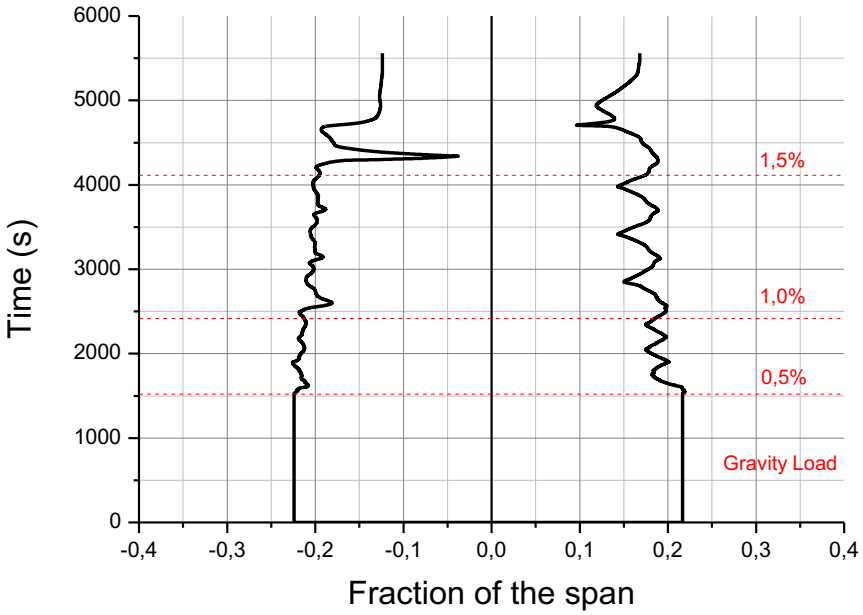

Figure 79 - Inflection Points C-Ref-L

Figure 80 displays the location of inflection points only for the positive side because there were some issues with the results from one of the displacement transducers positioned in the negative side and therefore, values obtained for the diagram were not acceptable.

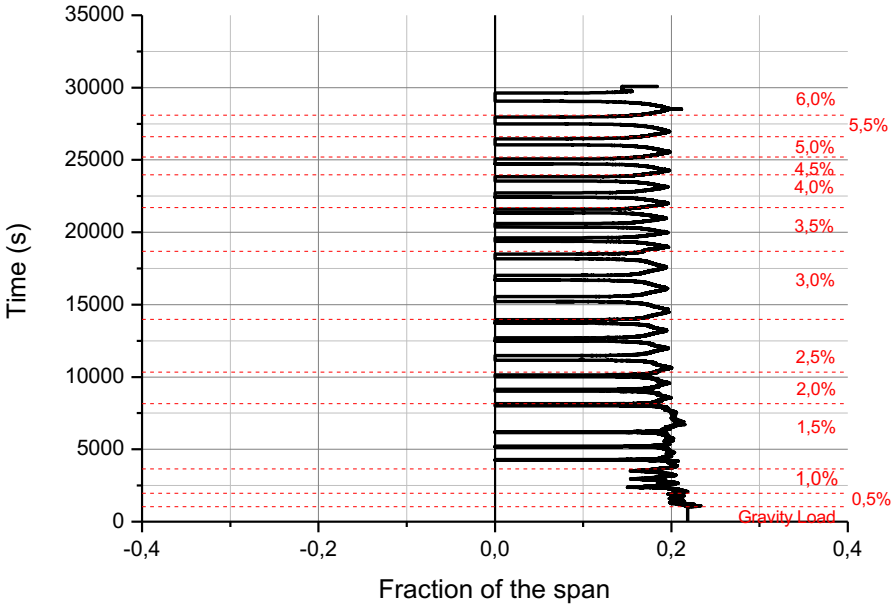

Figure 80 - Inflection Points C-SSR5-L

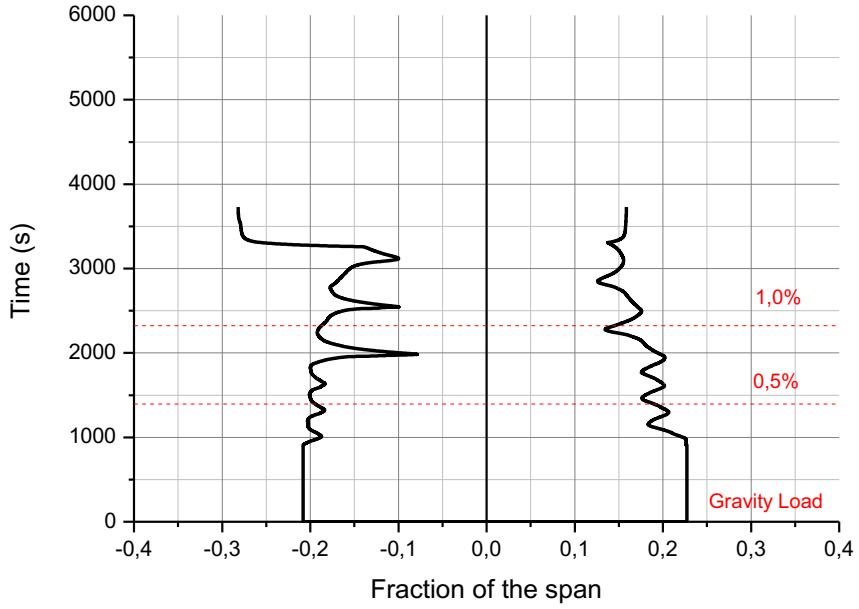

Figure 81 - Inflection Points C-Ref-H

As the experiments initiated with the application of only gravity load, at that point all three specimens showed locations of the inflection points varying from 20,5% to 22,5%, all relatively close to the theoretical value of 22%.

With horizontal displacements being imposed the inflection points moved along the span. When the horizontal force was being applied from North to South to a slab it can be seen that both inflection points move towards the North direction and the opposite happens when the direction of the force was reversed. Also, when looking at the diagrams above it is clear that the inflection points move towards the column as the test continues.

From the figures presented above, it is noticeable that inflection points reached the column only for the specimen supporting higher drifts (C-SSR5-L). Since the vertical load was kept constant during the entire test, as higher drifts were applied to C-SSR5-L the moments originated by the gravity load were less significant than the ones from horizontal forces and positive moments appeared near the column.

4.5.3 E-W deflection

Displacement transducers were also positioned aligned with the center line of the E-W direction, perpendicular to the horizontal loading direction. Figures 82-84 below show the vertical displacements obtained for the first cycle of every drift for all specimens. These deflections are present due to the distribution of gravity loads and are increased throughout the experiment as a result of the deterioration of bending stiffness of the slab caused by horizontal loading.

From Figures 82-84 the same can be concluded as before for the displacements in the N-S direction, specimen C-Ref-H show a higher stiffness than the other two slabs and there was not a big difference between the values obtained for specimen C-Ref-L and C-SSR5-L for the same drift levels. Also in this direction there was a vertical displacement when only gravity load was applied (drift 0,0%) and as the test advanced with horizontal displacements the vertical displacements grew as well.

The displacement transducer in specimen C-SSR5-L positioned +250mm from the center of the column did not work properly during the test, therefore it is not shown in Figure 83.

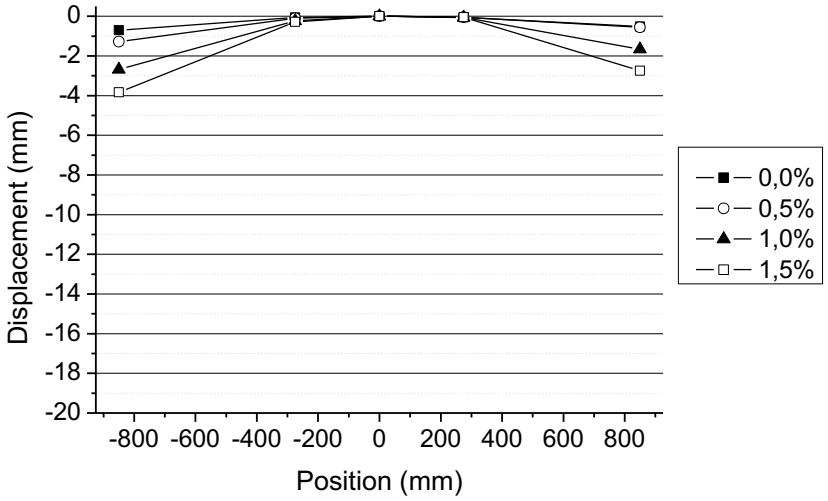

Figure 82 – E-W deflection C-Ref-L

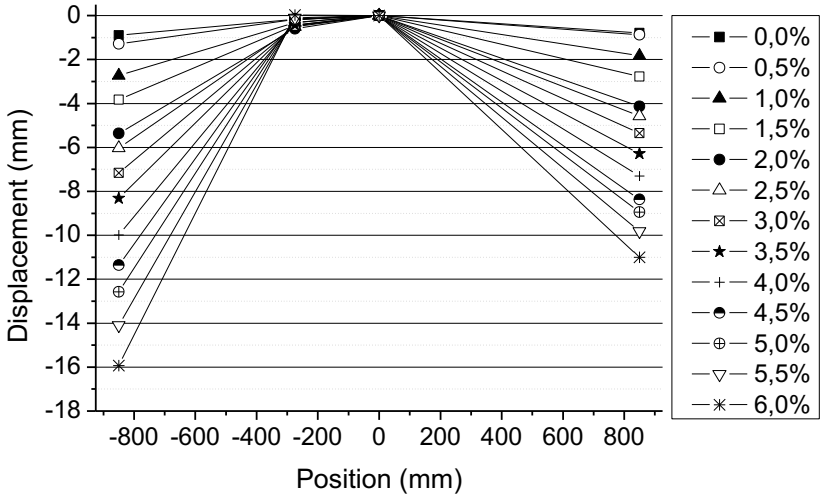

Figure 83 – E-W deflection C-SSR5-L

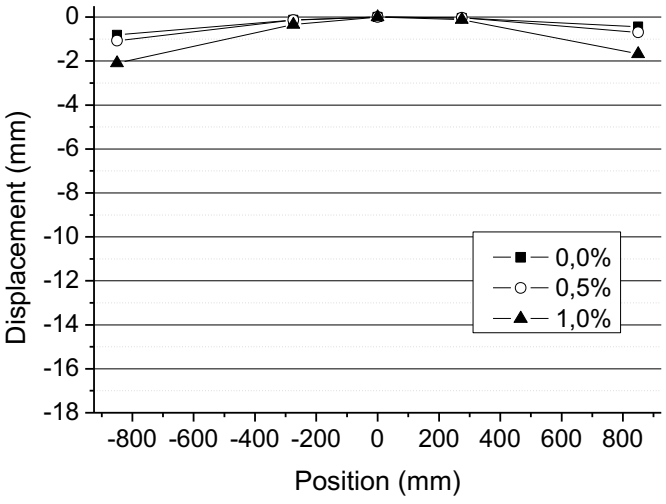

Figure 84 – E-W deflection C-Ref-H

4.6 Lateral Stiffness

Diagrams with lateral stiffness values for all three specimens are shown in Figure 85. Behavior for both low flexural reinforced specimens was similar, the small differences could be related to differences in the material properties (Table 13) or GSR (Table 14). Slab C-SSR5-L started with a quick degradation and it started to slow down after reaching a 2,5% drift ratio. In the slab with high flexural reinforcement ratio, C-Ref-H, stiffness was higher but with a quicker degradation with the drift ratio increase. Values shown in Figure 85 include all cycles and it is noticeable a degradation caused by the repetition of cycles, represented by a decrease in stiffness for the same drift level.

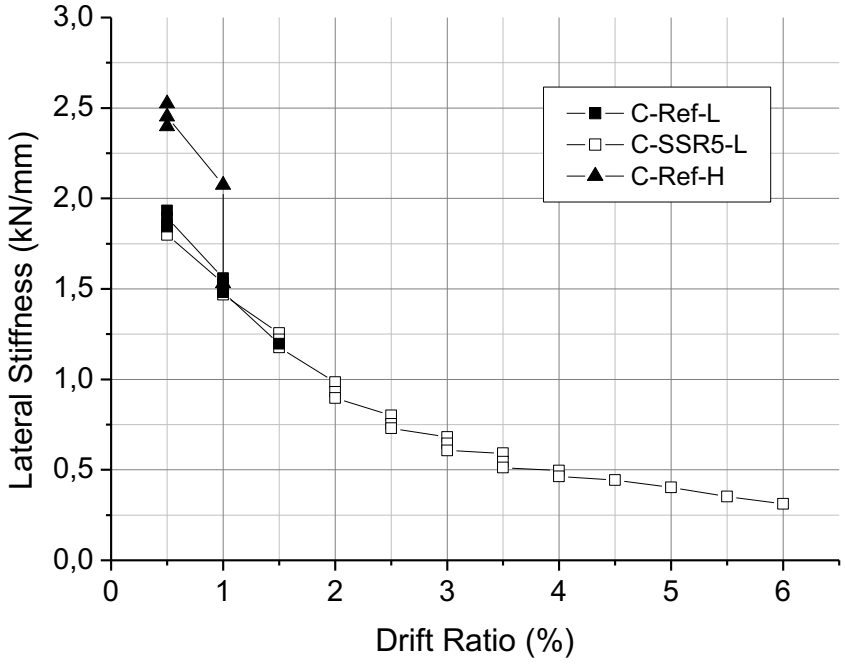

Figure 85 - Lateral Stiffness

4.7 Strain

4.7.1 Strain for top longitudinal reinforcement

For every strain measurement location in flexural reinforcement there were two strain gauges installed. Therefore, the results presented in Figures 86-88 are either the average value

between both measurements or the value for only one strain gauge in the cases one of the strain gauges did not work properly. Results for each row of strain gauges are shown for the loading direction in which strain values were higher. Every missing point in the diagram means that yielding was reached or that the strain gauge stopped working. The yielding value considered is marked in every diagram with a dashed line and the complete strain diagrams are displayed in Appendix A.

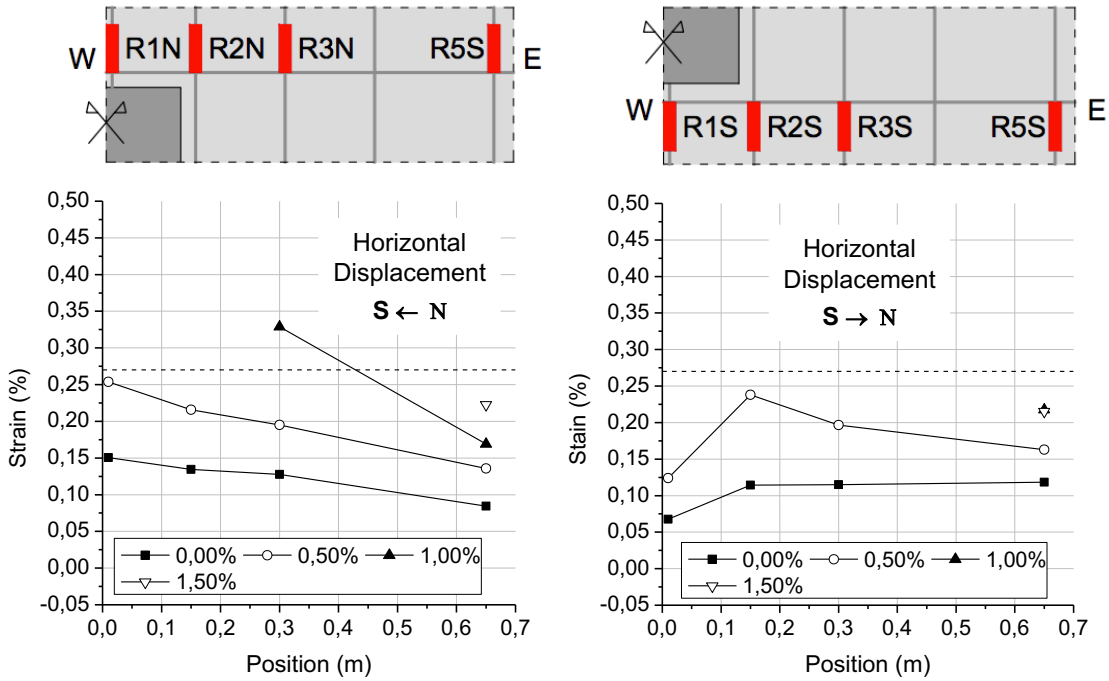

Figure 86 - Strain values for top longitudinal reinforcement - C-Ref-L

In all specimens yielding was first reached in top reinforcement bars located near the column, at approximately 0,50% drifts. Whereas in more distanced strain gauges, smaller values were noted throughout the experiment. As C-SSR5-L supported higher drifts than the other two specimens, yielding of all instrumented reinforcement bars was detected at approximately 2,50% drifts. For specimens failing in punching, it is noticeable that, near failure, strain values in C-Ref-L were much higher and closer to yielding when compared to C-Ref-H due to the smaller flexural reinforcement ratio.

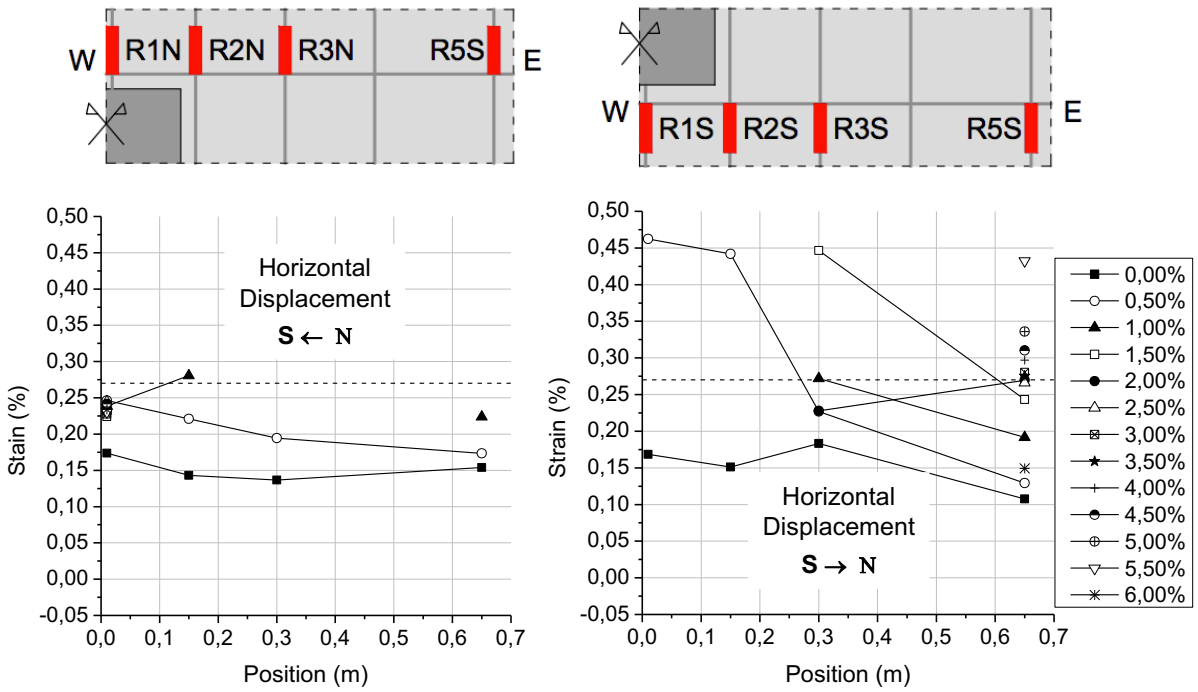

Figure 87 - Strain values for top longitudinal reinforcement - C-SSR5-L

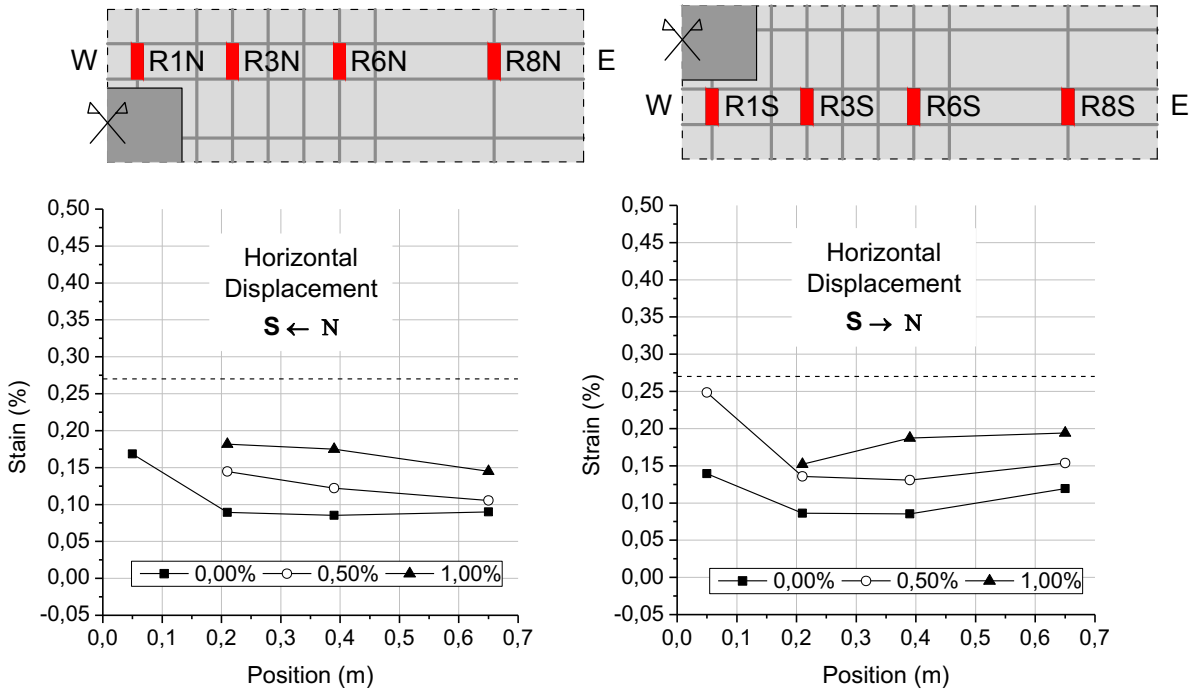

Figure 88 - Strain values for top longitudinal reinforcement - C-Ref-H

4.7.2 Strain for bottom longitudinal reinforcement

Strain measurements for bottom flexural reinforcement are shown below in Figures 89-91. Results are much lower for bottom reinforcement than the ones obtained for top bars. Yielding was only seen in the shear reinforced slab, starting at around 3,00% drifts. For C-Ref-L and C-Ref-H, bars located closer to the edge of the slab had higher strain during the entire experiment.

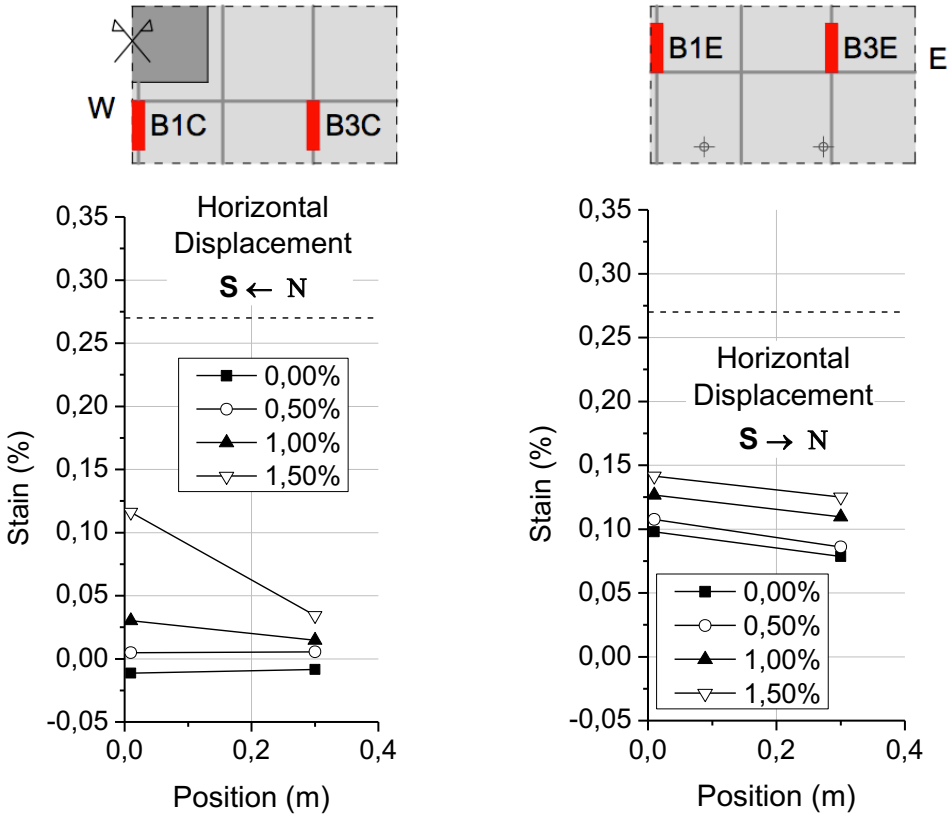

Figure 89 - Strain values for bottom longitudinal reinforcement - C-Ref-L

Strain results for bottom reinforcement is consistent with the conclusions taken from strain at top reinforcement, values for the specimen with high flexural reinforcement ratio are once again much smaller and further from yielding when compared to specimens C-Ref-L and C-SSR5-L.

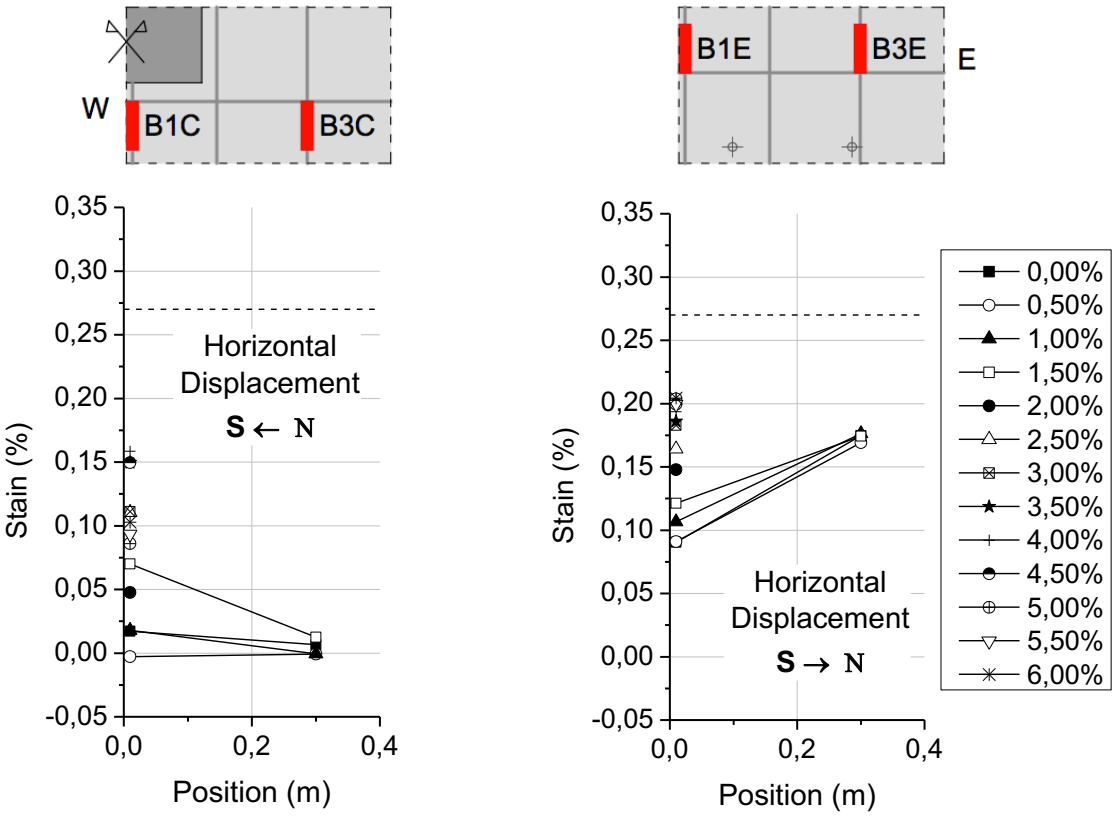

Figure 90 - Strain values for bottom longitudinal reinforcement - C-SSR5-L

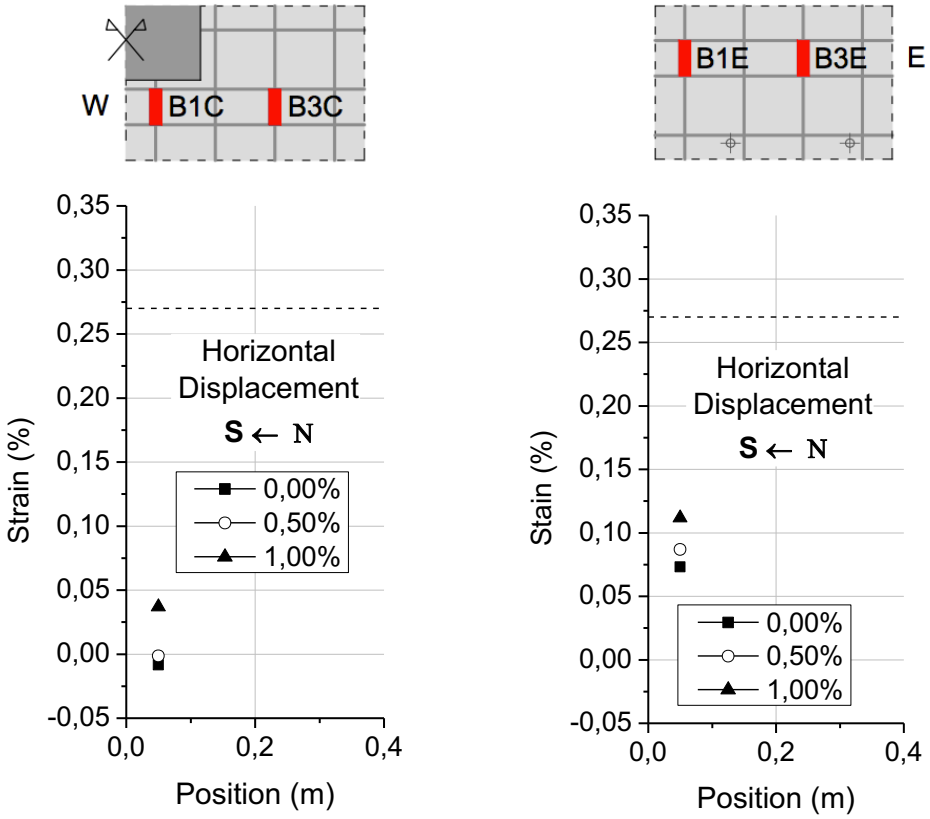

Figure 91 - Strain values for bottom longitudinal reinforcement - C-Ref-H

4.7.3 Strain for punching shear reinforcement

The measured strain values for punching shear reinforcement are shown in Figures 92-94. Results are displayed for every instrumented row of studs with the horizontal displacements being applied in both N-S and S-N directions. Strain measurements are mostly higher in the studs closer to the column, although most of the results below show that the highest strain values are in the second row of studs. During most of the test strain measurements were not close to yielding but they increased as higher drifts were applied and yielding was only detected by a stud located in the second perimeter of shear reinforcement. This could be explained by the strain gauge being located in the middle of a second row stud, where it is expected to be crossed by the shear crack.

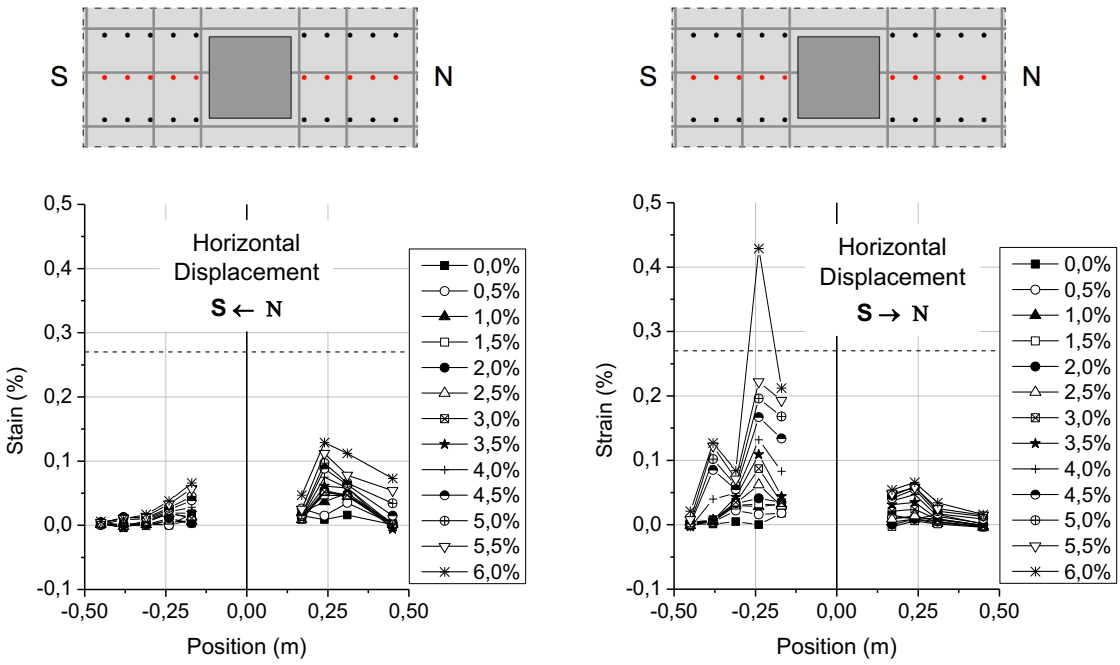

Figure 92 - Strain values for the center row of studs in C-SSR5-L

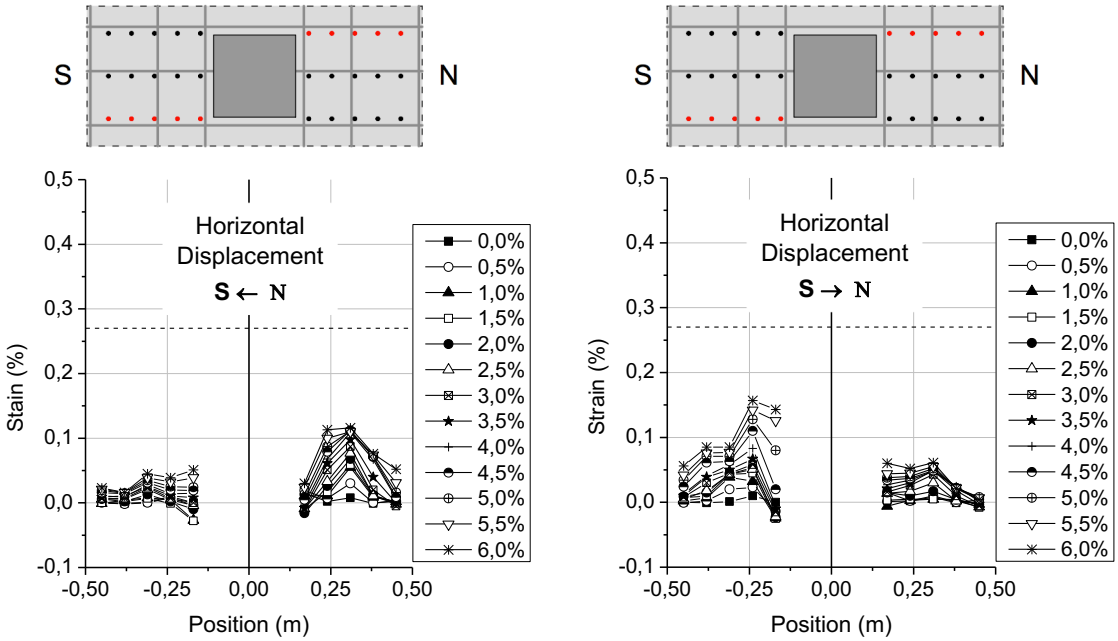

Figure 93 - Strain values for the edge row of studs in C-SSR5-L

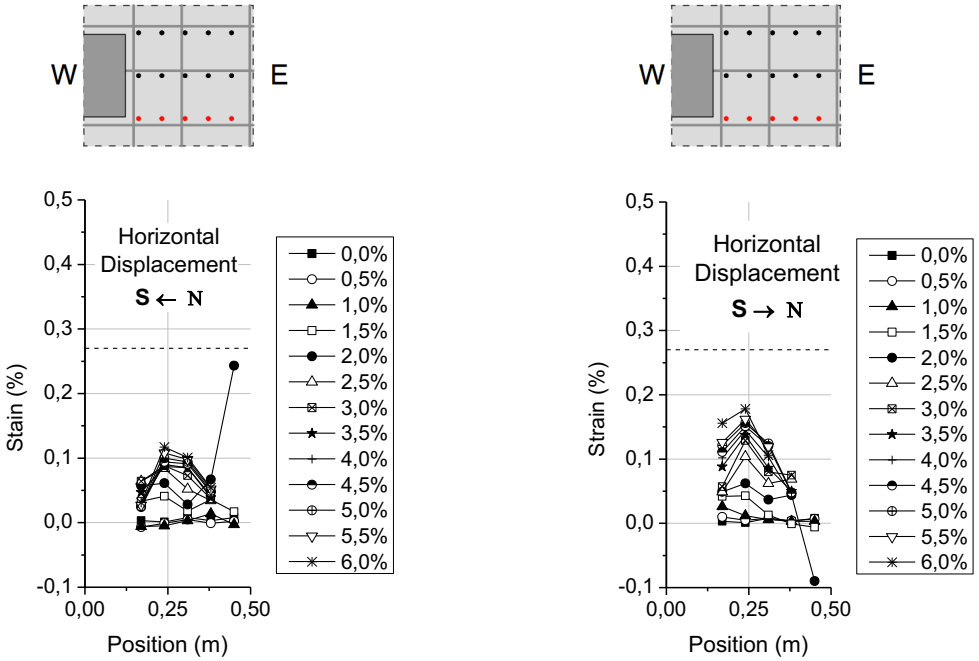

Figure 94 - Strain values for the east row of studs in C-SSR5-L

Chapter 5

5 Comparison with previous experimental campaigns

This chapter focus on comparing the results obtained in this dissertation with previous experimental campaigns also developed at FCT/UNL. Therefore, two specimens with same overall dimensions as the three slabs tested during this work (4,15 x 1,85 x 0,15 m^3) and a reinforcement ratio of ρ=0,96% are hereby presented and compared. The two slabs were chosen due to the similarities in GSR and the variation of flexural reinforcement ratio in order to allow reasonable comparisons.

The first slab chosen, C-50, was tested by Almeida et al. (2016) with no punching shear reinforcement and a GSR of 52%. The second specimen, C-SSR3, is from Isufi et al. (2019), designed with three rows of studs around the column and a 55% GSR. The properties from all specimens and vertical loads are shown in Table 16 (values were obtained according to Eurocode 2, by equation (32)). Results may differ from values shown in Almeida et al. (2016) due to values of k being limited to 2 in the calculations made for this dissertation. Top reinforcement for both C-50 and C-SSR3 was composed by ø12mm bars with spacing varying from 100mm to 200mm in the column region and ø10mm bars every 100mm near the edge of the slab, and for bottom reinforcement ø10mm bars spaced at 100mm were used. Shear reinforcement used in C-SSR3 is detailed in Figure 95.

Table 16 - Details of the compared specimens

Specimen	d (mm)	ρ (%)	f_c (MPa)	V_g (kN)	V_0 (kN)	GSR
C-Ref-L	117	0,64	31,3	165	284	58%
C-SSR5-L	117	0,64	46,6	182	323	56%
C-Ref-H	118	1,34	41,1	219	400	55%
C-50*	118	0,96	52,4	203	389	52%
C-SSR3 **	118	0,96	41,2	196	359	55%

*Specimen published in Almeida et al. (2016); ** Specimen published in Isufi et al. (2019)

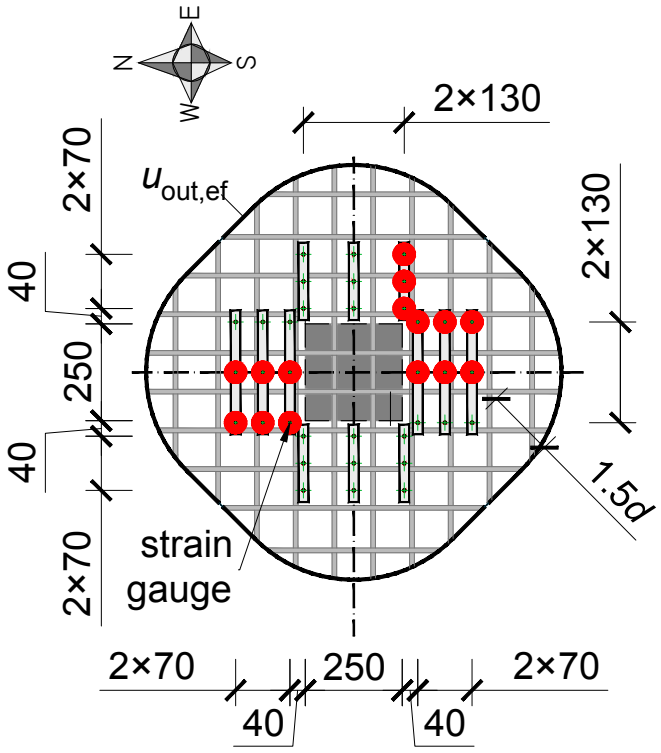

Figure 95 - Layout for studs used in C-SSR3 (Isufi et al., 2019)

The test setup and protocol for these tests were the same used in this dissertation, with constant vertical load and cyclic horizontal displacements. Both specimens failed during the tests with a punching shear failure. A summary of results obtained during the experiments is displayed in Table 17, listing the maximum horizontal force attained during the test with the respective unbalanced moment and drift ratio, failure drift and also failure mode of each specimen.

Table 17 - Results of comparison specimens

Specimen	Max Horizontal Force (kN)	Unbalanced Moment (kN.m)	Drift (%)	Failure Drift (%)	Failure Mode
C-Ref-L	36,40	72,80	1,50	1,50	Punching
C-SSR5-L	41,92	83,80	3,00	>6,00	Flexural yielding (no failure)
C-Ref-H	44,08	88,16	-1,00	1,00	Punching
C-50*	37,40	74,80	1,10	1,00	Punching
C-SSR3 **	60,40	120,70	3,50	4,00	Flexure-Punching

*Specimen published in Almeida et al. (2016); ** Specimen published in Isufi et al. (2019)

5.1 Non-shear reinforced specimens

Results show that the reduction in flexural reinforcement from 0,96% to 0,64% did not influence much on the horizontal force at failure of non-shear reinforced specimens, as seen in Figure 96, whereas the increase from 0,96% to 1,34% increased strength in around 17% (Table 17).

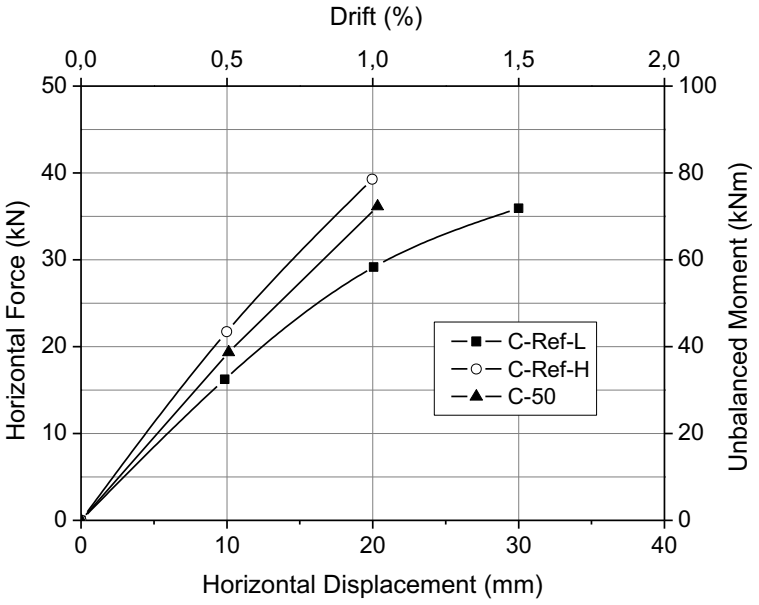

Figure 96 - Force x Displacement for non-shear reinforced specimens

Regarding maximum drifts, C-Ref-L had the highest failure drift among non-shear reinforced specimens, failing at the first cycle of 1,5% drifts. The other two slabs failed at the same drift ratio of 1,0%, C-50 during the second cycle and C-Ref-H in the third and last cycle.

Even with the highest gravity load being applied to C-Ref-H, increasing the flexural reinforcement resulted in longitudinal deflections approximately 30% lower than C-50 during the first phase of the test. The vertical displacement at mid-span, for positive cycles, for these three non-shear reinforced slabs can be seen in Figure 97. The degradation of the specimens is noticeable by the steps shown in the figure, with displacement growing not only with higher drifts but also with the repetition of drift levels.

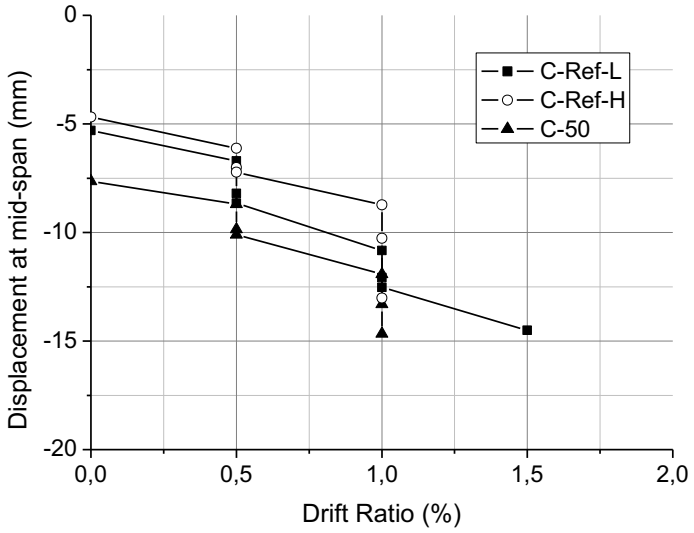

Figure 97 - Vertical displacement at mid-span for non-shear reinforced specimens

Figure 98 displays lateral stiffness for non-shear reinforced slabs during the first cycle of each drift ratio. Values are relatable with the flexural reinforcement ratio of the specimens, with C-Ref-H presenting higher values but also a slightly stepper degradation when elevating the drift ratio, whereas degradation in C-50 and C-Ref-L were similar

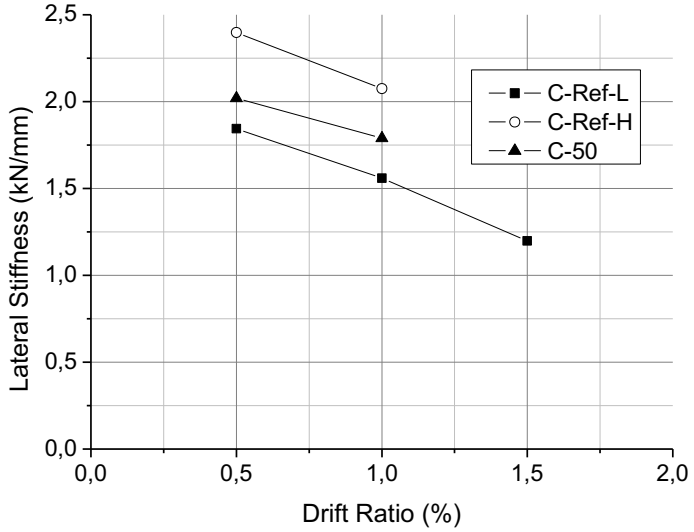

Figure 98 - Lateral Stiffness for non-shear reinforced specimens

For both C-Ref-L and C-Ref-H strain values for top longitudinal reinforcement near the column were similar to C-50, reaching yielding near the 1,0% drift (Refer to Almeida et al.

(2016) for detailed strain values). At mid-span, strain values in C-50 were much lower than the other two slabs, especially from C-Ref-L.

5.2 Shear reinforced specimens

For shear-reinforcement specimens the reduction of flexural reinforcement ratio from 0,96% to 0,64% reduced the maximum horizontal force in 30%. The increase in number of perimeters of studs increased the maximum drift capacity from 4,0% to 6,0%, with C-SSR5-L not failing during the experiment. A drift capacity increase was also noticed in results from Isufi et al. (2019) for specimens C-SSR5a and C-SSR5b, both with five perimeters of studs and ρ =0,96%, that reached 6,0% and 5,5% drifts, respectively. Both C-SSR3 and C-SSR5-L behaved similarly during the tests, reaching a horizontal plateau at about 2,5% drifts, as displayed in Figure 99.

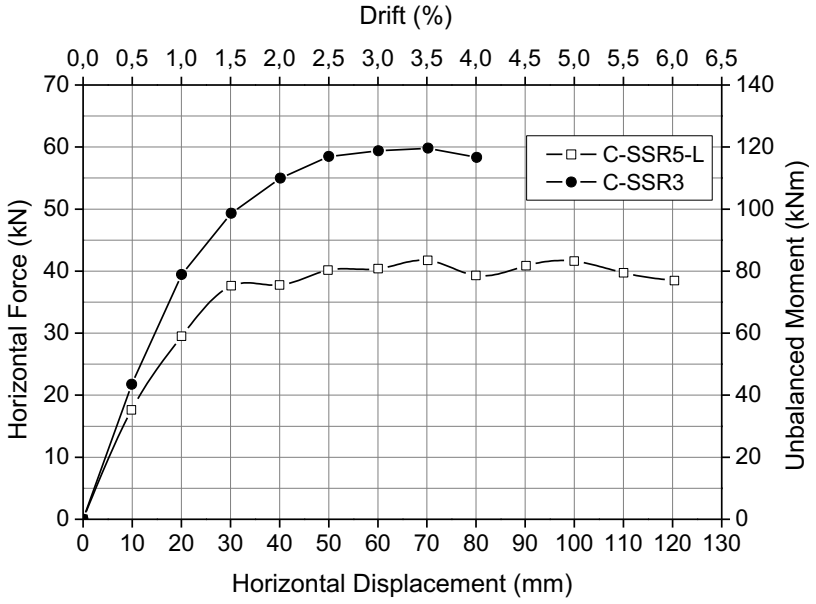

Figure 99 - Force x Displacement for shear reinforced specimens

Vertical displacements at mid-span for both C-SSR5-L and C-SSR3 are displayed in Figure 100. For the first drifts values were comparable between the two slabs but starting at 1,5% drifts displacements for C-SSR5-L started to increase faster. At a 4,0% drift ratio, as C-SSR3 was near failure, displacement in C-SSR5-L was around 45% bigger than in the median flexure reinforced slab (C-SSR3).

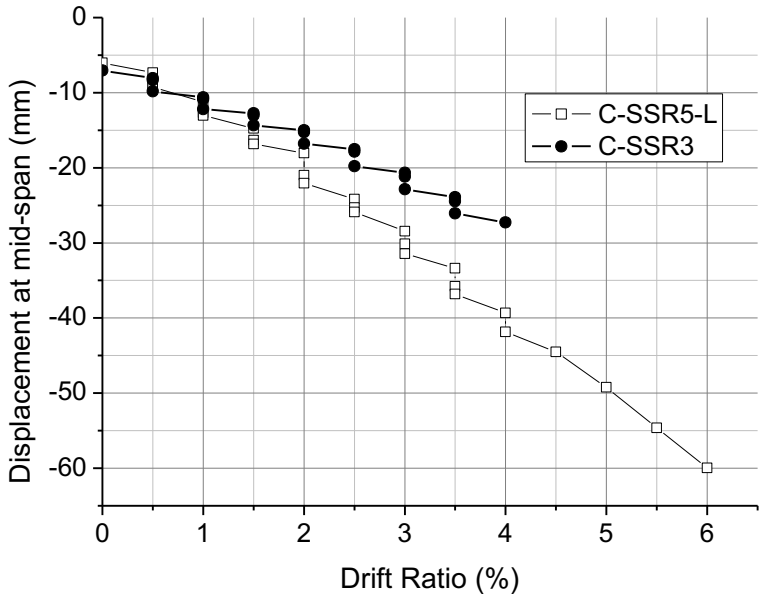

Figure 100 – Vertical displacement at mid-span for shear reinforced specimens

Stiffness in C-SSSR3 was initially higher but degradation in both reinforced specimens are comparable throughout the tests, as seen in Figure 101, where the difference between both curves is kept almost constant until failure of C-SSR3.

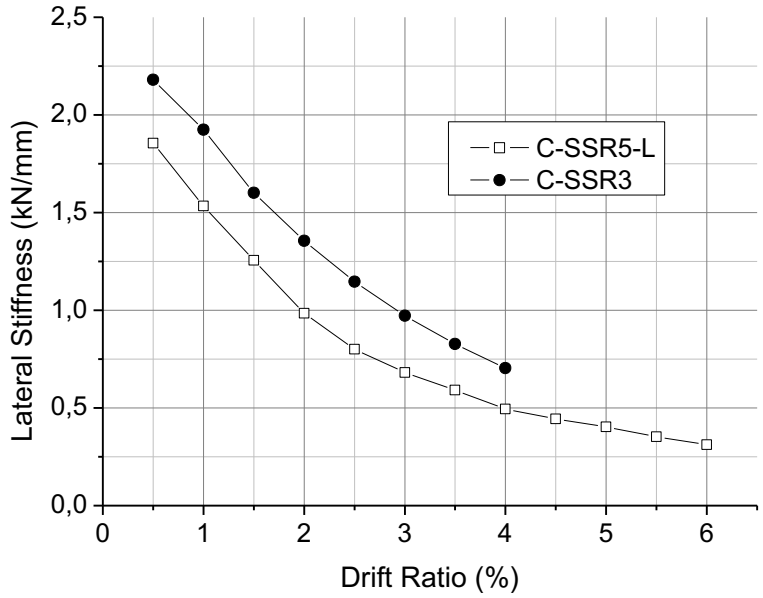

Figure 101 - Lateral stiffness for shear reinforced specimens

Strain measurements along the shear-reinforced slabs was similar, with yielding of top flexural reinforcement being noticed at around 2,5% drift ratios for both C-SSR3 and C-SSR5-

L. For shear reinforcement, the second row of studs measured higher strain values in both slabs, relating to the crack of the specimens. Refer to Isufi et al. (2019) for detailed strain information.

Chapter 6

6 Conclusions and recommendations for future studies

This chapter contains the main conclusions obtained from the results presented and discussed previously in this dissertation, regarding an experimental campaign with three flat slabs with varying flexural reinforcement ratio under constant gravity load and horizontal cyclic displacements. Some comparisons were made with specimens tested in previous experimental campaigns using the same test setup. Later on the chapter some recommendations for future experimental campaigns and researches will be listed.

6.1 Conclusions

The main conclusions taken from this experimental campaign are:

- Flexural reinforcement ratio proved to have effects on the punching shear resistance and drift capacity of flat slabs under lateral loading. Both specimens with low flexural reinforcement tested during this experimental campaign supported higher drifts when compared to median and high flexural reinforced slabs;
- Reducing the flexural reinforcement ratio in specimens C-Ref-L and C-SSR5-L (ρ=0,64%) resulted in larger deflections in mid-span when compared to specimens with a ρ=0,96% (C-50 and C-SSR3) and a ρ=1,34% (C-Ref-H);
- Similar to results obtained during previous experimental campaigns, here also specimens with no shear reinforcement did not attain high drift ratios, with the highest drift attained being 1,5%. Whereas the use of studs as shear reinforcement improved the drift capacity of specimen C-SSR5-L, with the slab-column connection supporting a 6,0% drift, which is considered very high for a real structure;
- The increase in flexural reinforcement ratio for C-Ref-H increased the specimen's capacity regarding unbalanced moments, showing a high level of stiffness and a more brittle rupture than specimen C-Ref-L. For specimens with shear reinforcement, C-SSR5-L and C-SSR3, the tests showed that when punching shear

reinforcement is sufficient to prevent punching failure, the unbalanced moment capacity of slab column-connections is proportional to the flexural reinforcement ratio;

- Repetition of reversed cyclic horizontal displacements caused a considerable stiffness deterioration rate in all slabs here described. Energy dissipation capacity increased when failure was approaching and consequently more damage was evident in all specimens towards the end of each test;

6.2 Recommendations for future research

- More studies regarding specimens with high flexural reinforcement ratio and studs as specific shear reinforcement to allow more comparisons with the specimens here presented and previous studies;
- More experimental campaigns with varying gravity shear ratio for a better understanding of the effects on the drift capacity;
- Explore the use of other punching shear reinforcement systems in specimens with the same characteristics as the ones presented in this thesis for an analysis on the effectiveness of different reinforcement systems;

References

ACI-ASCE Committee 318. Building Code Requirements for Structural Concrete (ACI318-19). 2019

Almeida, A. F. O., Inácio, M. M. G., Lúcio, V. J. G., Ramos, A. P. Punching behavior of RC flat slabs under reversed horizontal cyclic loading. 2016. Engineering Structures 117: pp. 204-219.

Almeida, A. F. O., Alcobia, B., Ornelas, M., Marreiros, R., Ramos, A. P. Behaviour of reinforced-concrete flat slabs with stirrups under reversed horizontal cyclic loading. 2018. Magazine of Concrete Research: 72:7, pp. 339-356.

Badawy, M., Saafan, M., Elwan, S., Elzeiny, S. and Abdelrahman, A. Punching shear resistance of flat slabs by shear heads. International Journal of Engineering Research and Development. Vol. 13 No 11, pp. 47-66. 2017.

Bartolac, M., Damjanović, D., Duvnjak, I. Punching strength of flat slabs with and without shear reinforcement. Građevinar. 2015

Birkle, G. Punching of flat slabs: The influence of slab thickness and stud layout. PHD Thesis, The University of Calgary, 2004.

Binici, B. Punching shear strengthening of reinforced concrete slabs using fiber reinforced polymers. PHD Thesis, The University of Texas at Austin, 2003.

Corley, W. G., Hawkins, N. M. Shear head Reinforcement for slabs. ACI Journal, Vol. 65 No. 10, pp. 811-824. 1968.

De Oliveira, M., Pereira Filho, M., Oliveira, D., Ferreira, M., Melo, G. (2013). Punching resistance of internal slab-column connections with double-headed shear studs. Revista IBRACON de Estruturas e Materiais.

Drakatos, I., Muttoni, A., Beyer, K. Internal slab-column connections under monotonic and cyclic imposed rotations. Engineering Structures. Vol. 123, pp. 501-516. 2016.

Einpaul, J., Brantschen, F., Ruiz, M. F. and Muttoni, A. Performance of punching shear reinforcement under gravity loading: influence of type and detailing. ACI Structural Journal, Vol. 113, No. 4, pp. 827-838. 2016.

Emam, M., Marzouk, H. and Hilal, S. Seismic response of slab-column connections constructed with high-strength concrete. ACI Structural Journal, Vol. 94, No. 2, pp. 197-204. 1997.

Erdogan, H. Improvement of punching strength of flat plates by using carbon fiber reinforced polymer (CFRP) dowels. PHD Thesis. The Graduate School of Natural and Applied Sciences of Middle East Technical University. 2010.

Ferreira, M. P. Punção em lajes lisas de concreto armado com armaduras de cisalhamento e momentos desbalanceados. PHD Thesis. Faculdade de Tecnologia da Universidade de Brasilia. 2010. (In Portuguese)

Ferreira, M. P., Barros, R. N. M., Pereira Filho, M. J. M., Tapajós, L. S., Quaresma, F. S. One-Way Shear Resistance of RC Members with Unconnected Stirrups. Latin American Journal of Solids Structures, Rio de Janeiro. Vol. 13, n. 15, p. 2970-2990. 2016.

fib – International Federation for Structural Concrete. *fib* Model Code 2010 for concrete structures. 2010.

Gouveia, N. D., Faria, D. M. V., Ramos, A. P. Assessment of SFRC flat slab punching behavior – part II: reversed horizontal cyclic loading. 2018. Magazine of Concrete Research: 71:1, pp. 26-42.

Hawkins, N. M. Siesmic response of reinforced concrete flat plate structures. Proceedings of the Seventh World Conference on Earthquake Engineering, Istanbul, Turkey, Sept. 9-13, pp. 33-40. 1980.

Isufi, B. Ramos, A. P., Lúcio, V. Reversed horizontal cyclic loading tests of flat slab specimens with studs as shear reinforcement. 2019. Structural concrete 20: pp. 330-347.

Mabrouk, R. T. S., Bakr, A. and Abdalla, H. Effect of flexural and shear reinforcement on the punching behavior of reinforced concrete flat slabs. Alexandria Engineering Journal. Vol. 56, pp. 591-599. 2017.

Marzouk, H, Osman, M., and Hussein, A. Cyclic loading of high-strength lightweight concrete slabs. ACI Structural Journal, Vol. 98 No. 2. pp. 207–214. 2001.

Muttoni, A. and Schwartz, J. Behavior of Beams and Punching in Slabs without Shear Reinforcement. IABSE Colloquium. Vol. 62, pp. 703-708. 1991.

Muttoni, A. Punching Shear Strength of Reinforced Concrete Slabs without Transverse Reinforcement. ACI Structural Journal, Vol. 105 No. 4. pp. 440-450. 2008.

Newswise. Study on the influence of column size and slab slenderness on punching strength. 2016. Access in October 2020: <https://www.newswise.com/articles/study-on-the-influence-of-column-size-and-slab-slenderness-on-punching-strength>

NP EN 1992-1-1. Eurocódigo 2 – Projeto de Estruturas de Betão Armado: Regras gerais e regras para edifícios. 2010.

NP EN 12390-3. Ensaios de betão endurecido – Parte 3: Resistência à compressão dos provetes de ensaio. 2003.

NP EN 12390-6. Ensaios de betão endurecido – Parte 6: Resistência à tracção por compressão de provetes. 2003.

Rabello, F. T. Análise comparativa de normas para a punção em lajes de concreto armado. 2010. Universidade Federal de Santa Catarina. Available from: <https://repositorio.ufsc.br/handle/123456789 /94391>. Acesso em: 30 mar. 2017.

Ramos, A., Marreiros, R., Almeida, A., Isufi, B. and Inácio, M. Punching of flat slabs under reversed horizontal cyclic loading. ACI-fib International Symposium, Vol 315, pp. 253-272. 2017.

Robertson, I. N., Kawai, T., Lee, J. and Enomoto, B. Cyclic testing of slab-column connections with shear reinforcement. ACI Structural Journal, Vol. 99, No. 5, pp. 605-613. 2002.

Robertson, I. N. and Johnson, G. P. Cyclic lateral loading of non-ductile slab-column connections. ACI Structural Journal, Vol. 103, No. 3, pp. 356-364. 2006.

Ruiz, M. F. and Muttoni, A. Application of Critical Shear Crack Theory to Punching of Reinforced Concrete Slabs with Transverse Reinforcement. ACI Structural Journal. Vol. 106, No. 4, pp. 485-494. 2009.

Ruiz, M. F., Muttoni, A. and Kunz, J. Strengthening of flat slabs against punching shear using post-installed shear reinforcement. ACI Structural Journal. Vol. 107. No. 4. pp. 434-442. 2010.

Schmidt, P., Kueres, D. and Hegger, J. Punching shear behavior of reinforced concrete flat slabs with a varying amount of shear reinforcement. Structural Concrete. Vol. 21. pp. 235-246. 2020.

Sissakis, K. and Sheikh, S. A. Strenghtening concrete slabs for punching shear with carbon fiber-reinforced polymer laminates. ACI Structural Journal. Vol. 104, No. 1. pp. 49-59. 2007.

SlabSTRESS – Slab STructural RESponse for Seismic European Design. 2020. Available from: <http://www.slabstress.org>

Swanson, D. Christchurch Earthquake Reconnaissance Part 1: The First 3 days [2011]. Available from: <http://www.reidmiddleton.com/reidourblog/5-2/>.

Tan, Y. and Teng, S. Interior slab-rectangular column connections under biaxial lateral loadings. ACI Special Publication, No 232, pp. 147-174. 2005.

APPENDIX A

In this appendix are displayed the diagrams for strain values measured through the entire test. First are presented the strain for flexural reinforcement, top and bottom, for each specimen, followed by the values obtained for the studs used in specimen C-SSR5-L.

For longitudinal bars, two strain gauges were placed at each position therefore the values here presented are the mean values of both measurements. In some of the figures below values for strain are not shown for the entire test, this means that strain gauges in that position stopped working due to yielding of the bar or malfunction of the strain gauge.

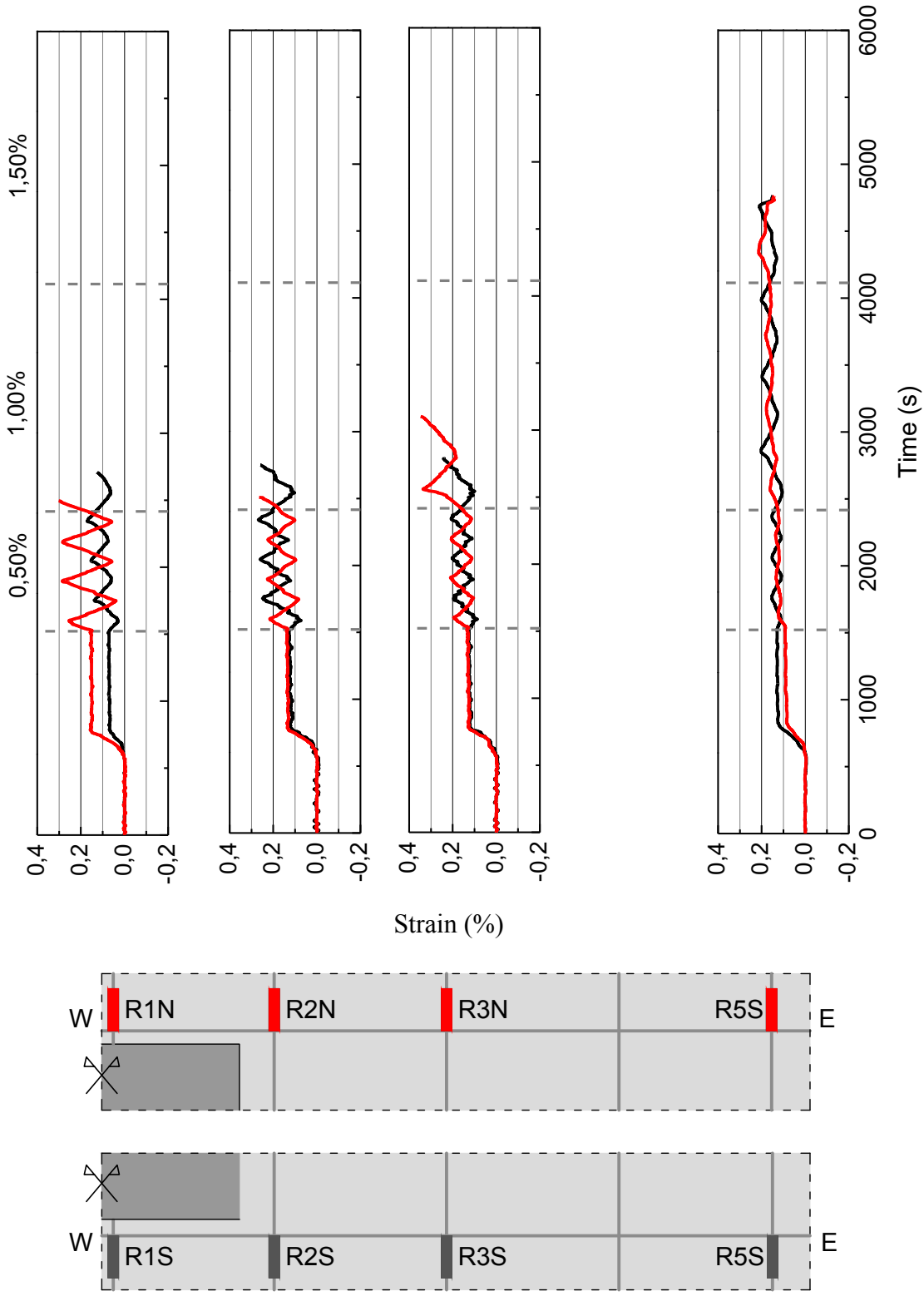

Figure A. 1 - Top reinforcement strain measurements for C-Ref-L

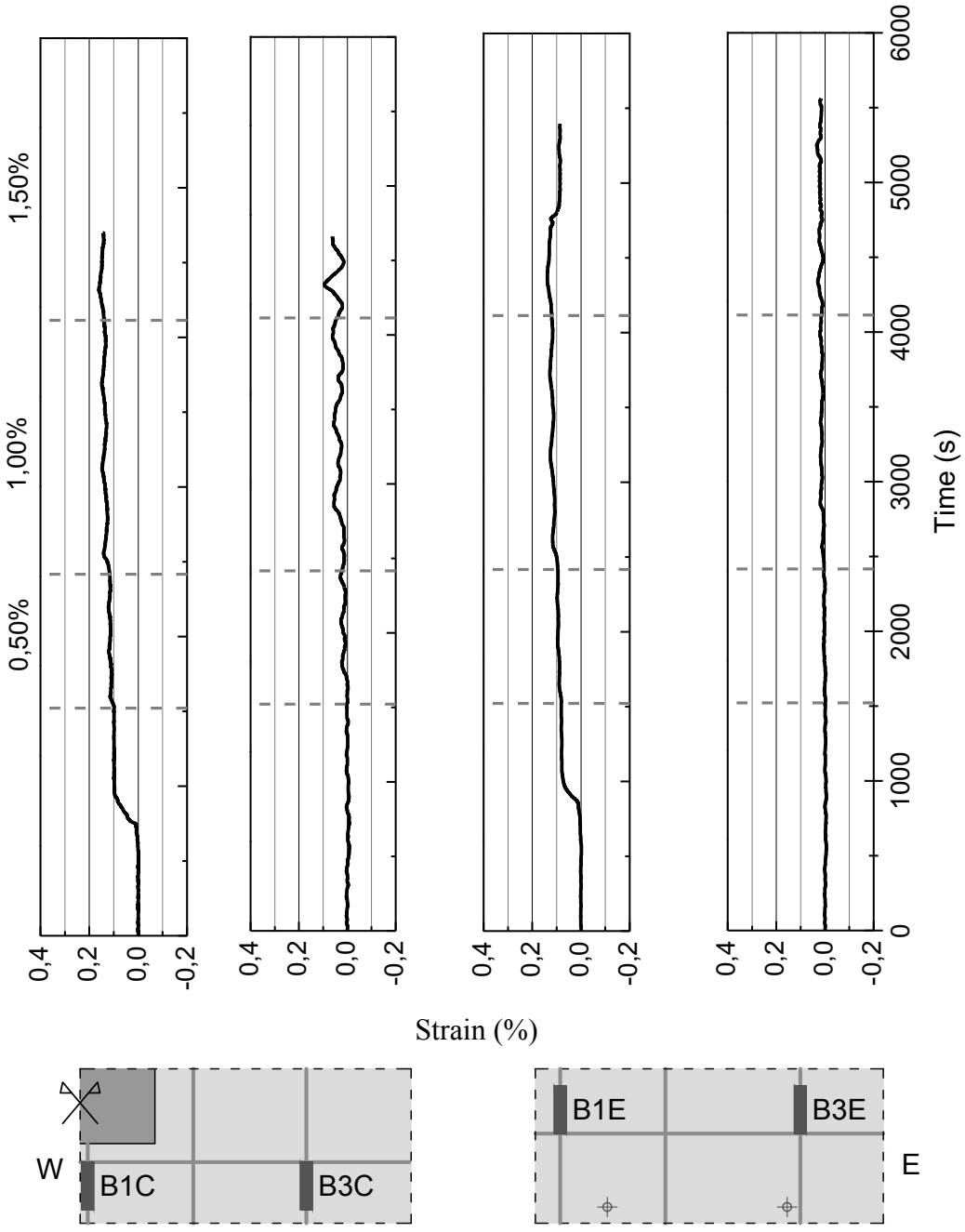

Figure A. 2 - Bottom reinforcement strain measurements for C-Ref-L

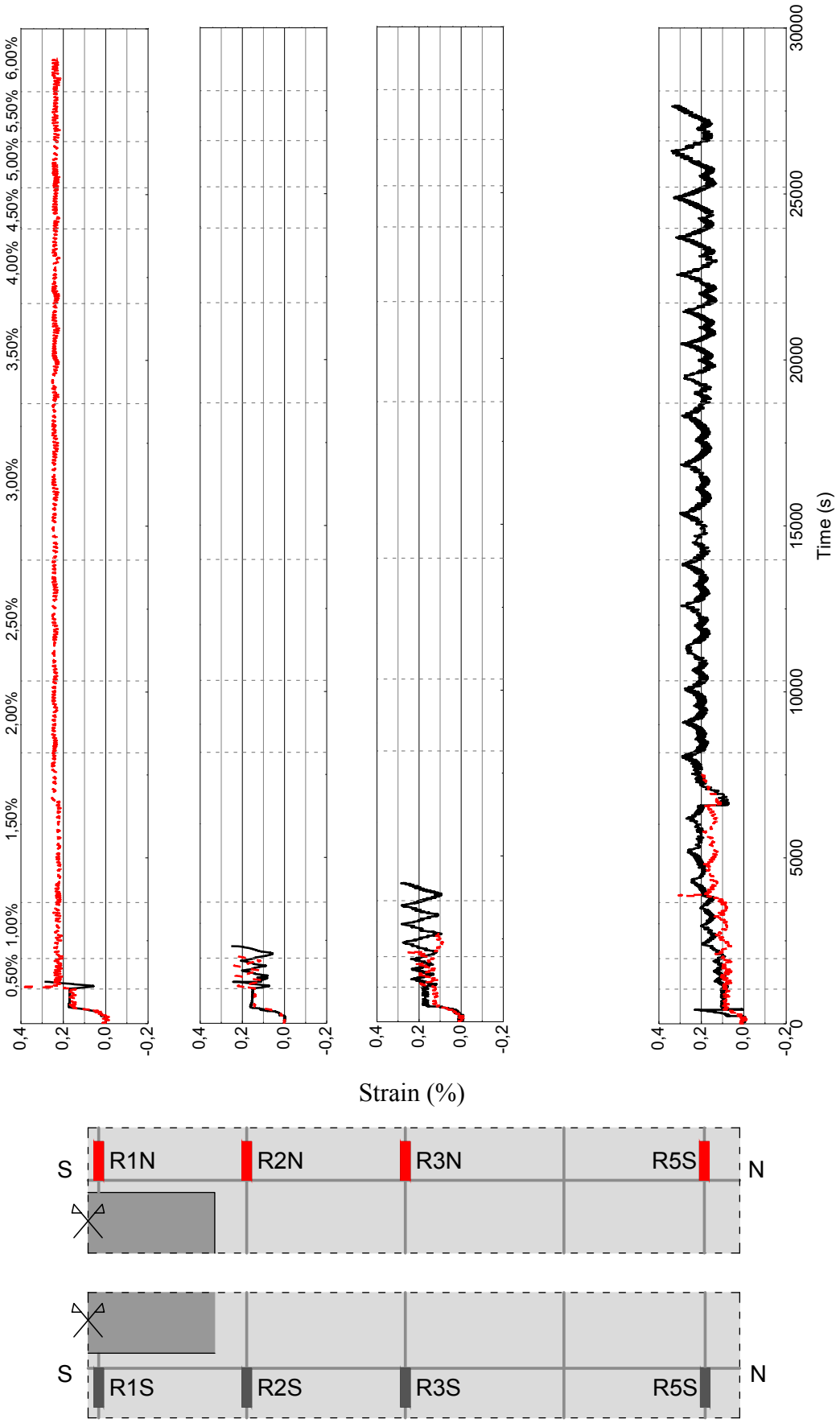

Figure A. 3 - Top reinforcement strain measurements for C-SSR5-L

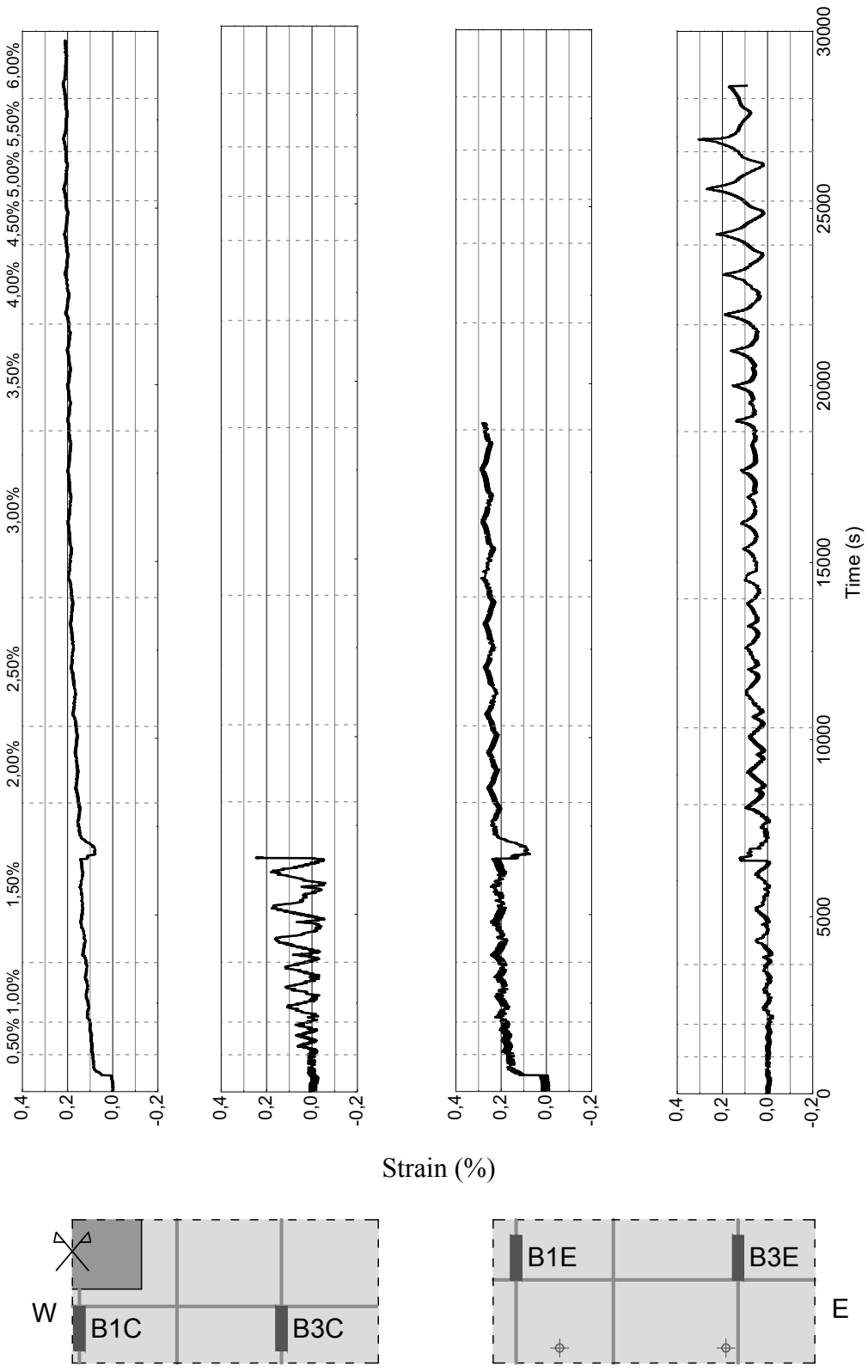

Figure A. 4 - Bottom reinforcement strain measurements for C-SSR5-L

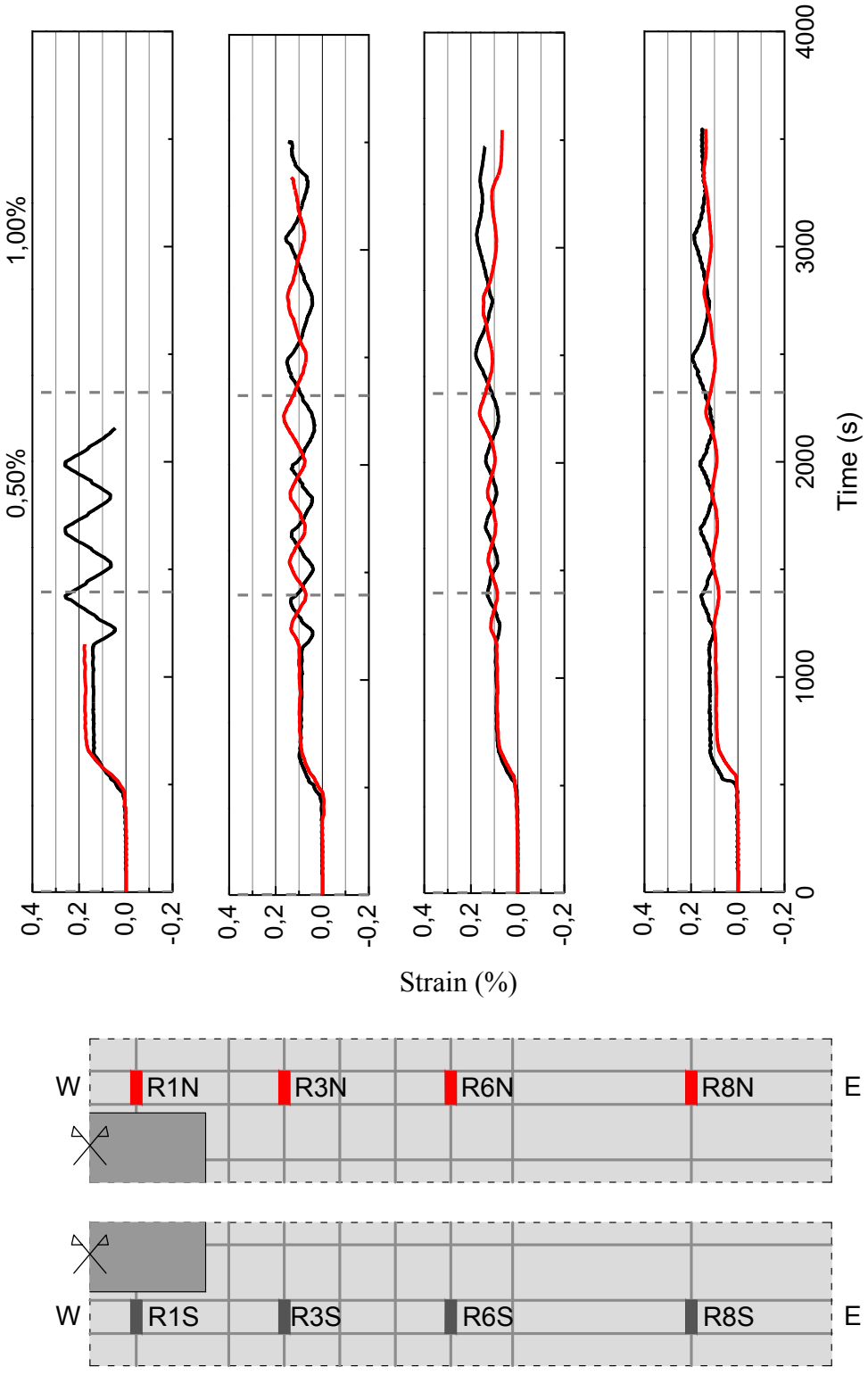

Figure A. 5 - Top reinforcement strain measurements for C-Ref-H

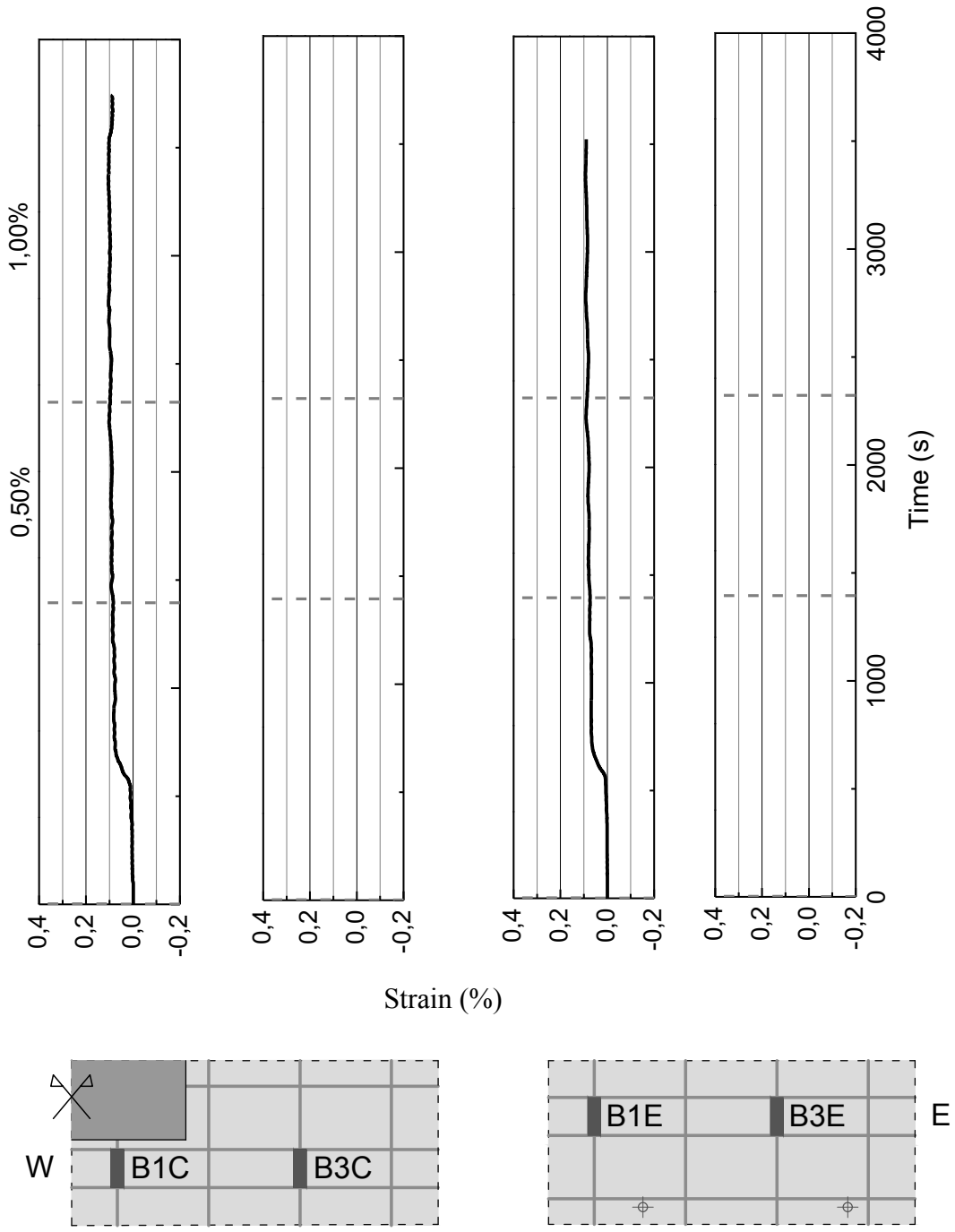

Figure A. 6 - Bottom reinforcement strain measurements for C-Ref-H

*Strain gauge positioned at B3C and B3E did not function correctly during the test

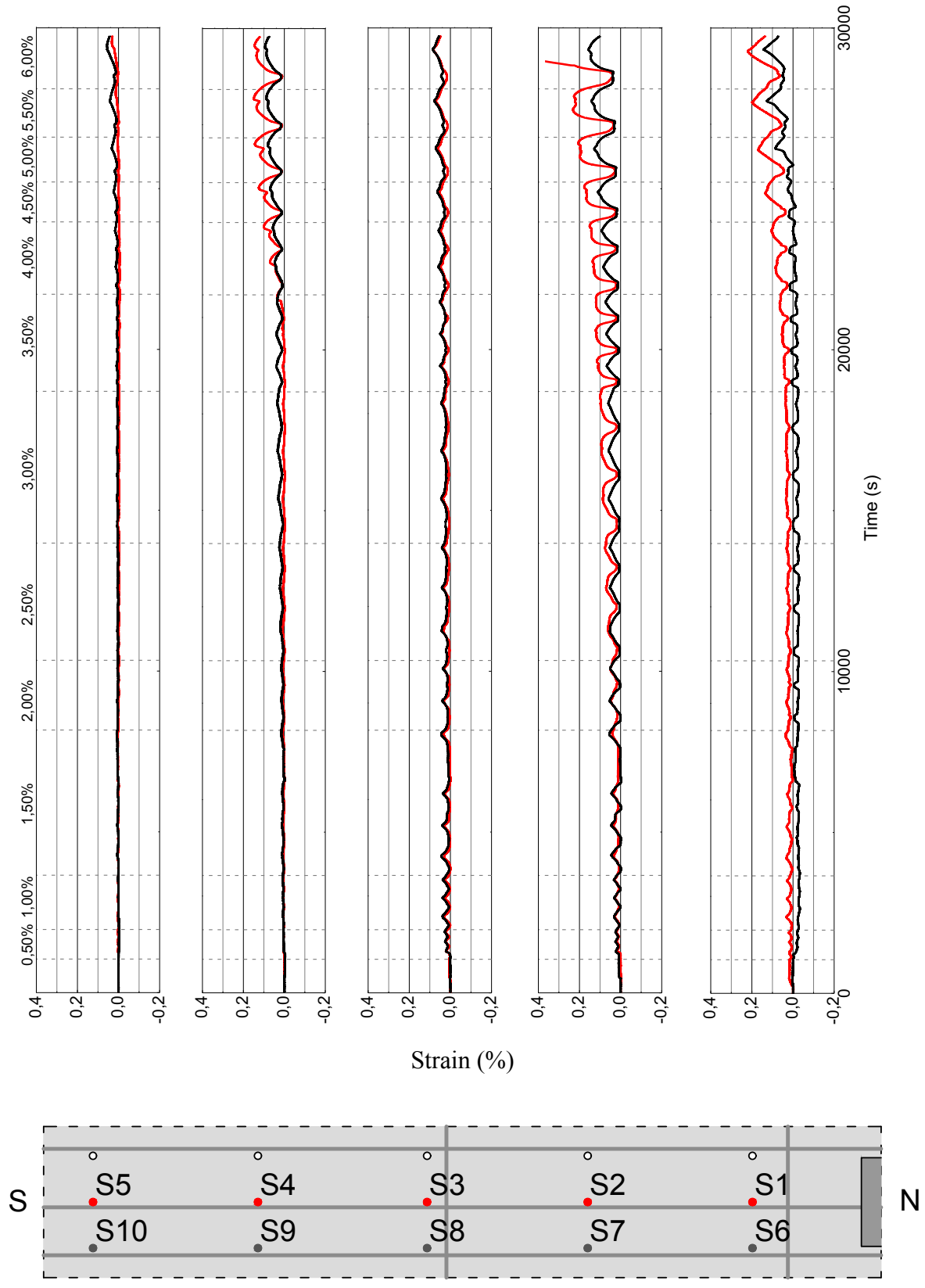

Figure A. 7 - South studs strain measurements for C-SSR5-L

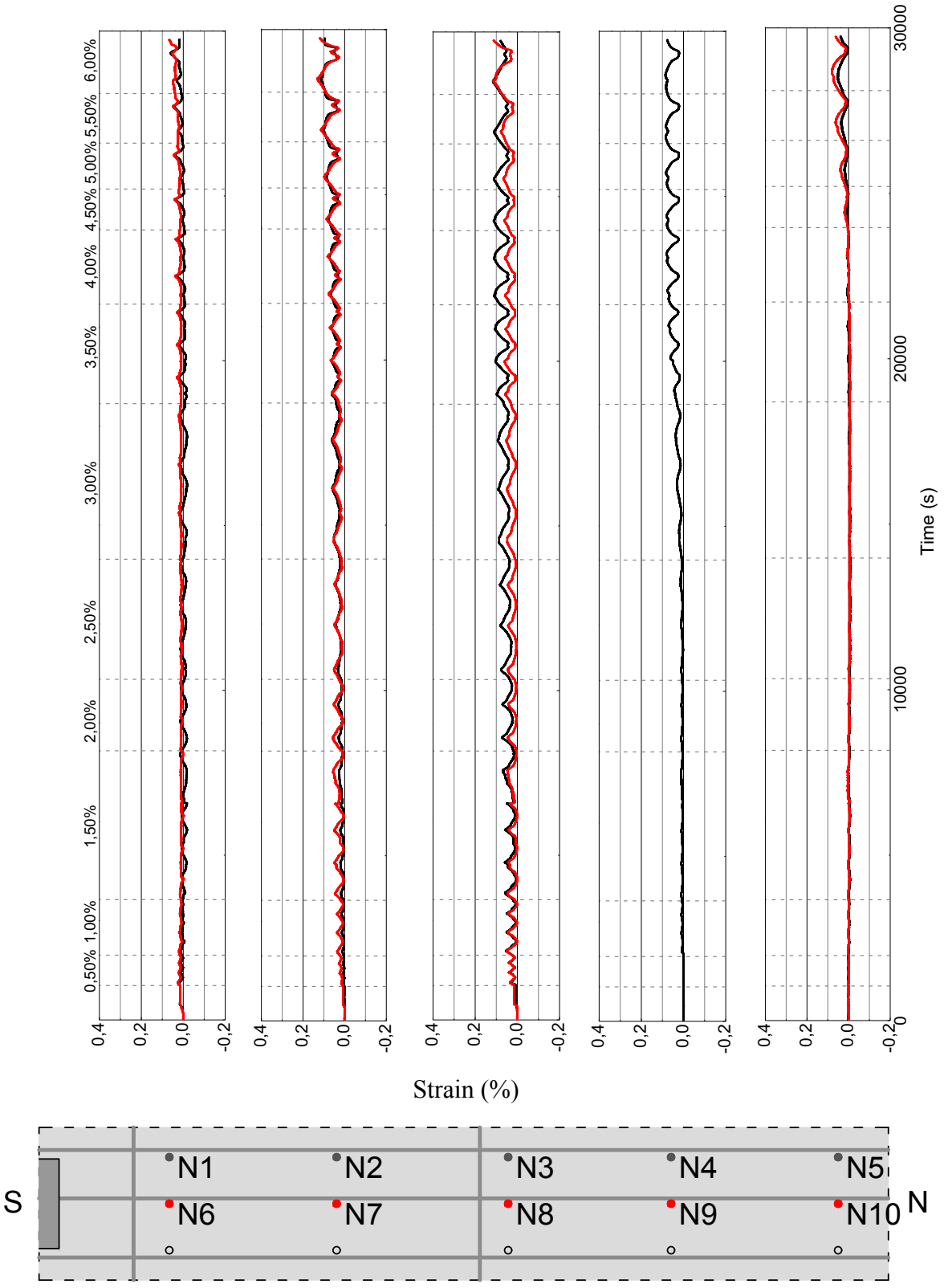

Figure A. 8 - North studs strain measurement for C-SSR5-L

*Strain gauge installed in stud N9 did not function correctly during the test

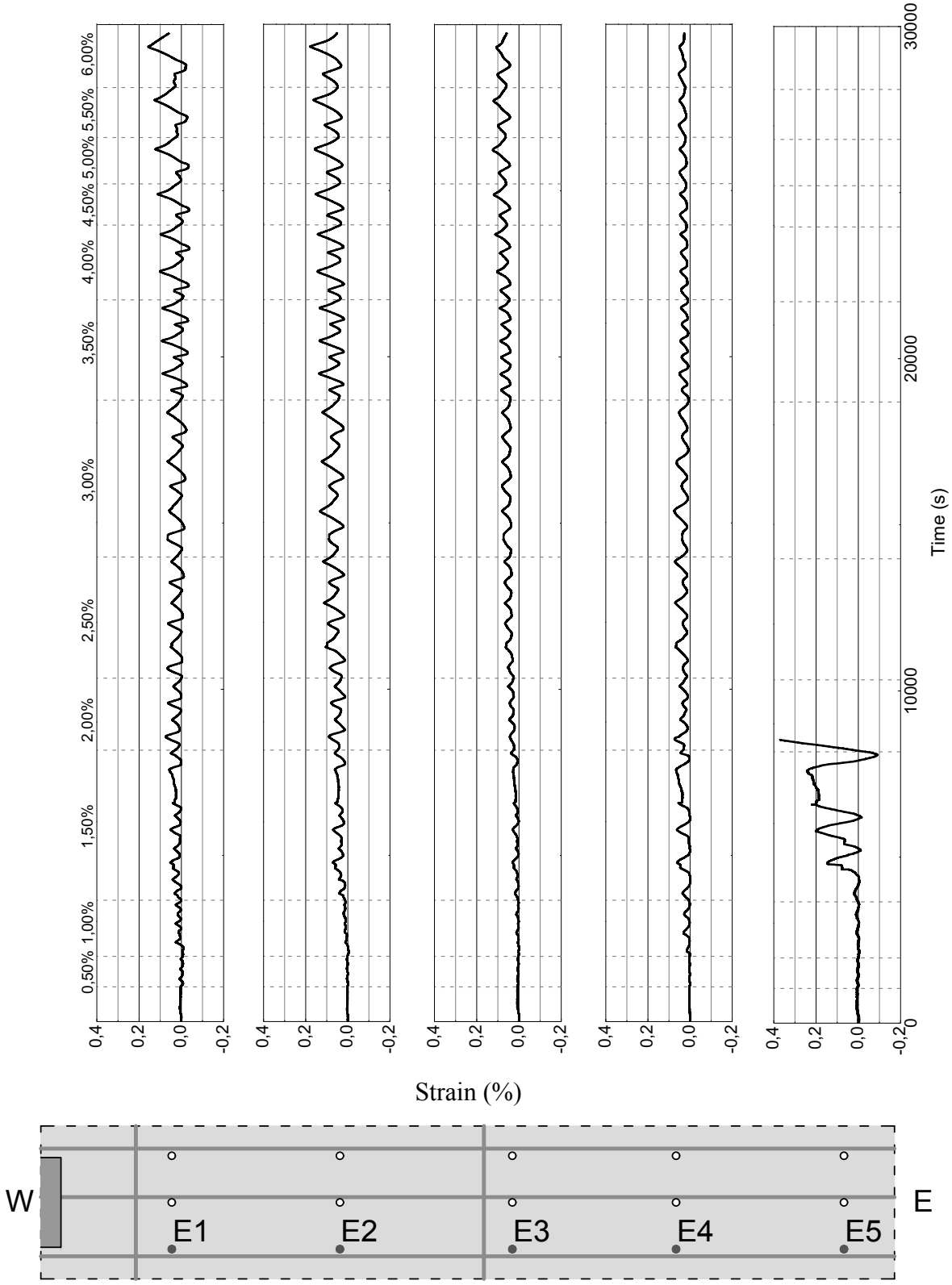

Figure A. 9 - East studs strain measurements for C-SSR5-L